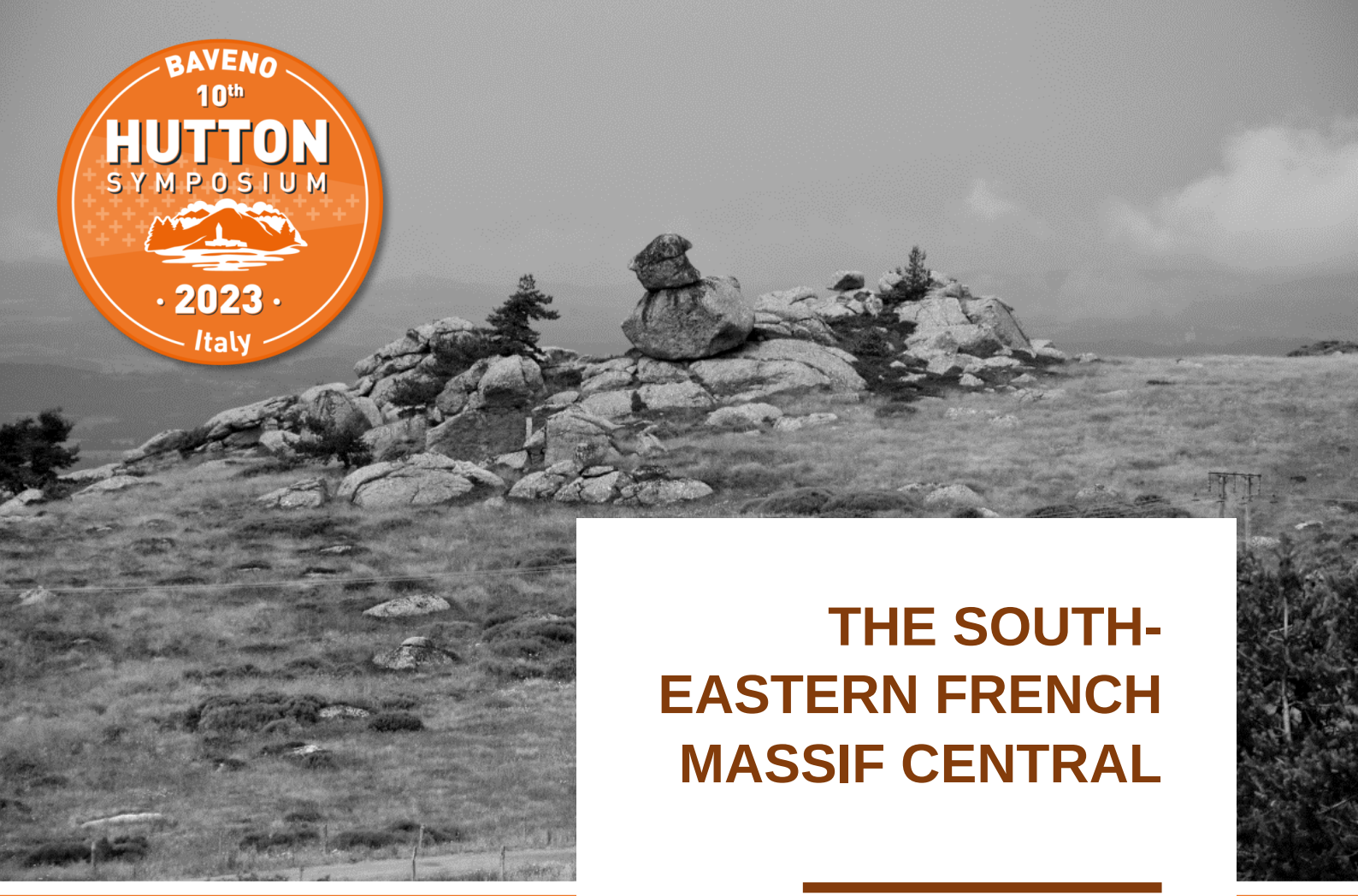

THE SOUTH-EASTERN FRENCH MASSIF CENTRAL

Hutton Symposium on Granites and Related Rocks

Pre-conference field trip

4 – 9 September 2023

Oscar LAURENT[1], Pierre BOUILHOL[2], Alain CHAUVET[3]

[1]CNRS, Géosciences Environnement Toulouse, France
[2]Centre de Recherches Pétrographiques et Géochimiques, Université de Lorraine, Nancy, France
[3]CNRS, Géosciences Montpellier, France

Table of contents

Information

Abstract

This field trip will take you to a journey through the Variscan crust of the eastern French Massif Central in the Carboniferous (**Figure 1**), offering the opportunity to investigate the anatomy of a crustal-scale, late orogenic magmatic system. We will examine the different structural levels of this system from the near surface to the mid-crust, starting from shallow granite plutons, associated silicic sub-volcanic rocks, lamprophyres and hydrothermal ore-forming systems. We will progressively travel deeper through the transition from low-grade country rocks to mid-crustal migmatites; eventually to the heart of the famous Velay complex, Europe's largest diatexite-granite dome. The characteristics of the exposed rocks will also lead us to discuss the nature of the complementary and concealed lowermost crust.

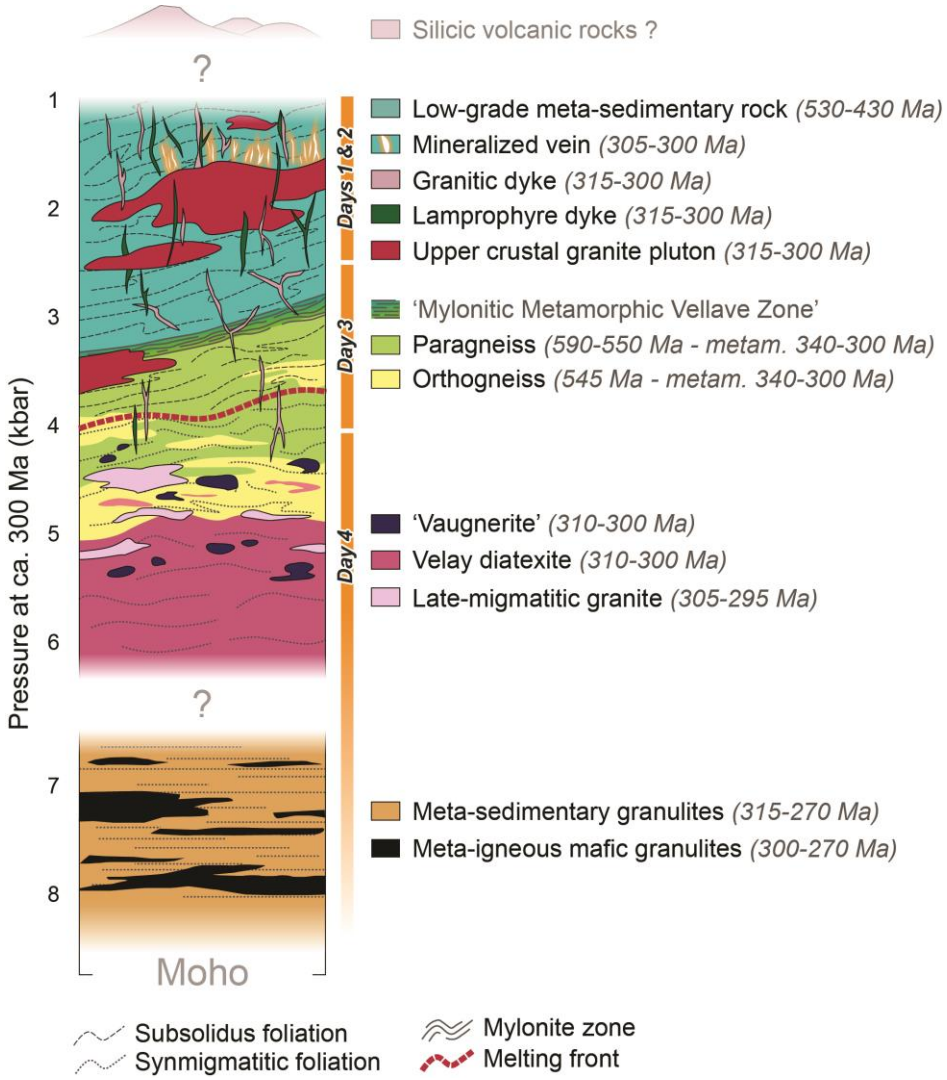

Figure 1 : A sketch vertical section through the late Carboniferous orogenic crust of the southeastern French Massif Central, highlighting the lithologies, structures and ages relevant to the field trip and objectives of each day.

This nearly continuous section through the Variscan upper- and mid-crust offers the opportunity to investigate many of the key topics relevant to the scientific program of the 10th Hutton Symposium on granites and related rocks. In particular, we will discuss the genetic and structural links between all components of the Carboniferous magmatic system; the processes of melt generation and transfer at different scales in space and time; the role of mantle-derived magmas in the genesis of late-orogenic granites; and implications for the magmatic-hydrothermal transition and the formation of ore deposits.

Eventually, this will lead us to discuss the importance of such magmatism for the genesis, reworking and stabilization of the continental crust in the context of Phanerozoic plate tectonics.

The field takes place in the scenic southeastern French Massif Central, home of the Cévennes National Park (https://www.cevennes-parcnational.fr/) and UNESCO Monts d'Ardèche Geopark (http://www.geopark-monts-ardeche.fr/), renowned for their unique geological heritage and preserved wilderness. In addition to visiting fascinating outcrops, you will discover a region of beautiful landscapes, traditional small villages, clear mountain streams, picturesque winding roads and experience the local hospitality and taste for invigorating country food.

Keywords: late-orogenic magmatism, granite, migmatite, magmatic-hydrothermal transition, continental crust, Massif Central, Velay dome, Cévennes

Program Summary

The general field trip location and detailed itinerary are shown in **Figure 2**; the different structural levels corresponding to each day are indicated on **Figure 1**.

Day 0 – **Monday 4th of September**. This is a transfer day, during which the participants picked up in either Lyon or Montpellier will travel to the Cévennes area. Special icebreaker dinner and overnight in Saint-Roman-de-Tousque.

Day 1 – Tuesday 5th of September. The first day will be dedicated to magmatic processes which contributed to build up the Aigoual pluton, a shallow granitic laccolith emplaced in regional low-grade meta-sedimentary rocks (the Cévennes schists), with a focus on **magma chamber and mush dynamics in shallow granitoid plutons** and how **interactions between mafic and silicic magmas** play a role in the formation of these plutons and associated volcanism. The day will start with the observation of a peculiar border facies of the Aigoual granite, containing high proportions of K-feldspar megacrysts and microgranular mafic enclaves at Saint-Jean-du-Gard (stop 1.1). We will then examine the physical and chemical effects of interactions between lamprophyre and granite in composite dykes at Rousses (stop 1.2) and on a broader scale, study the spatial geometry of these dykes and how they potentially connect with surface volcanism through one outcrop (stop 1.3) and panoramic viewpoint (stop 1.4) around Barre-des-Cévennes. End of the day and overnight in Saint-Roman-de-Tousque.

Day 2 – Wednesday 6th of September. This second day will be spent around the Mont Lozère batholith with emphasis on **the magmatic-hydrothermal transition** and **processes leading to the formation of intrusion-related ore** (gold ± antimony) **deposits**. The first stop in Cocurès (stop 2.1) will allow to investigate the relationships between high-silica equigranular granite (the Bougès unit) and aplitic dykes; and zones enriched in miarolitic cavities associated with pegmatoidal dykes and mineral layering. The next two outcrops in Pont-de-Montvert (stop 2.2) and Vialas (stop 2.3) will also allow to examine similar structures but in the K-feldspar porphyritic facies of the Mont Lozère batholith (the Pont-de-Montvert unit), as well as the intrusive contact of this granite in the Cévennes schists at locality 2.3. Finally, hydrothermal imprint and alteration within the Cévennes schists, related to the emplacement of the Mont Lozère batholith, will be examined at the Travers section (stop 2.4) and, if time and logistics permit, a short venture in a disused artisanal gold mining gallery at Pont-de-Rastel (optional stop 2.5). End of the day and overnight in Villefort.

Day 3 – Thursday 7th of September. During this day, we will progressively "deepen" in the crustal section, starting from the **transition between the low-grade Cévennes schists towards the underlying migmatites** that form the southernmost margin of the Velay dome. This transition is a zone of abrupt changes in metamorphic grade and complex structural record, both related to the exhumation of the migmatitic mid-crust, which can be observed along a short transect south of Saint-Laurent-les-Bains (stop 3.1). In the Luc area, we will discuss **the nature and geological significance of the main pre-Variscan lithologies** and their **importance as protoliths of Carboniferous migmatites** based on unmolten examples of paragneisses (stop 3.2) and orthogneisses (stop 3.3). We will then sit close to the melting front and have a look at a nice example of metatexite developed in orthogneisses in Borne (stop 3.4). The last stop of the day at Col de Meyrand (stop 3.5) is a mainly touristic lookout point, which yet allows to glimpse the large-scale structure of the southern margin of the Velay dome from landscape analysis. End of the day and overnight in Beaumont.

Day 4 – Friday 8th of September. On the last day of the trip, we reach the core of the Velay dome, i.e. parts of the Carboniferous crust that were exhumed from the deepest levels (up to 6 kbar), to discuss

how large migmatitic domes form, **what are the melting processes** and the **nature of the complementary lower crust**. This will start at Pont-de-Bayzan where migmatites developed at the expense of meta-sedimentary rocks (stop 4.1) show a diversity of textures and compositions allowing to discuss the different melting reactions, heat sources, and melt transfer processes. The next outcrops in Antraigues (stop 4.2) and Péreyres (stops 4.3, 4.4 and 4.5) will give an overview of the petrological diversity of the Velay diatexites, in particular the spectacular and typical cordierite-rich cockades; large garnet and biotite phenocrysts; and restitic enclaves whose mineralogy allows to discuss the characteristics of Carboniferous melting and eventually the nature of the complementary lower crust. End of the day and overnight in Beaumont.

Day 5 – Saturday 9th of September. This is a transfer day to the 10th Hutton Symposium venue in Baveno, Italy. This will first include a drive to Chambéry (ca. 250 km, 3.5 hours), from where the field trip participants will be able to reach Baveno (ca. 450 km, 6.5 hours) with connections in Milano Porta Garibaldi and (logistics pending) Malpensa Airport. Estimated time of arrival in Baveno is 7:30 pm.

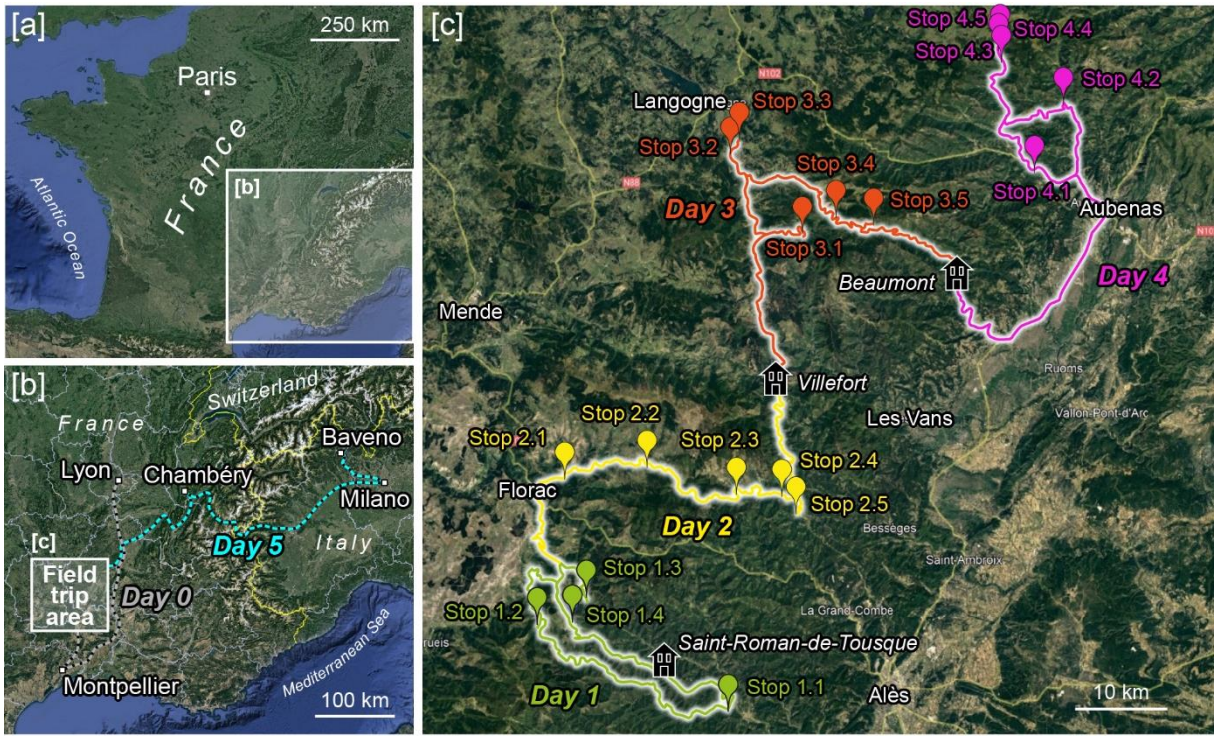

Figure 2 : Overview of the field trip area location [a,b] and itinerary [b,c] from Google Earth photos.

Safety

The late summer weather in southeastern Massif Central is usually warm (18–30°C), sunny with occasional afternoon storms, but the trip visits high hills / plateaus (900–1600 m a.s.l.) along the Atlantic / Mediterranean watershed where intense rain showers and cold spells may occur, rather unpredictably. Basic equipment must therefore include sun protection for head and skin, as well as warm clothes and waterproof jackets. Light field boots or running shoes are sufficient as only short walks/hikes are planned, most outcrops lying along roadsides and riverbeds. Several outcrops are located next to beautiful swimming holes in (cold) mountain streams, consider packing a swimming costume. Car sickness may be an issue as the trip frequently implies rather long drives on curvy mountain roads.

In case of serious need for immediate assistance, you may call the universal European emergency number **112** free of charge. Other useful numbers specific to the French authorities (only reachable with a French cell or fixed phone) are as follows:

- Emergency medical service (SAMU): **15** (medical/health issue, redirects to the nearest healthcare center)
- Police: **17** (in case of an accident, aggression, theft, etc.)
- Fire Brigade: **18** (in case of fire, weather emergency, etc.)

By their nature, excursions and field trips involve certain potential risks. Although field leaders will make their best to ensure participant's safety, and in particular issue instructions and advice, ensuring one own's safety remains each participant's responsibility.

In particular, it is to the responsibility of every field trip participant to:

- Familiarize themselves with the excursion program;
- Follow the field trip leaders' instructions and directions at all times;
- Always stay with the group whenever traveling on foot in the field and stopping at outcrops, as some of them are located in potentially hazardous environment (road side, slippery river bed, steep rocky surroundings, etc.);
- Wear adapted clothing and footwear;
- Be aware of his/her own physical limits and advise the leaders if he/she wishes to stop;
- Carry sufficient amounts of drinkable water (some may be provided along with lunch packages but likely not up to the amounts required for a regular day in the field);
- Advise the leaders about any health problem that may have an impact on his/her physical condition (e.g., asthma, diabetes, epilepsy, vertigo, heart condition, joint and/or back pain, car sickness, allergies, etc.) as well as carry and manage any personal medicine that may be required accordingly;
- Be in possession of valid travel documents, including visa where required;
- Behave at all times in a responsible and courteous way toward the other participants and excursion leaders;
- Inform the excursion leaders before leaving the group.

By participating to a field trip, participants agree to follow these guidelines and to release the organizers of the Conference, including the field trip guides and organizers, from all liability for injury, death or other loss or damage resulting from the participation to the trip, or the travel to or from the excursion.

Hospitals

Below are contact information for the nearest hospitals (see approximate location on **Figure 2**):

- **Day 1 and day 2:** Centre Hospitalier Alès Cévennes (Avenue du Dr. Jean Goubert, 30100 Alès; Phone nr.: +33 466 78 33 33)
- **Day 2 and day 3:** Hôpital Lozère (53 avenue du 8 Mai 1945, 48000 Mende; Phone nr.: +33 466 49 49 49)
- **Day 4:** Centre Hospitalier d'Ardèche Méridionale (14-16 Avenue de Bellande, 07205 Aubenas; Phone nr.: +33 475 35 60 60)

Overnight accommodation

Dinner, overnight and breakfast are booked in hiking lodges, country hotels or campsites (single or double rooms) as follows:

- **Day 0 and Day 1:** Village de Gîtes de Saint-Roman-de-Tousque (Saint-Roman-de-Tousque, 48110 Moissac-Vallée-Française; Phone nr.: +33 448 25 00 05) - https://www.cevennes-vallee-francaise.fr/
- **Day 2:** Camping le Mas des Sédariès (Rue du Mas des Sédariès, 48800 Villefort; Phone nr.: +33 466 46 25 20) - https://www.sedaries.com/
- **Day 3 and Day 4:** Le Sentier des Arches (Le Gua, 07110 Beaumont; Phone nr.: +33 475 39 44 09) - https://www.sentierdesarches.com/fr/

Lunch packages are provided by the hotels.

Excursion notes

Overview of the field area

The area we will visit, namely the Cévennes and Monts d'Ardèche regions, are located on the southeastern flank of the Massif Central. In this area, the Variscan basement has been continuously uplifted since the early Cenozoic in response to the Alpine orogeny. The Massif Central is a broad asymmetric plateau, as the eastern part has undergone a stronger uplift (up to ca. 1200–1700 m.a.s.l.) than the western part. The eastern margin thus represents a steep escarpment, the plateau lying 700–1200 m above the lowlands of the Rhône Valley. This escarpment, along which we will be travelling over these four days, is a maze of deeply incised valleys and steep and narrow ridges ("*serres*").

Because of this peculiar geomorphology, the eastern margin of the Massif Central represents the watershed between rivers flowing to the West and North to the Atlantic Ocean (Loire river and its tributaries) and those flowing east- and southwards to the Rhône Valley and eventually the Mediterranean Sea. This dichotomy also strongly affects the landscapes, vegetation, climate; as well as land use and local economy, which all vary spectacularly over short distances as they are very different on the "*Plateau*" and in the "*Vallée*".

Owing to the steep topography and to the proximity of the Mediterranean Sea to the South, the climate ranges from Mediterranean in the Rhône Valley (and adjoining lowlands around Montpellier, Alès, Aubenas, Privas); to semi-continental and even alpine-like on the highest points of the plateau (the summits are above the tree line). The lowlands grow olive trees, are covered with vineyards and hardly see any frost during the winter; whereas some 30 km away the plateau sits in pine forest with heather, blueberries and peatland and is commonly buried under tens of centimeters of snow for weeks. Along the escarpment, rains occur typically in autumn (late September to November), and tend to be concentrated over a few massive "*épisodes cévenols*" (generally about 200 mm in 24h, with a record at 607 mm in 24h).

In terms of human history, the area features evidence for a long-lived human occupation, starting with many megalithic monuments and painted caves dating back to the Stone Age. Several major roman cities existed in the Southern Rhône Valley. Medieval occupation was dense and most present villages existed already: Romanesque churches are ubiquitous, and every strategic hill is capped by a castle or a watch tower. In the XVIth century, the whole of southern France, in particular the Cévennes area, was affected by civil unrest during the wars of religion following the Protestant Reformation and this remote region became a shelter for protestants fleeing the persecutions.

The economy of the Cévennes and Monts d'Ardèche areas was first based on silk, as the mild climate allowed to grow mulberry trees on which the silk worm feeds. Silk was produced since the Middle Ages and boomed in the XVIIIth to XIXth centuries, feeding the famous silk weaving industry in Lyon. The agriculture has long been and is still mainly based on chestnut farming and cattle, goat and hog breeding (the latter mainly used for salted and cured meat such as "*saucisson*" etc.). Mining became a significant industrial activity in the region by the industrial revolution, including coal (from late Carboniferous basins fed by erosion of the Variscan orogenic belt), base metals together with silver and fluorine (dispersed mineralization in the Triassic cover or along Variscan faults re-activated in the Mesozoic) and gold, occurring as small lodes in the Cévennes mountains. It was followed by uranium (hosted in granites or at the unconformity between granite and Mesozoic sediments) in the second half of the XXth century.

The population in this rural area peaked in the mid-XIXth century but sharply declined in the XXth as the local industries (including mines) became unable to compete with national, then international counterparts. Later on, the development of the tertiary sector attracted more people towards large urban centers, notably lacking in the area. As an illustration, Beaumont, one of the villages where we'll be staying, has a population of 250 today, versus >1,300 inhabitants in 1850. Today, south-eastern Massif Central has a population of <500'000 inhabitants over a surface of 20'000 km^2 (half of the size of Switzerland), no town bigger than 25'000 and 75% of the population live in rural areas.

Starting in the late 70s however, the area underwent a certain revival based on tourism, which became the new pillar of the local economy. More recently, especially with the advent of internet and improved communications, a wave of young to middle-aged professionals came to the mountains and started small business either in the tourism sector, organic and small-scale farming, or working remotely via internet.

Geological background

The Variscan belt of Western Europe

The Variscan belt is a late-Palaeozoic orogenic belt, extending from the Appalachians to the West, to Central Europe to the East (**Figure 3**). The orogen records long-lived convergence between Gondwana and/or Gondwana-derived microcontinents to the South, and Laurussia-Avalonia to the North (Stampfli et al., 2002; Stampfli et al., 2013), and resulted in the assembly of Earth's latest supercontinent (Pangea) in the late Paleozoic (**Figure 3**). It forms most of the basement of Western Europe (**Figure 4**), covered by Mesozoic basins and affected by structures related to the Alpine cycle (Matte, 1986).

Although remnants of high-pressure metamorphism are present throughout the Variscan belt, it has long been recognized as a "hot" orogen characterized by abundant high-temperature (upper amphibolite to granulite facies) metamorphic rocks, including migmatites, and granitoids (see e.g. Franke, 2014; Vanderhaeghe et al., 2020; and references therein). These are best exposed in the high-grade core of the orogenic system referred to as the "Moldanubian zone" (Ballèvre et al., 2014) (i.e. the greenish domain in **Figure 4**), commonly regarded as the "internal zone" of the Variscan orogeny (Lardeaux et al., 2014).

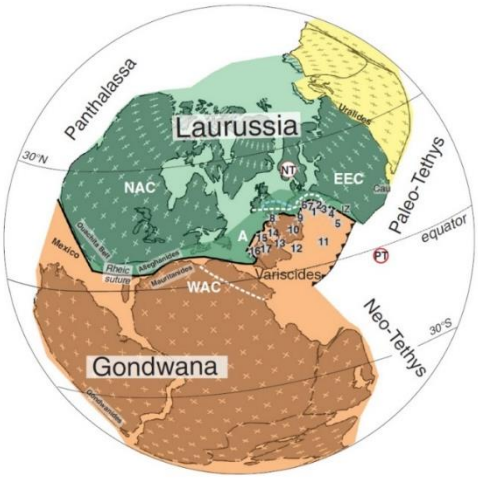

Figure 3 : Palaeogeographic reconstruction of the Pangea supercontinent ca. 250 Ma ago, highlighting the Variscan suture (Rheic suture) (after Kroner and Romer, 2013). Abbreviations: NAC – North American Craton; EEC – East European Craton; WAC – West African Craton; A – Avalonia; PT – Paleothetys; NT – Neothetys.

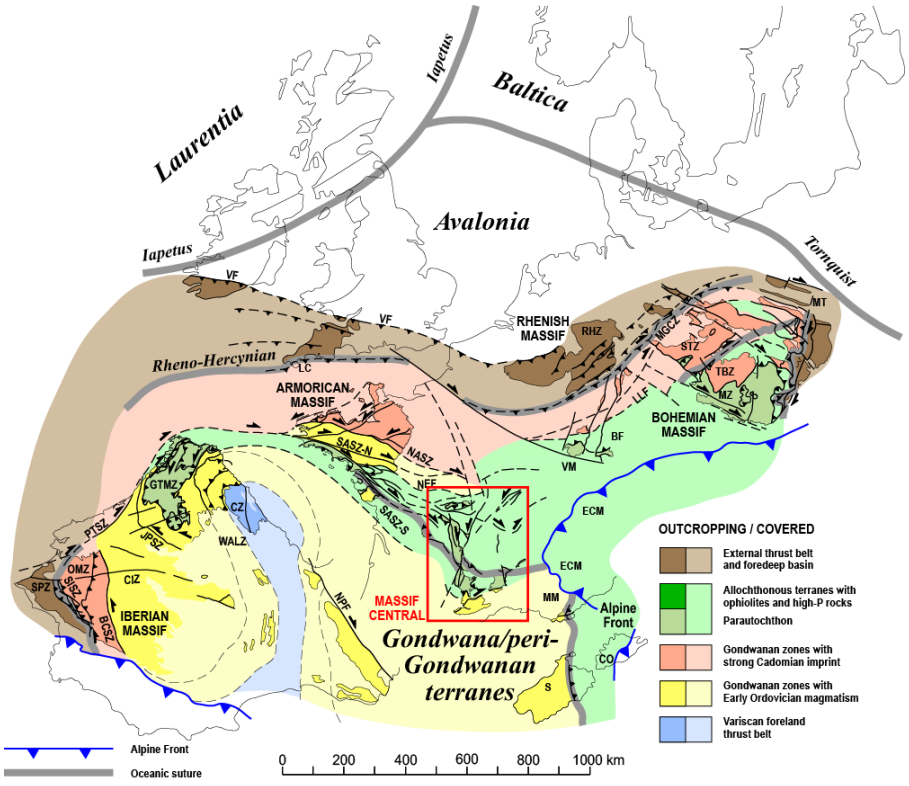

Figure 4 : Simplified geological map of the Variscan belt (Ballèvre et al., 2014). Zones: CIZ, Central Iberian; CZ, Cantabrian; GTMZ, Galicia–Tras-os-Montes; MGCZ, Mid-German Crystalline; MZ, Moldanubian; OMZ, Ossa-Morena; RHZ, Rheno-Hercynian; SPZ, South Portuguese; STZ, Saxo-Thuringian; TBZ, Tepla´-Barrandian; WALZ, West Asturian–Leonese. Shear zones/faults: BCSZ, Badajoz–Cordoba; JPSZ, Juzbado–Penalva; LLF, Lalaye–Lubine; MT, Moldanubian thrust; NASZ, North Armorican; NEF, Nort-sur-Erdre; NPF, North Pyrenean; PTSZ, Porto–Tomar; SASZ, South Armorican; SISZ, Southern Iberian; VF, Variscan front. BF, Black Forest; CO, Corsica; ECM, External Crystalline Massifs; LC, Lizard Complex; MM, Maures Massif; S, Sardinia; VM, Vosges Massif.

The French Massif Central

The French Massif Central (FMC) is a large (ca. 100,000 km^2; **Figure 5**) inlier of the Moldanubian zone in Central France. The eastern part of the FMC (E-FMC) refers to the terrains located east of the "Sillon Houiller" ("coal line"), a lithospheric-scale strike-slip fault flanked by several pull-apart, coal-bearing late Carboniferous basins (Burg et al., 1990; Thiery et al., 2009). The Limousin domain occurs West of the Sillon Houiller, and although its geological history is relatively comparable until ca. 320 Ma, it does not expose large, late Carboniferous (ca. 310-300 Ma) granite-migmatite domes as the E-FMC (Vanderhaeghe et al., 2020) and also misses the related, upper crustal granitic intrusions.

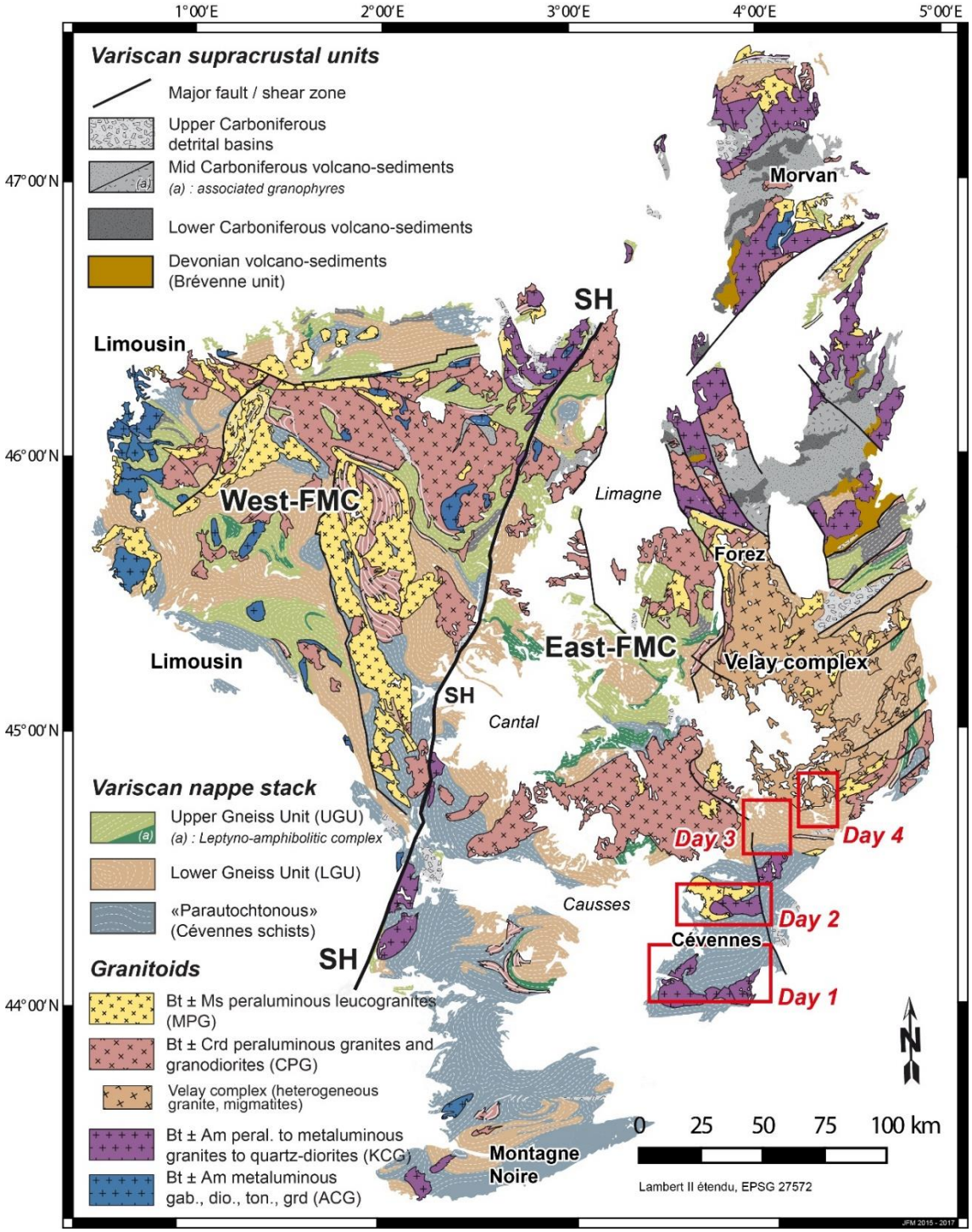

Figure 5 : Geological map of the French Massif Central, redrawn after Geological map of France to the 1/1 000 000 scale (Chantraine et al., 1996), omitting post-Variscan units. SH: Sillon Houiller. The red frames indicate the areas visited in this trip.

The building blocks of the continental crust in the E-FMC belong to the former northern margin of the Gondwana supercontinent (Nance et al., 1991; Matte, 2001; Zeh et al., 2001; Faure et al., 2009b; Kroner and Romer, 2013) and consist of Neoproterozoic to early Paleozoic meta-sedimentary and meta-igneous rocks. These rocks formed in relation to the Cadomian orogeny and in response to the break-up of the north Gondwana margin, and were affected by tectono-metamorphic and magmatic events during subsequent convergence between Gondwana and Laurussia (Matte, 1986; Nance et al., 1991; Matte, 2001; Faure et al., 2009b; Kroner and Romer, 2013) (see details in the next section).

As a result of this evolution, the Massif Central crust is structured as a stack of tectono-metamorphic nappes (with a south-verging attitude on a regional scale) developed during the Devonian and early Carboniferous (Matte, 1986; Ledru et al., 1989.; Matte, 2001). This nappe stack notionally comprises four main tectono-metamorphic units (Burg and Matte, 1978; Burg et al., 1984; Ledru et al., 1989; Faure et al., 2009b; Lardeaux et al., 2014), which are from the bottom to the top (and from South to North) (**Figure 5**):

- The **"para-autochtonous" unit** (**PAU**) made of low-grade (greenschist- to lower amphibolite-facies) meta-sedimentary rocks ("Schistes des Cévennes" and equivalent units; Faure et al., 1999), likely deposited from the Cambrian to the Ordovician (Faure et al., 2009a; Couzinié et al., 2022);
- The **"lower gneiss unit"** (**LGU**), an amphibolite-facies unit of ortho- and paragneisses having late Ediacarian to early Cambrian protoliths (Chelle-Michou et al., 2017; Couzinié et al., 2017, 2019). In the E-FMC, the LGU underwent pervasive, long-lived and low-pressure (<6 kbar) melting during the Carboniferous (Montel et al., 1992; Barbey et al., 1999, 2015), resulting in the development of migmatites and a large, granite-cored anatectic complex referred to as the Velay Dome (see below; Dupraz and Didier, 1988; Lagarde et al., 1994; Ledru et al., 2001);
- The **"upper gneiss unit"** (**UGU**), an amphibolite-facies unit of ortho- and paragneisses having early Cambrian to Ordovician protoliths (Duthou et al., 1984; Chelle-Michou et al., 2017; Lotout et al., 2017). Those underwent partial melting too, but to a lesser extent than the LGU and at higher pressure (>8 kbar) and older (late Devonian) ages of ca. 360 Ma (Gardien et al., 2011). The base of the UGU is marked by a ca. 490–480 Ma-old bimodal magmatic association (amphibolites and meta-rhyolites or granites; Pin and Lancelot, 1982; Briand et al., 1991), locally known as the "**leptyno-amphibolic complex**" (**LAC**). Within and immediately below the LAC, the UGU contains characteristic relicts of high-pressure granulites (Gardien et al., 1990; Mercier et al., 1991; Gardien, 1993), possibly ultra-high-pressure (coesite-bearing) eclogites (Lardeaux et al., 2001) and boudins of mantle peridotite (Bernard-Griffiths and Jahn, 1981; Gardien et al., 1990).
- **Low-grade** (lower greenschist-facies) **volcano-sedimentary associations** (Feybesse et al., 1988). This comprises the Brévenne basin in the E-FMC, interpreted as a Devonian (ca. 366 Ma-old; Pin and Paquette, 1997) back-arc (Bébien, 1970; Sider and Ohnenstetter, 1986).

In the field trip area, we will mainly focus on rocks of the PAU and LGU (**Figure 5**). The lateral continuity of these different nappes at the scale of the Massif Central is a debated issue (see Vanderhaeghe et al., 2020 and references therein). This will be one possible topic of discussion at the occasion of Day 3, as stop 3.1 sits at the contact between the two units.

In the E-FMC, the nappe stack is intimately associated with granitic rocks s.l. While the PAU and low-grade volcano-sedimentary rocks have been intruded by Carboniferous (340-300 Ma; Laurent et al., 2017) granitic plutons, the LGU features one of Europe's largest granite-diatexite dome, the ca. 310-300 Ma Velay Complex (Ledru et al., 2001; Barbey et al., 2015; Vanderhaeghe et al., 2020) (**Figure 5**). These are the main focus of this trip and are described in more detail in the next sections.

Crustal evolution and geological history of the E-FMC

The constitutive rocks of the different Variscan nappes of the E-FMC described above belong to the former northern margin of the Gondwana supercontinent (Nance et al., 1991; Matte, 2001; Zeh et al., 2001; Faure et al., 2009b; Kroner and Romer, 2013; Stampfli et al., 2013) (**Figure 4**). The oldest rocks identified so far are indeed meta-sediments deposited in the Ediacarian (590–550 Ma) and fed by detritus from Archean to Neoproterozoic Gondwanian terranes (Chelle-Michou et al., 2017; Couzinié et al., 2019), produced through the combined action of the Pan-African orogenies and Neoproterozoic glaciations (Squire et al., 2006; Meinhold et al., 2013). The protoliths of these rocks were once part of a thick (pluri-kilometer) succession of siliciclastic marine sediments deposited in the context of the

Neoproterozoic Cadomian accretionary orogenic system developed along the north Gondwana margin (Nance et al., 1991; Garfunkel, 2015), possibly in a back-arc setting (Linnemann et al., 2014; Couzinié et al., 2019). These were associated with unevenly distributed, and generally minor amounts of magmatic rocks (Linnemann et al., 2014). Throughout Western Europe, and in the E-FMC in particular, ages and Hf isotopic compositions of detrital zircons within these Ediacaran sediments clearly point to a derivation from northern Africa (West African Craton, Saharan Metacraton, Arabian-Nubian shield), with a mixture of old cratonic crust (Meso-/Neoarchean and Paleoproterozoic) and a juvenile Neoproterozoic (0.9–0.6 Ga) component (see Chelle-Michou et al. 2017; Couzinié et al., 2019 and references therein) (**Figure 6**a).

The Ediacaran meta-sedimentary rocks were then intruded by two main generations of igneous rocks (now orthogneisses). The first emplaced near the Ediacarian-Cambrian boundary (ca. 545 Ma; Caen-Vachette, 1979; R'Kha Chaham et al., 1990; Mougeot et al., 1997; Be Mezeme et al., 2006; Couzinié et al., 2017) in the context of inversion of the Cadomian back-arc basin (**Figure 6**b). The second generation corresponds to a well-known magmatic flare-up in the early Ordovician (490–470 Ma) throughout Western Europe (Berger et al., 2006; Melleton et al., 2010; Nance et al., 2010; Von Raumer et al., 2013a; Villaseca et al., 2015; von Raumer et al., 2015; Gutiérrez-Alonso et al., 2016; Chelle-Michou et al., 2017). Although this timing is coeval with the opening of the Rheic Ocean and northward drifting of Avalonia away from the north Gondwana margin (**Figure 6**b), igneous rocks of that age are widespread far to the south of the Rheic suture (see **Figure 4**), including in the E-FMC. This suggests that a smaller oceanic domain existed between the north Gondwana margin and an intervening terrane (Armorica), i.e. the "Galicia-Brittany Ocean" (Matte, 2001) or "Massif Central-Moldanubian Ocean" (Tait et al., 1997). Alternatively, the area may have consisted of an ocean-continent transition or hyperextended north Gondwana margin (Lardeaux et al., 2014). This context was favorable to further sediment deposition, explaining the purported Ordovician deposition age of some of the E-FMC meta-sedimentary rocks, notably in the PAU (Cévennes schists; Faure et al., 2009a; Couzinié et al., 2022).

In the E-FMC, both generations of orthogneisses are silicic, peraluminous in composition and show zircon Hf isotopic compositions compatible with partial melting of the Ediacaran meta-sedimentary rocks (**Figure 6**a). They are coeval with minor volumes of mafic rocks with juvenile Hf isotopic characteristics (**Figure 6**a), indicating a non-negligible contribution of depleted mantle melting in both cases, in the form of arc or back-arc magmas for the Ediacaran-Cambrian event; and MORB or passive margin basalts for the early Ordovician event.

Rifting and opening of oceanic basin(s) in the early Paleozoic were followed by subduction and associated HP-LT to HP-HT metamorphism, marking the onset of the Variscan cycle (***Figure 6***b). This metamorphic event (M1), originally dated to the Silurian to early Devonian, was recently re-evaluated to be mainly mid- to late-Devonian (390–360 Ma) (Paquette et al., 2017; Lotout et al., 2018; Benmammar et al., 2020) (**Figure 6**c). It was temporally associated with emplacement of arc-related calc-alkaline tonalites to granodiorites (Bernard-Griffiths et al., 1985; Peiffer, 1986; Shaw et al., 1993; Pin and Paquette, 2002; Rossi and Pin, 2008) and bimodal volcanics with back-arc affinity (Bébien, 1970; Sider and Ohnenstetter, 1986; Pin and Paquette, 1997).

Collision proper started at 360–350 Ma (**Figure 6**c), with nappe stacking (Burg et al., 1984) characterized by a top-to-the-NW D2 phase followed by a top-S D3 event (Faure et al., 2009b); Barrowian metamorphism (M2); and formation of large peraluminous granite intrusions in the northern MCF (Cartannaz et al., 2007). Following collision, NW–SE extension started at ca. 330 Ma (D4 of Faure et al., 2009), associated with HT/LP metamorphism (M3 in Montel et al., 1992) (**Figure 6**c). The Variscan events end up in the formation of the large Velay granite–migmatite dome at 310–300 Ma, possibly corresponding to a local M4 metamorphic phase at high temperatures and shallow depths (820 °C, 4 kbar; Montel et al., 1992). The late Carboniferous period (340–300 Ma) is also characterized by the emplacement of voluminous granitoids (Laurent et al., 2017) (see details in the next section). Together with the extent of melting recorded in the Velay dome, this event implies a substantial input of extra heat to the crust, from (i) increased heat flux through the Moho, due to peeling off of the lithospheric root of the belt (Laurent et al., 2017; Vanderhaeghe et al., 2020); and/or (ii) mantle-derived magmatism (Ledru et al., 2001).

The details of the Variscan geodynamic evolution is still debated, particularly in the case of the FMC. In particular, the timing, vergence and location of the subduction zones are still unclear, and several hypotheses are presented in the literature. A "monocyclic" model entails that the nappe stack of the FMC results from continuous North-verging subduction from the Silurian to the Carboniferous; whereas a "polycyclic" model proposes that a switch from North- to South-verging subduction happened in the late Devonian (see **Figure 7** for a summary).

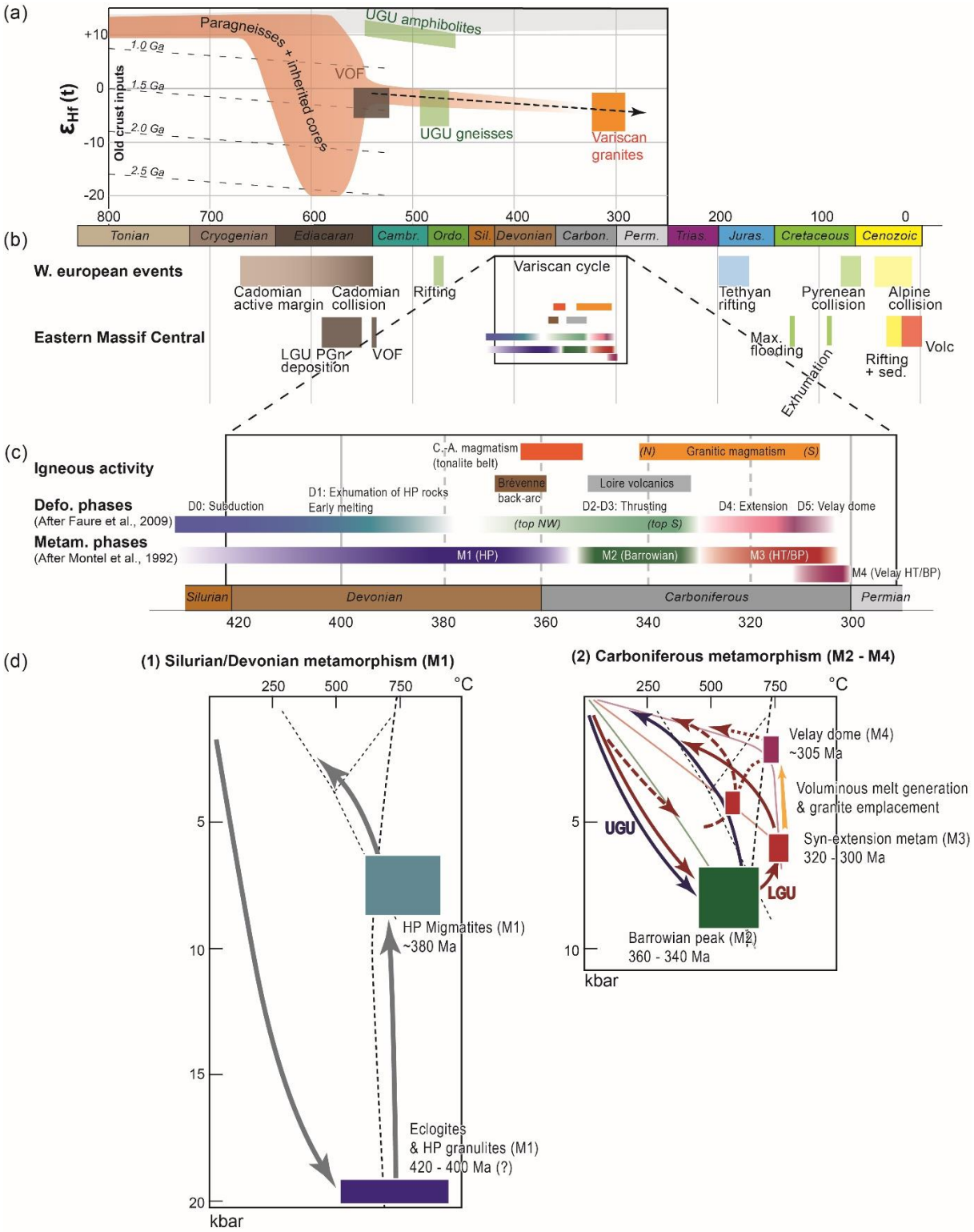

Figure 6 : Summary of geological events and crustal development in the French Massif Central. (a) Schematic zircon $\varepsilon Hf_{(t)}$ – time evolution patterns (after Couzinié et al., 2016, 2017, 2019; Chelle-Michou et al., 2017; Moyen et al., 2017 and unpublished data). (b) Summary of the geological events in France; three main orogenic cycles (Cadomian, Variscan and Alpine) have occurred since the late Precambrian. During the alpine cycle, the earliest phase corresponds to collision with Iberia (Pyrénées), followed by the Alps s.s., and the West European Rift System. (c) Details of the Variscan cycle in the Eastern Massif Central (the sequence of events is similar in most of the Moldanubian domain – in France, Limousin, S. Brittany, Vosges, etc.—until ca. 320—310 Ma; the Velay event however is unique to the Eastern FMC). Note the mismatch between the numbering of deformation phases (after Faure et al., 2009b), and the metamorphic phases (using the Southern Velay terminology of Montel et al., 1992). (d) Synthetic P—T—t paths in the French Massif Central (modified after Vanderhaeghe et al., 2020).

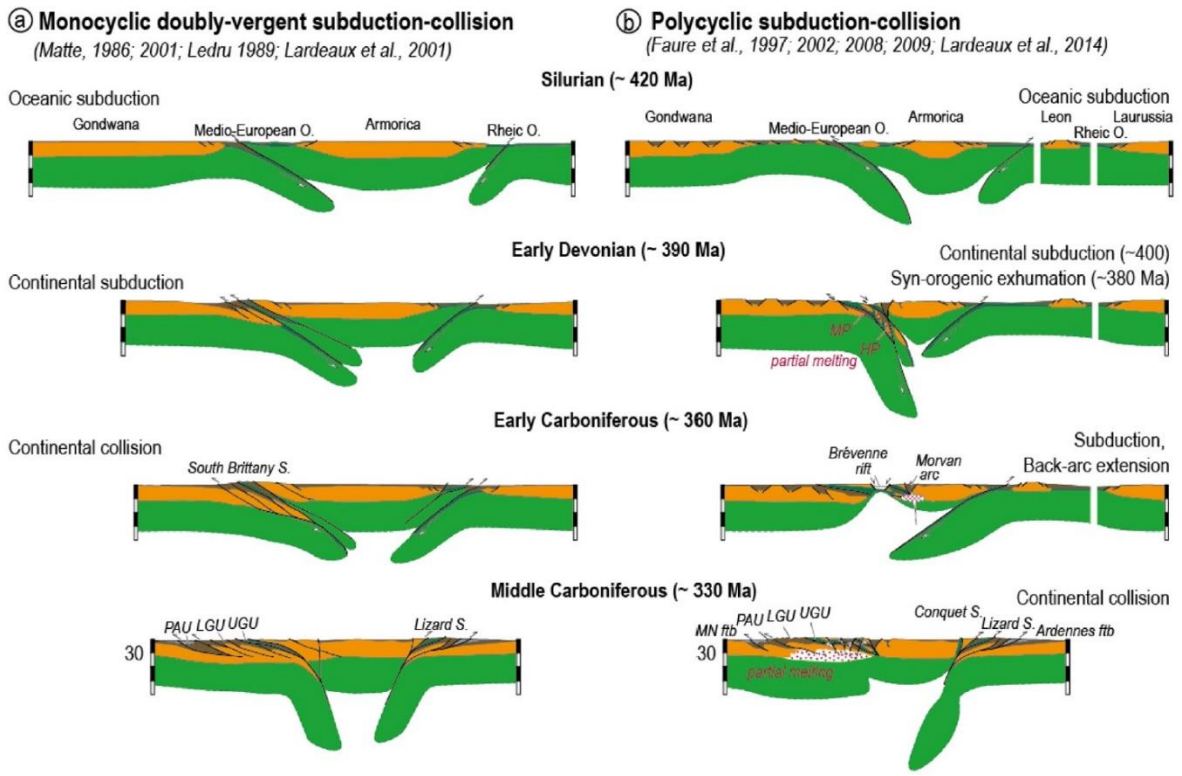

Figure 7 : Summary of different hypotheses proposed to explain the geodynamic evolution of the Variscan belt from the Silurian to the Middle Carboniferous (Vanderhaeghe et al., 2020) (see also **Figure 11**).

In contrast to zircons from Ediacarian sediments, which indicate contributions from Mesoarchean to Neoproterozoic crustal components, those from younger igneous rocks (Ediacaran-Cambrian, Ordovician orthogneisses and the Carboniferous, Variscan granitoids) plot along a rough linear trend of decreasing $\varepsilon Hf_{(t)}$ towards younger ages (**Figure 6**a) corresponding to a time-integrated $^{176}Lu/^{177}Hf$ ratio typical of average crust (ca. 0.01). A similar pattern has been observed for both Sr (Duthou et al., 1984) and Nd (Turpin et al., 1990) isotopes. This pattern is irrespective of the petrogenetic diversity of the rocks plotting along the trend (including strongly peraluminous granites/orthogneisses; slightly metaluminous to moderately peraluminous diorites/granodiorites; and metaluminous intermediate to mafic rocks). The trend shows that the isotopic identity of the E-FMC crust (and even lithosphere) was essentially acquired by the end of the Cadomian orogeny, and that all subsequent events contributed mainly to its reworking, through a range of geological processes.

Following the Variscan orogeny, the FMC and notably the eastern edge was affected by development of the Tethyan passive margin. This resulted in the deposition of a typical succession of continental Permian to Triassic sediments (sandstone and conglomerates with evaporites locally); lower Jurassic shallow-water carbonaceous facies; upper Jurassic and lower Cretacenous deep-water limestones; and mid-Cretaceous massive reef limestones (the “Urgonian” facies). Epicontinental seas around the Tethys developed relatively thin equivalents of this succession, for instance in the Causses and Cévennes area. These form isolated mounds and flat-lying, high plateaus of Triassic to lower Jurassic sediments that uncomformably rest on top of the Variscan basement.

Starting from the late Cretaceous, the opening of the Bay of Biscay and the Pyrenean collision caused uplift and exhumation of the European basement. Large portions of the Massif Central were exhumed at that time (fission track ages of 130–110 Ma) (Barbarand et al., 2001). Tertiary extension associated with the West European Rift system further enhanced exhumation and led to the relatively high elevation of the E-FMC relative to other Variscan inliers in Western Europe. Rifting proper occurred in the Oligocene and resulted in the formation of N—S trending grabens filled by lacustrine to shallow marine sediments. The uplift (Miocene to present) occurred along a N—S axis, ca. 50 km West of the Rhône Valley, forming a significant mountain range (1200–1700 m). The uplift resulted in deeply incised valleys and favored the development of karstic morphology in the limestones. The post-Variscan erosion surface is still preserved (often capped by alterites), and forms plateaus at altitudes of typically 1000 m in our region of interest.

Intra-continental volcanism started in the Oligocene, but peaked in Miocene to Pliocene, with the development of large stratovolcanoes (Cantal, Mont-Dore) and basaltic provinces (Aubrac, Velay, Devès). This activity extended into historical times (900,000 to <6,000 years), mostly in the form of scattered monogenic volcanoes and associated flows, including the iconic Chaîne des Puys near Clermont-Ferrand and several edifices in the field trip area. Lavas are typically alkaline basalts, rich in mantle peridotite nodules; and less common andesites, trachy-andesites, trachytes and phonolites.

Granitoids of the E-FMC, the Velay Complex and vaugnérites

Variscan granitoids are abundantly exposed in the E-FMC (see **Figure 5**), like in many other areas of the belt in Western Europe (Finger et al., 1997; Bea et al., 1999; Fernandez-Suarez et al., 2000; Janoušek et al., 2000; Rossi and Pin, 2008). Intrusive granitoid bodies can be classified in two groups:

- Strongly peraluminous, **muscovite-** (± garnet, tourmaline) or **cordierite-bearing granites and granodiorites**, respectively corresponding to "**MPG**" and "**CPG**" in the classification of Barbarin (1999). While MPG can be either biotite-bearing (two-mica granites) or biotite-free, CPG are always biotite-bearing, and cordierite ranges from abundant to absent (Barbey et al., 1999). These granites usually form laccoliths and small bodies around and within the Velay Dome (Ledru et al., 2001) (**Figure 5**).
- Slightly to mildly peraluminous, **K-feldspar porphyritic calc-alkaline quartz-diorites, granodiorites and granites** (**KCG** in the sense of Barbarin, 1999). They are commonly (but not always) amphibole-bearing, always biotite-rich, and never contain muscovite. They contain microgranular mafic enclaves (MME: Didier and Barbarin, 1991) and are spatially associated with "*vaugnérites*" (see below). In contrast with CPG and MPG, KCG always emplaced at higher structural levels in low-grade country rocks (**Figure 5**).

The Velay Complex is a large (up to 100 km wide) granite-migmatite dome bounded by extensional shear zones, and roughly concentric with a heterogeneous, cordierite-bearing granite-diatexite core surrounded by a migmatitic rim, grading into unmolten gneisses (**Figure 5**). The crystallization of the Velay granite-diatexite core is dated at 310-300 Ma (Mougeot et al., 1997; Couzinié et al., 2014, 2021; Chelle-Michou et al., 2017; Laurent et al., 2017). The heterogeneous granitic phase at the core of the complex can be considered as a CPG, although it is unique by its size and relationship with migmatites.

The E-FMC also includes ubiquitous, yet small volumes of "**vaugnérites**", which are mafic to intermediate, potassic plutonic rocks akin to lamprophyres (Michon, 1987; Sabatier, 1991). Similar rocks (termed "*durbachites*" or "*redwitzites*") are found throughout the Variscan belt (Holub, 1997; Siebel and Chen, 2009; von Raumer et al., 2013b). Vaugnérites range from diorite to syenite and consist of biotite, amphibole, clinopyroxene, plagioclase, with subordinate orthopyroxene, K-feldspar and quartz (Sabatier, 1991). They crop out as enclaves (1-100 m) in granites and migmatites, but can also form sills and dykes (Couzinié et al., 2014).

The main major-element geochemical traits of the Variscan granitoids and vaugnérites are presented in **Figure 8**. While MPG and CPG (including the Velay granite) are generally silicic, strongly peraluminous and show a wide range of Mg# values (from 10-50 in MPG and Velay granite vs. 30-60 in other CPG), vaugnérites are clearly more mafic (45-65 wt.% SiO_2), metaluminous and magnesian (Mg# = 50-80). KCG show somewhat intermediate characteristics between the two end-members.

The petrographic and geochemical characteristics of CPG-MPG and Velay granite clearly suggest a crustal source. This is confirmed by their richness in inherited zircons (Couzinié et al., 2014; Chelle-Michou et al., 2017; Laurent et al. 2017); bulk-rock Sr—Nd isotopic analyses overlap with those of ortho- and paragneisses (Duthou et al., 1984; Pin and Duthou, 1990; Turpin et al., 1990; Williamson et al., 1996, 1997; Downes et al., 1997) (**Figure 9**); and chemical and chronological complementarity with lower crustal xenoliths of meta-sedimentary granulites (Villaros et al., 2018; Laurent et al., 2023) brought up mainly by Cenozoic volcanoes. Vaugnérites, on the other hand, are typical post-collisional mafic magmas (PCMM) that stem from an enriched (lithospheric) mantle source (Couzinié et al., 2016). The origin of KCG is more debated. Their slightly more mafic character than CPG-MPG (**Figure 8**), systematic association with vaugnérites (Barbarin, 1988) and lack of inherited zircons (Laurent et al., 2017) favor that they derive from differentiation of mantle-derived magmas, i.e. vaugnérites (Moyen et al., 2017). On the other hand, the common occurrence of mafic enclaves (MME) and magma mixing textures in KCG as well as their intermediate major- and trace-element characteristics between vaugnérites and CPG-MPG, suggest that KCG may rather derive by mixing between these respectively mantle-derived and crust-derived magmas (Downes et al., 1997; Solgadi et al., 2007).

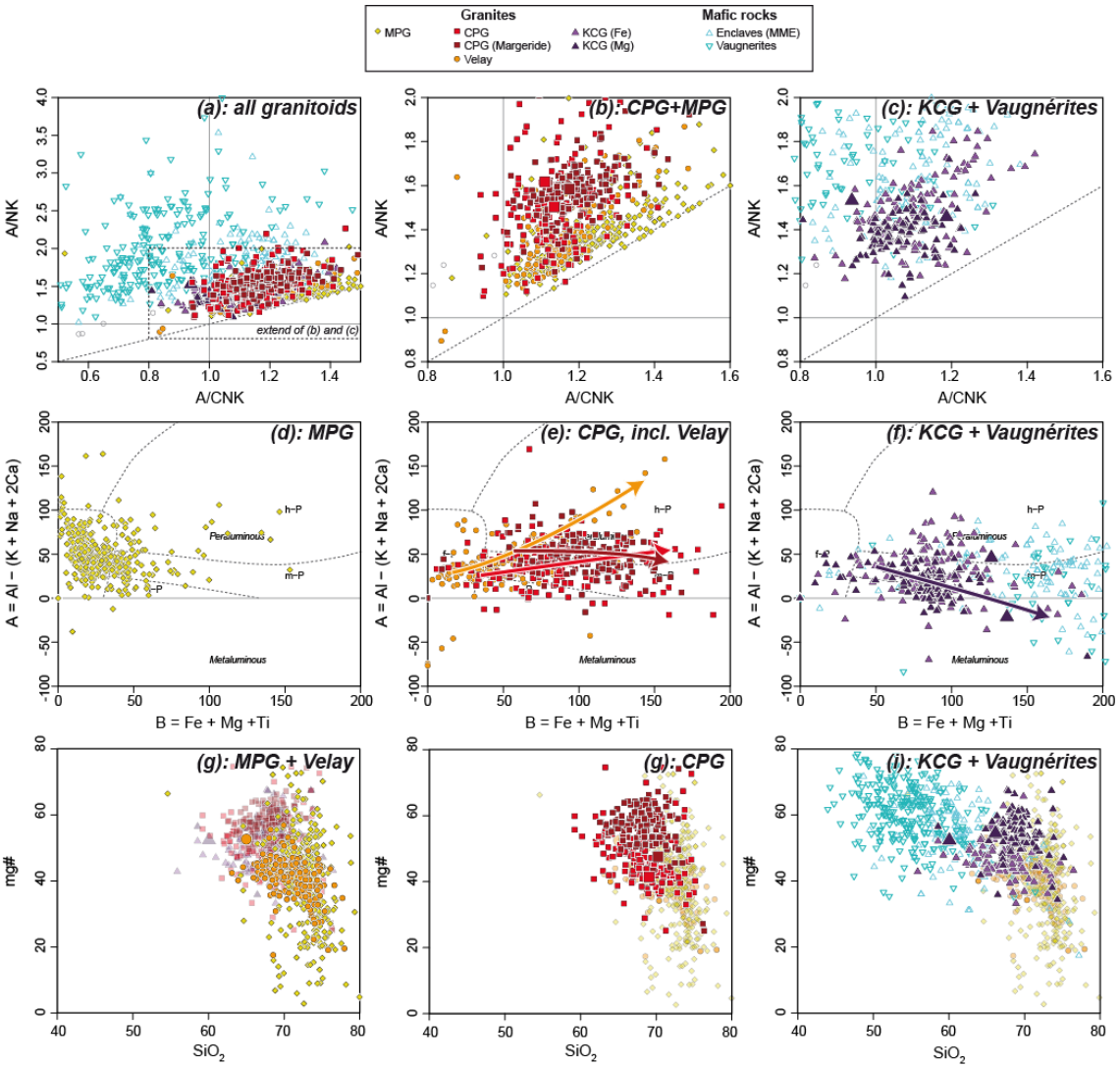

Figure 8 : Major-element geochemistry of granitoids and vaugnérites of the E-FMC, plotted in the A/CNK (molar Al_2O_3 / [$CaO+Na_2O+K_2O$]) vs. A/NK diagram (Shand, 1943) (upper panels); the A–B diagram (Debon and Lefort, 1983) (middle panels); and Mg# (molar MgO/[MgO+FeO]) vs. SiO_2 diagrams (lower panels) (Moyen et al., 2017).

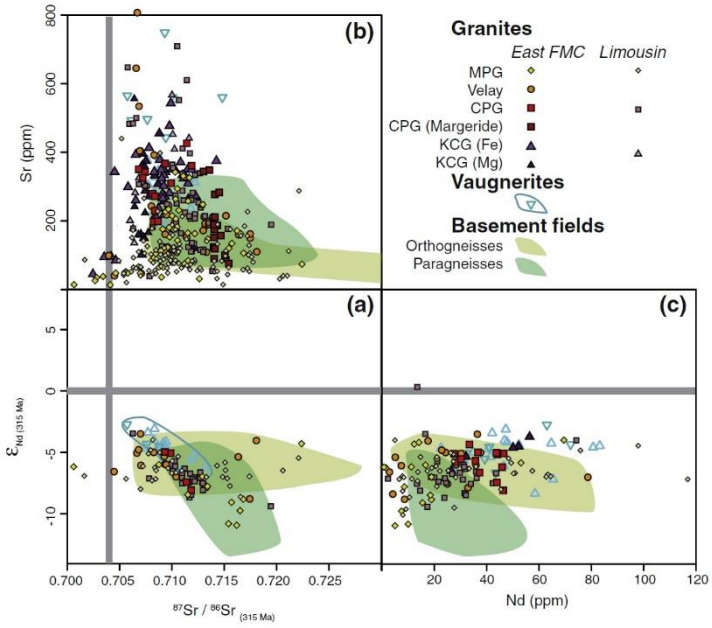

Figure 9 : Bulk-rock Sr-Nd elemental and isotopic composition of the E-FMC granitoids and main crustal lithologies (ortho- and paragneisses) (Moyen et al., 2017).

Altogether, the formation of Carboniferous granitoids in the E-FMC likely resulted from a lithospheric-scale thermal anomaly, likely the removal of the orogenic mantle root and increase of the mantle heat flux through the Moho (Henk et al., 2000; von Raumer et al., 2013a; Laurent et al., 2017, 2023). This triggered widespread lower crustal melting, possible interaction with mantle-derived melts (vaugnérites), extraction of the resulting granitic magmas and their upwards transfer. The emplacement ages of granitoids throughout the E-FMC shows a consistent N–S decrease from ca. 340 Ma in the North to ca. 310-300 Ma in the South (**Figure 10**), taken as evidence for a southward propagation of the thermal anomaly and therefore of lithospheric mantle delamination (Laurent et al., 2017; Vanderhaeghe et al., 2020) (**Figure 11**). Hot, relatively H_2O-poor magmas such as KCG and some CPG rose up to high crustal levels, forming large granitic plutons; whereas cooler, H_2O-rich CPG and MPG ponded in the mid-crust (Villaros et al., 2018; Laurent et al., 2023). There, heat advection and H_2O release upon crystallization would have enhanced partial melting of the middle crust (Barbey et al., 2015; Villaros et al., 2018; Couzinié et al., 2021) and thereby build up a widespread partially molten layer, which laterally spread during late-orogenic extension (**Figure 11**) and was eventually exhumed and crystallized at 310-300 Ma (**Figure 10**) to form the Velay dome (Vanderhaeghe et al., 2020).

The investigated crustal section (**Figure 1**) is the result of all of these processes and allows to examine their expression at different structural levels.

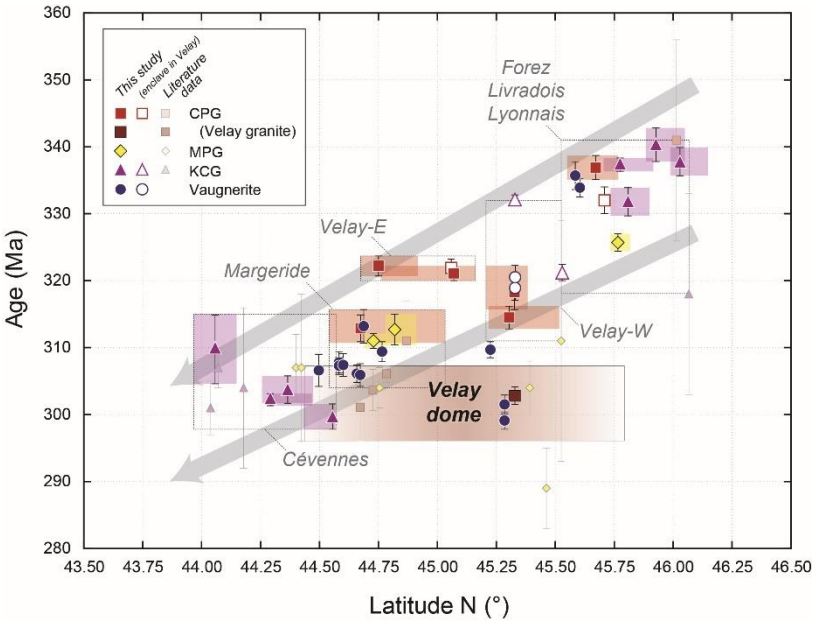

Figure 10 : Zircon and monazite U-Pb crystallization ages of Variscan granitoids in the E-FMC, plotted as a function of latitude (in degrees) and showing the southwards migration of magmatism (modified from Laurent et al., 2017, with addition of new ages obtained since then).

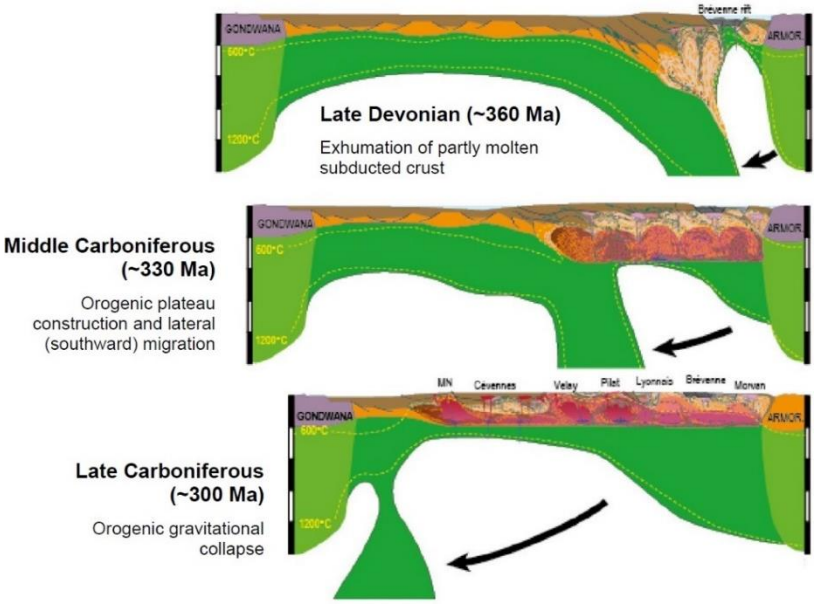

Figure 11 : Schematic South – North cross-section at the lithospheric scale showing a possible geodynamic evolution to explain the late-Variscan geological record of the E-FMC, in particular the abundance of Carboniferous granitoids and the presence of the Velay granite–diatexite dome. Southwards delamination of the lithospheric mantle root is triggered by decoupling with partially molten, subducted continental crust in the late Devonian; and triggers in turn widespread melting in the Carboniferous. Modified from Vanderhaeghe et al. (2020).

Itinerary

Day 1

The Cévennes domain (**Figure 12**) is part of the Parautochtonous Unit (PAU) of the FMC nappe stack and mainly consists of greenschist-facies mica- and quartz-schists, with minor quartzite, calc-silicate- and paragneisses, collectively named the "**Cévennes schists**" (Brouder, 1963; Faure et al., 1999, 2001; Barbey et al., 2015). These are interleaved with several orthogneiss massifs (Peyrolles, Cézarenque–Joyeuse) forming decametre- to (several) kilometre-thick concordant bodies (Brouder, 1963; Weisbrod and Marignac, 1968; Roger, 1969; Couzinié et al., 2022). Ages obtained both on volcano-sedimentary units and on orthogneisses generally point to Cambrian to Ordovician emplacement ages (530-430 Ma) for the whole sequence (Faure et al., 2009a; Couzinié et al., 2021).

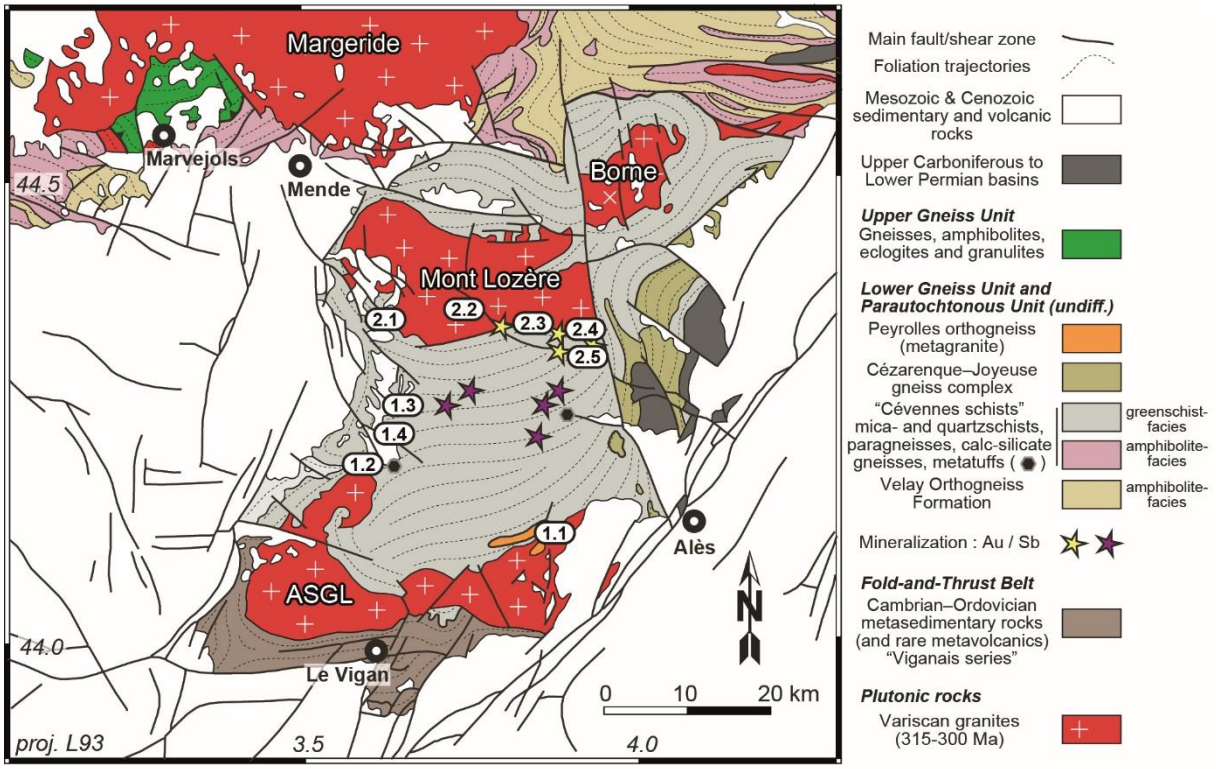

Figure 12 : Geological map of the Cévennes domain (modified after Couzinié et al., 2022), showing the location of the field trip stops for days 1 and 2 (numbered ellipses). ASGL = Aigoual – Saint-Guiral – Liron pluton.

The main tectono-metamorphic phase (corresponding at the scale of the FMC to the D3-M2 event *sensu* Faure et al., 2009b; see **Figure 6**) that affected the Cévennes schists produced a near-horizontal schistosity with a N–S stretching and mineral lineation, associated with top-to-the-S nappe stacking (Toteu and Macaudière, 1984; Faure et al., 2009b). This event took place at 340–330 Ma (Ar-Ar dating of micas and amphibole; Caron, 1994), under greenschist to lower amphibolite facies conditions (up to ca. 500 °C and 5 kbar; Arnaud et al., 2004) with a general southward decrease of metamorphic grade. The Viganais series, located in the southernmost part of the area (**Figure 12**), is a fold-and-thrust belt made of barely metamorphosed Cambrian-Ordovician sediments (Faure et al., 2009a).

The Cévennes schists were intruded by two major plutonic complexes of (dominantly) KCG affinity (**Figure 12**), the ca. 315-305 Ma (Brichau et al., 2008; Werle et al., 2023) **Aigoual–Saint-Guiral–Liron pluton**, thereafter simplified to "**Aigoual pluton**"; and the ca. 305-300 Ma (Brichau et al., 2008; Laurent et al., 2017) Mont Lozère batholith (see day 2). The Aigoual pluton forms a gently N-dipping laccolith (Faure et al., 1999; Talbot et al., 2005) that separates the Cévennes schists from the Viganais domain. The granite typically cuts across pre-existing thrust contacts (Talbot et al., 2005) and is surrounded by a thermal aureole (a few hundred meters, up to a kilometer wide) in the low-grade meta-sedimentary rocks. Thermo-barometric data on hornfels from the aureole indicate shallow emplacement pressures, as low as 1 to 2 kbar (Najoui et al., 2000).

The Aigoual pluton consists of two main lithological types, showing transitional contacts: (i) a dominant, K-feldspar porphyritic granite; and (ii) a so-called “microgranitic” type, i.e. porphyry-like granites and hybrid rocks closely associated with lamprophyres in the NW part of the pluton (**Figure 13**). The pluton, which suffered very little sub-solidus deformation, has been the topic of a detailed AMS study (Talbot et al., 2004). The rocks display variable magnetic fabrics, corresponding to an interplay between magma emplacement dynamics and regional deformation during crystallization. The general NW-SE to E-W trending magnetic lineation is consistent with the direction of a regional extensional event that was synchronous with magma emplacement (**Figure 13**) and post-dated the major episode of N–S directed nappe stacking in the Cévennes schists (Faure et al., 2009a); while local NNE-SSW directions in the northern and western parts of the pluton relate to local magma flow in dykes (see stop 1.2). The magnetic foliation defines a broad dome in the southwestern part of the pluton (**Figure 13**) interpreted as reflecting inflation of the magma reservoir above a possible feeder zone (Talbot et al., 2005).

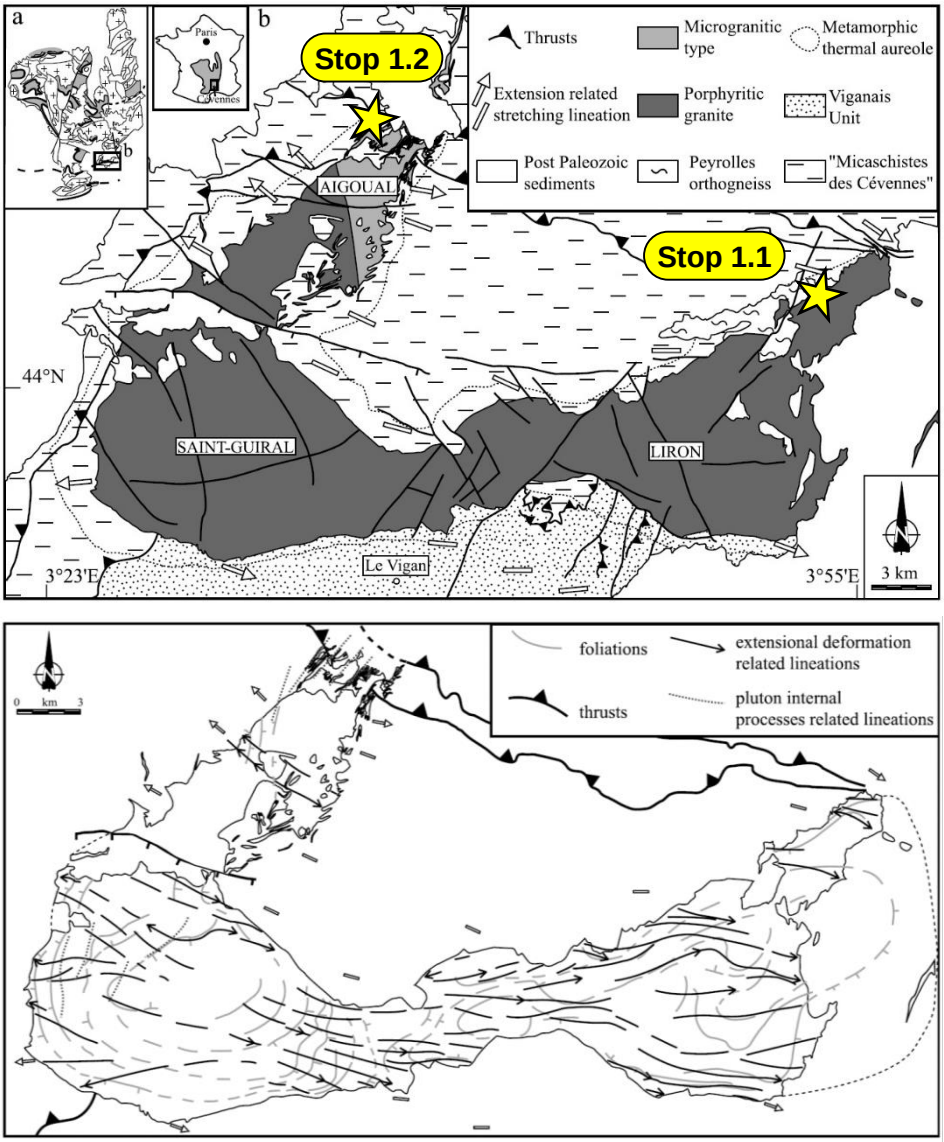

Figure 13 : Top: sketch structural and geological map of the Aigoual pluton and country rocks, showing the location of the first two stops of the day; and bottom: map of magnetic fabrics in the Aigoual pluton as determined by AMS. Both figures are from Talbot et al. (2005).

The aims of the day are to investigate the magma chamber dynamics in the Aigoual pluton, notably discuss the processes leading to the construction of such a shallow laccolith and the extraction and transfer of magmas potentially linking the reservoir with silicic eruptions. The origin of KCG magmas will also be a key point of discussion: do they form through melting of lower crustal (mafic?) rocks, interactions between crustal and mantle melts, or direct differentiation of the latter?

Stop 1.1 – Porphyritic Aigoual granite, megacrysts and mafic enclaves

Coordinates: Lat. 44°6'42.8" N; Long. 3°51'36.1'' E

Location: Gardon de Saint-Jean river bed, ca. 2 km West of Saint-Jean-du-Gard close to the D907/D260 crossroads

This outcrop is located at the northeastern tip of the Aigoual pluton, at the contact with the country rock. The pluton is structurally located below the country rocks, which form the surrounding topography; and given the generally northward dipping attitude of the intrusion (Faure et al., 1999; Talbot et al., 2005), this outcrop is possibly located in the former reservoir roof. There, it is intrusive in the Peyroles orthogneiss (a large xenolith thereof is exposed on the southernmost part of the outcrop), one of the meta-igneous units interlayered with the "Cévennes schists". The granitic protolith of the orthogneiss crystallized at 433 ± 4 Ma as dated by U-Pb on zircon by LA-ICP-MS (Faure et al., 2009a). There, the granite has been dated (**Figure 14**) at 308.1 ± 2.8 Ma by Ar-Ar on biotite ; 307 ± 3 Ma by TIMS U-Pb on zircon (Brichau et al., 2008) and 313.0 ± 3.2 Ma by LA-ICP-MS U-Pb on zircon (Werle et al., 2023).

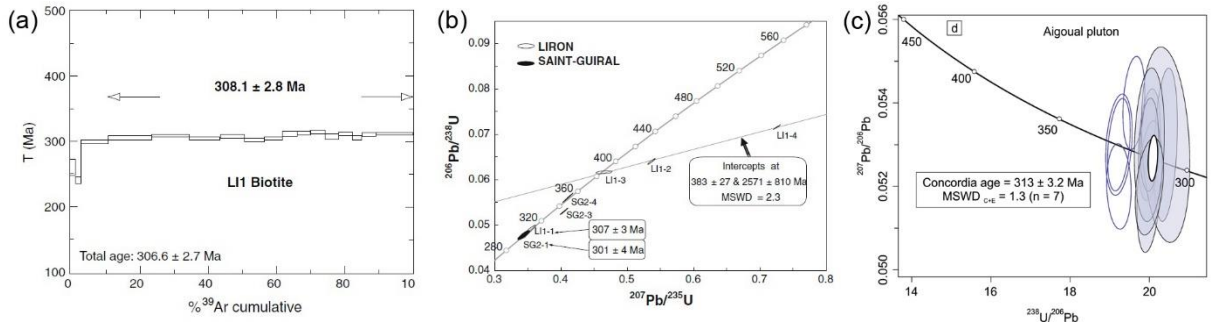

Figure 14 : Summary of age data obtained on the Aigoual (Liron) granite at the Saint-Jean-du-Gard outcrop. (a) Ar-Ar data on biotite and (b) U-Pb (TIMS) on zircon from Brichau et al. (2008); (c) U-Pb (LA-ICP-MS) on zircon from Werle et al. (2023).

The main petrographic type of the Aigoual pluton is a typical KCG: it consists of biotite- and locally amphibole-bearing, K-feldspar porphyritic granite, rich in rounded, fine-grained mafic enclaves (a few cm to a few dm size) and some elongated xenoliths of the country rocks (schists and paragneisses mainly). At stop 1.1, it is a rather silica-poor (66.2 wt.% SiO_2) granodiorite (Brichau et al., 2008).The main mafic mineral is biotite, both in the granodiorite and in the associated mafic enclaves (**Figure 15**).

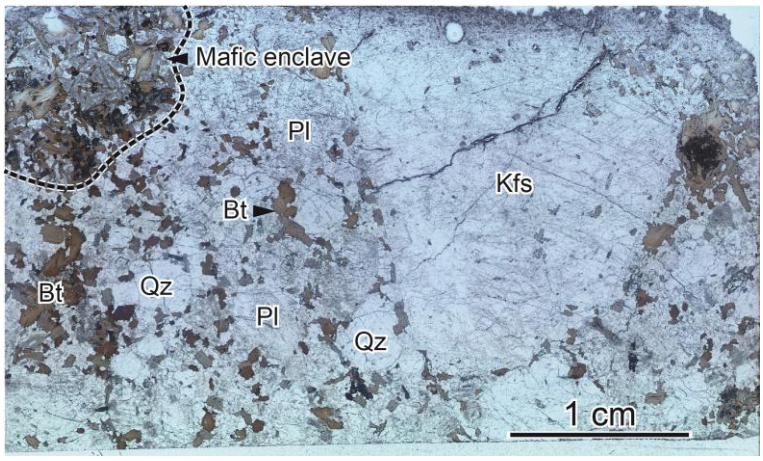

Figure 15 : Thin section scan of a sample of granodiorite from stop 1.1 (sample from H. Fest), containing a large K-feldspar phenocryst and part of mafic enclave. Note the texture of biotite grains clustering in-between quartz and feldspar phenocrysts.

The rock shows spectacular variations in terms of grain size, mineral proportions (in particular in the case of K-feldspar megacrysts), and other structures (**Figure 16**). Local K-feldspar accumulations defining cumulate-like structures with interstitial domains that consist of relatively dark, mafic granite. The granite may be locally very rich in mafic enclaves, forming clusters ("enclave graveyards") several meters across. The magma chamber and/or crystallization dynamics able to produce such structures are quite elusive, although the texture on the thin section scale (**Figure 15**) may suggest infiltration of a relatively potassic mafic magma (biotite-rich, similar to the lamprophyres of stop 1.2) in a granitic mush.

Figure 16 : Some examples of the accumulation of K-feldspar megacrysts and mafic enclaves, and relationships between both, that can be observed at stop 1.1.

Stop 1.2 – Composite granite – lamprophyre dyke

Coordinates: Lat. 44°12'04.8" N; Long. 3°35'23.7'' E

Location: Along the D119 road ca. 0.5 km South of Rousses.

The northern termination of the Aigoual pluton grades into a NE–SW to NNE–SSW trending dyke swarm (**Figure 17**), extending far North into the Cévennes schists (>10 km away from the pluton margin, see stop 1.3). AMS studies revealed magnetic fabrics consistent with the orientation and dip of the dykes, interpreted as reflecting magma flow in the conduits (Talbot et al., 2005) (**Figure 17**). The dykes are typically 100–1500 m long and a few tens of meters wide. LA-ICP-MS zircon U-Pb dating of both the dykes and the nearby main body of the Aigoual pluton (**Figure 18**) yielded the same ages of 313–311 (± 3) Ma (Werle et al., 2023).

Most of the north Aigoual dykes are composite and display a lamprophyre margin grading to a granitic core. The granite is a porphyry containing quartz, feldspar, biotite and rare clinopyroxene phenocrysts in fine-grained matrix (**Figure 19**a–c).

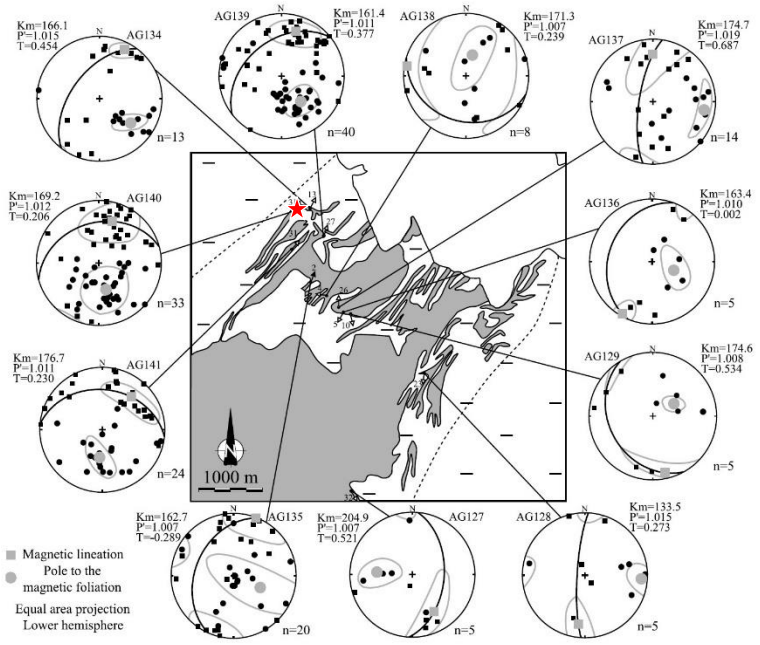

Figure 17 : Simplified geological map of the northwestern termination of the Aigoual pluton (granite/dykes in grey; Cévennes schists in dashed white) showing the dyke swarm and AMS results on several localities (Talbot et al., 2005). The red star corresponds to stop 1.2.

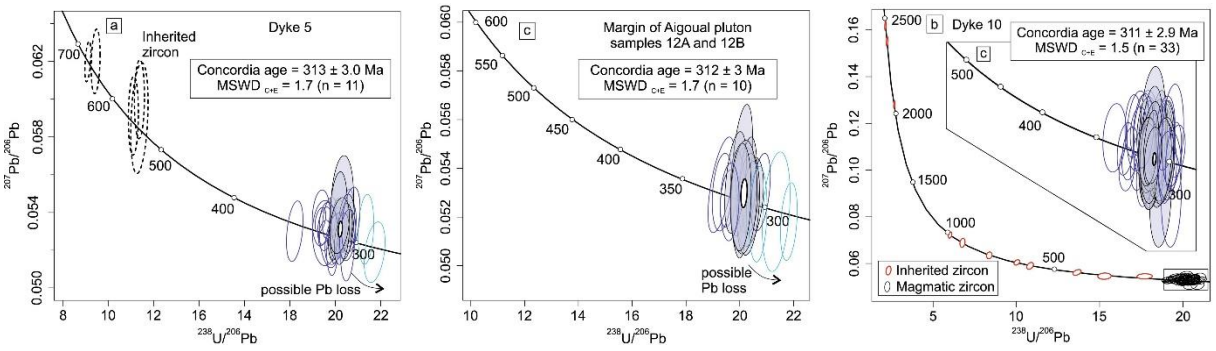

Figure 18 : LA-ICP-MS zircon U-Pb dating on the northwestern Aigoual dykes and main granite (Werle et al., 2023).

The lamprophyres also show a porphyritic texture with mainly biotite-phlogopite, plagioclase and rare amphibole phenocrysts in a very fined-grained matrix containing K-feldspar, plagioclase and quartz (**Figure 19**d–f). One petrographic characteristic of the lamprophyres is the presence of carbonate, in the form of ocelli or as interstitial phases between silicates (Werle et al., 2023) (**Figure 19**e,f). Pseudomorphs after olivine were also identified (Sabourdy, 1975). This, together with the high Mg# of some phlogopite phenocrysts (up to 0.75), supports an origin for lamprophyres through direct mantle melting (Werle et al., 2023).

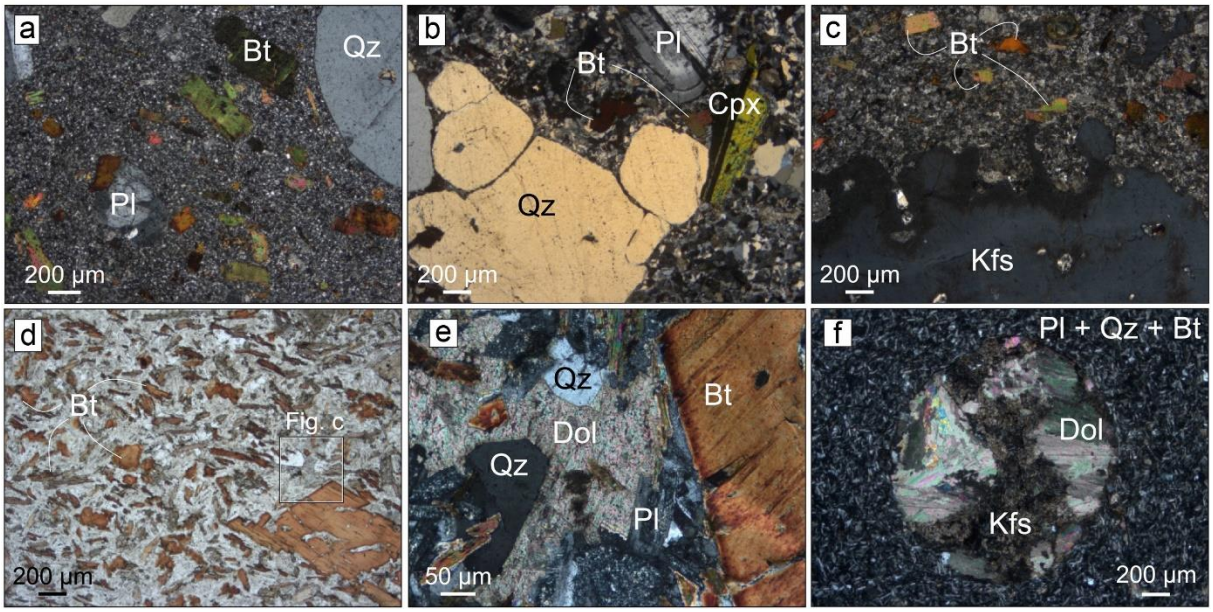

Figure 19 : Thin section photomicrographs of the hybrid porphyry granite (a–c) and lamprophyre (d–e) forming the composite dykes as exposed at stop 1.2 (modified from Werle et al., 2023). (e) and (f) show details of the texture of carbonate (mainly dolomite) in the lamprophyre.

The dyke exposed at stop 1.2 is one of the outermost dykes of the swarm (**Figure 17**). It dips gently (30° to 40°) to the NNW (**Figure 20**), in agreement with magnetic fabrics obtained by AMS at this locality. The (sharp) contact between the Cévennes schists and the marginal lamprophyre facies, containing few, large K-feldspar phenocrysts, is well exposed in the river bed, accessible by walking down the pathway starting from the road.

Figure 20 : Aerial oblique (merged drone) view of the dyke at stop 1.2 (J.F. Moyen, unpub. data), looking West and showing the generally north-dipping attitude of the dyke. The dashed line depicts the approximate position of the contact between the dyke and the Cévennes schists; and the yellow ellipse points to vehicles for scale.

The roadside outcrop illustrates well the progressive nature of the transition from the lamprophyre margin to the granite core (**Figure 21**). Petrographically, the transition mainly corresponds to an increase in the size and abundance of phenocrysts (most strikingly of K-feldspar), which tend to become less rounded and more euhedral; and the disappearance of amphibole and appearance of quartz (Sabourdy, 1975; Werle et al., 2023). The latter occasionally shows ocellar textures in the intermediate zone between lamprophyre ad granite. Chemically, bulk-rock compositions show consistent variations along transects perpendicular to the dyke walls, with SiO_2 typically increasing from 55-60 wt.% at the rim to 70-75 wt.% in the core and MgO, FeO_t, CaO, P_2O_5 decreasing concomitantly (**Figure 21**).

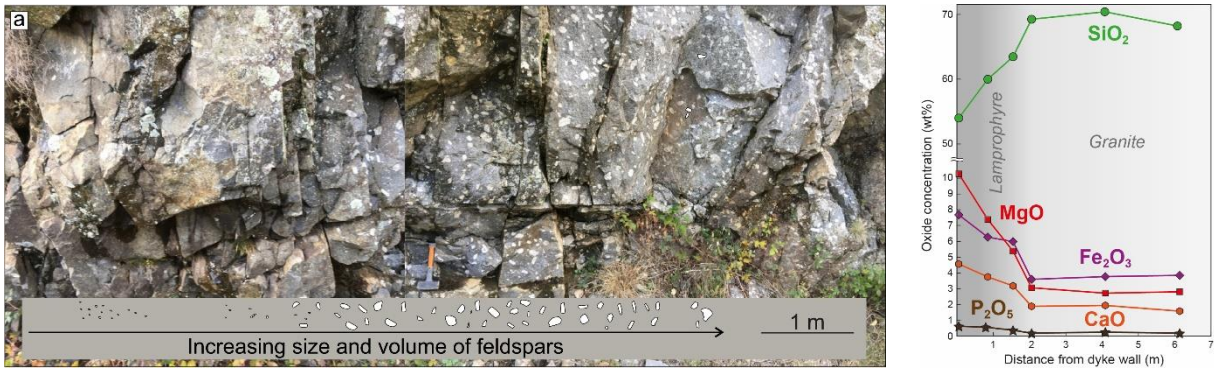

Figure 21 : Transition between lamprophyre and granite in the dyke at stop 1.2, in terms of textural (left, Werle et al., 2023) and bulk-rock compositional (right, modified from Sabourdy, 1975) variations.

Nevertheless, taken together, lamprophyres and granites tend to define well-separated compositional fields, rather than continuous mixing trends, for major and trace elements (**Figure 22**) as well as radiogenic (Sr, Nd) and stable (O) isotopes (Werle et al., 2023). Interestingly, the composition of the main, porphyritic type of the Aigoual granite is systematically intermediate between those of lamprophyre and granite end-members (**Figure 22**).

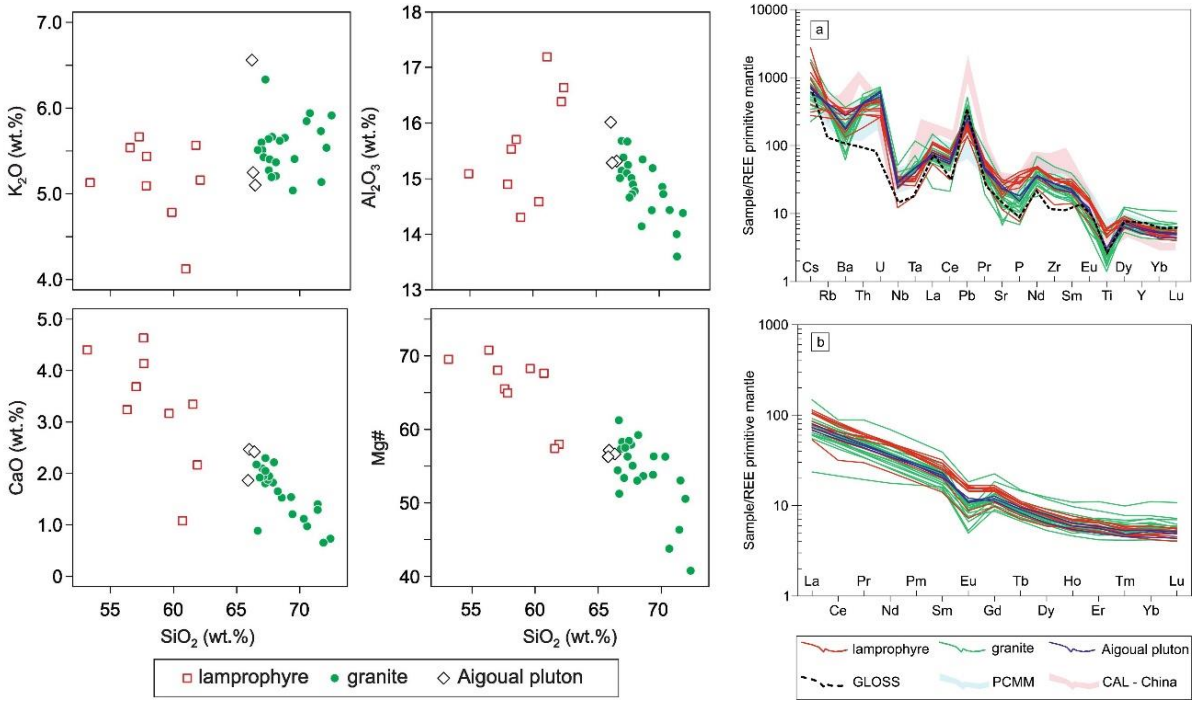

Figure 22 : Selected Harker plots and trace element spidergrams (concentrations normalized to Primitive Mantle values of McDonough and Sun, 1995) illustrating the compositional range between lamprophyres, granites in the dykes and the main body of the Aigoual pluton (Werle et al., 2023).

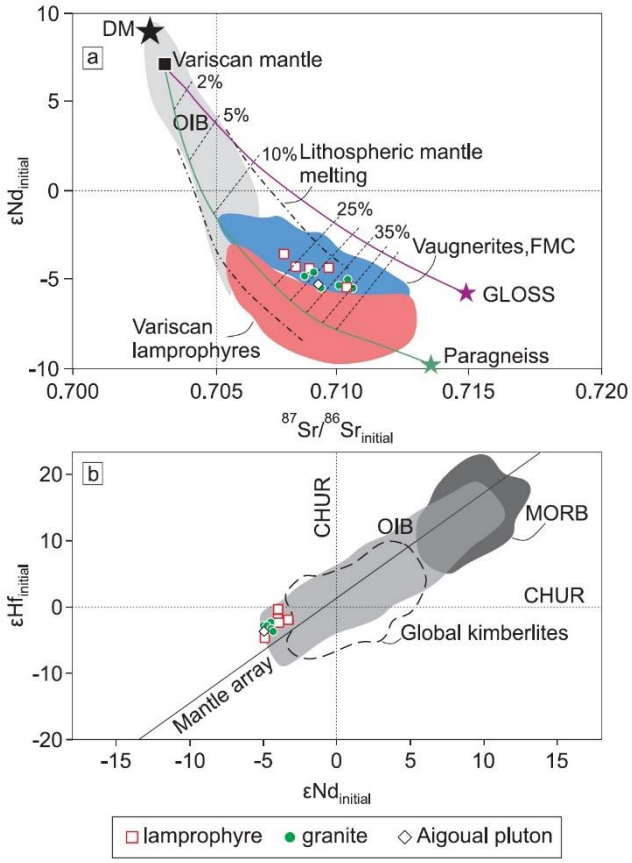

In terms of radiogenic isotopes, bulk-rock Sr–Nd and zircon Hf isotopic compositions clearly show a dominant influence of a crustal source for both lamprophyres and granites (**Figure 23**). In the case of lamprophyres, this can be reconciled with their generally low SiO_2, high Mg# and Ni-Cr contents by a genetic mechanism through partial melting of an enriched, lithospheric mantle source, metasomatized prior to melting by components derived from subduction of rocks similar to those of the local continental crust (**Figure 23**). A similar mechanism has been proposed to explain the origin of "vaugnérites" (Couzinié et al., 2016), of which the lamprophyres would thus be relatively shallow equivalents.

Figure 23 : (a) Bulk-rock Nd vs. Sr isotopic compositions and (b) zircon Hf vs. bulk-rock Nd isotopic compositions for the Aigoual dykes (lamprophyre and granite) and main pluton, compared to the isotopic compositions of vaugnérites, Variscan lamprophyres and other mantle-derived rocks (Werle et al., 2023). The curves in (a) represent mixing trends between a Variscan mantle source and different crustal components (Global Subducting Sediment – GLOSS; and a E-FMC paragneiss).

Stop 1.3 – A sub-volcanic offshoot of the Aigoual pluton: the Barre dyke

Coordinates: Lat. 44°13'45.5" N; Long. 3°39'35.7'' E

Location: Along the D983 road ca. 2 km South of Barre-des-Cévennes.

The northern part of the Aigoual dyke swarm is concealed under Mesozoic sediments of the Can de l'Hospitalet plateau. On the other side of the plateau, however, a N-S trending granite porphyry dyke (and minor satellite intrusions) intrudes the Cévennes schists (**Figure 24**), referred here to as the Barre dyke. It shows the same mineralogical assemblage (quartz, K-feldspar, plagioclase, biotite with minor amphibole) and comparable texures as some of the lithologies in the main dyke swarm. This, together with the situation and general orientation of the Barre dyke, suggests that it represents an offshoot that extends the main swarm up to ca. 10 km north of the Aigoual pluton.

The study of several localities along the Barre dyke reveals consistent textural variations along strike (**Figure 24**). At stop 1.3, which is in a small satellite intrusion approximately halfway to the northernmost tip of the dyke, the rock has a crystal-rich porphyry texture defined by abundant (>60 vol.%), pluri-millimetric phenocrysts of altered plagioclase with subordinate quartz, biotite and K-feldspar (the latter occasionally reaching a few centimeters in size) in a fine-grained matrix. The rock also contains rounded, fine-grained mafic enclaves. About 5 km North, close to the termination of the dyke, the rock is mineralogically similar but shows much less phenocrysts (<25 vol.%) and an even finer-grained groundmass. A comparable, crystal-poor lithofacies can be observed at the margin of the intrusion at stop 1.3 (about 50-100 m North of the main outcrop along the road), closer to the contact with the Cévennes schists.

These textural variations may indicate a transition from deeper to shallower emplacement conditions from South to North, consistent with the general north-dipping attitude of the Aigoual pluton. If the pluton emplaced at ca. 6 km depth (~2 kbar) and was tilted 25° to 30° to the North, the northernmost termination of the 10 km-long Barre dyke would correspond to paleo-depths of 0.2 to 1.3 km. This near-volcanic environment agrees with the rock textures and in particular the presence of globular and embayed quartz containing melt and hourglass inclusions (**Figure 24**), which are typical features observed in rhyolites.

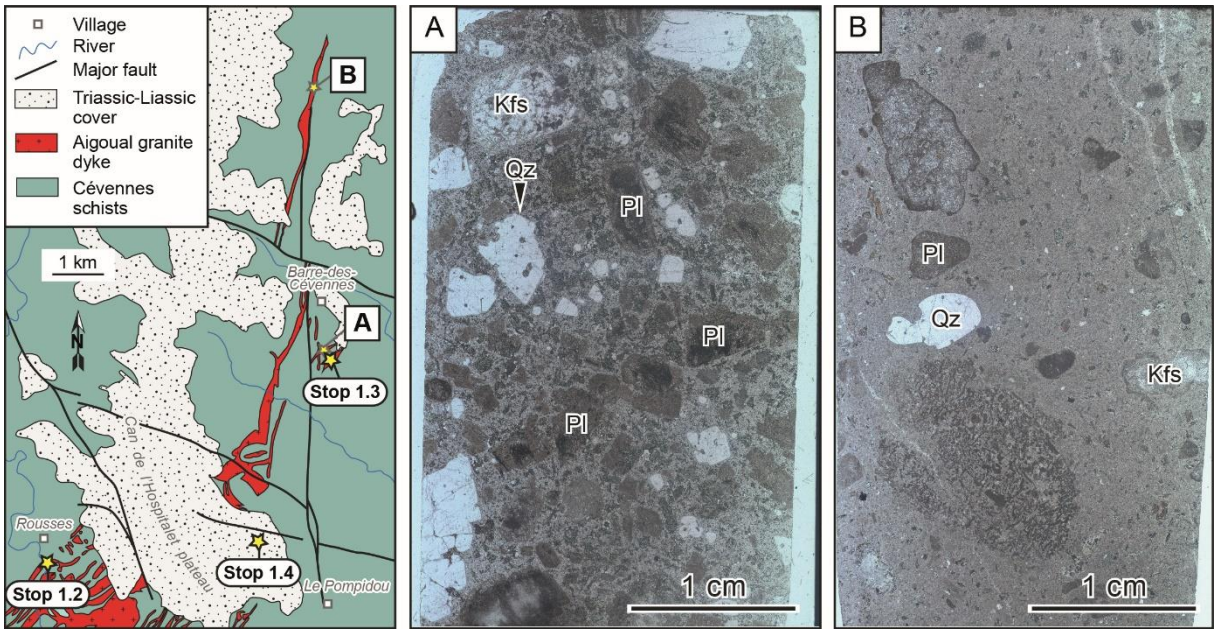

Figure 24 : Sketch geological map of the Barre dyke (left) showing the positions of stops 1.2 to 1.4 and sampling localities for the two samples for which thin section scans are shown in (A) and (B) (samples from H. Fest). Mineral abbreviations: Kfs = K-feldspar; Pl = plagioclase (altered); Qz = quartz.

Stop 1.4 – Panoramic view on the Barre dyke and Aigoual pluton

Coordinates: Lat. 44°12'14.0" N; Long. 3°38'24.5'' E

Location: Southeastern edge of the Can de l'Hospitalet plateau, off the D9 road ca. 1.5 km NW of Le Pompidou.

This viewpoint sits on lower Jurassic sedimentary rocks of the Can de l'Hospitalet plateau (**Figure 24**) and allows to clearly picture the 3D geometry of the Aigoual pluton and associated Barre dyke. The dyke can be easily spotted in the landscape facing North (**Figure 25**), whereas the high and gently dipping plateau to the SW corresponds to the pluton. Note the slight ESE dip of the dyke and the presence of satellite intrusions on the eastern flank of the valley, which correspond to the outcrops visited earlier at stop 1.3.

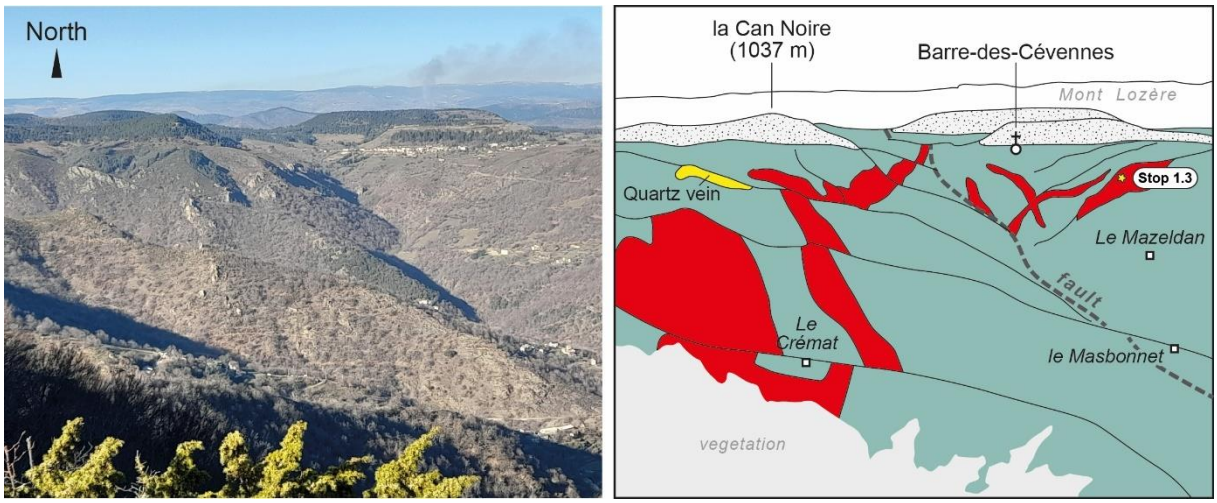

Figure 25 : Panoramic view towards the North at stop 1.4 and geological interpretation of the landscape (right), using the same color scheme as the map of **Figure 24**.

Day 2

The Mont Lozère batholith represents the second major granitic intrusion of the Cévennes domain (**Figure 12**) and forms the eponym mountain (1699 m). It consists of several plutons (**Figure 26**), which emplaced as laccoliths, no thicker than a few kilometers and in a sub-horizontal position, or dipping slightly to the North as shown by geophysical data (Talbot et al., 2004) (**Figure 27**). In contrast to the Aigoual pluton, these different plutons were attributed to different petrological types:

- The **Pont de Montvert pluton** consists of biotite- and locally amphibole-bearing K-feldspar porphyritic granites and granodiorites of KCG affinity, dated by various methods at ca. 305–302 Ma (Brichau et al., 2008; François, 2009; Laurent et al., 2017).
- The **Signaux pluton** is more strongly peraluminous, with three distinct facies: the **Bougès** and **Finiels** two-mica granites (MPG), dated respectively at 304 ± 3 Ma (LA-ICP-MS U-Pb on zircon; unpublished data) and 303 ± 3 Ma (TIMS U-Pb on zircon; Brichau et al., 2008); and the **Laubies** biotite + cordierite granite (CPG), associated with vaugnérites dated at 305.7 ± 3.2 Ma (LA-ICP-MS U-Pb on zircon; unpublished data).

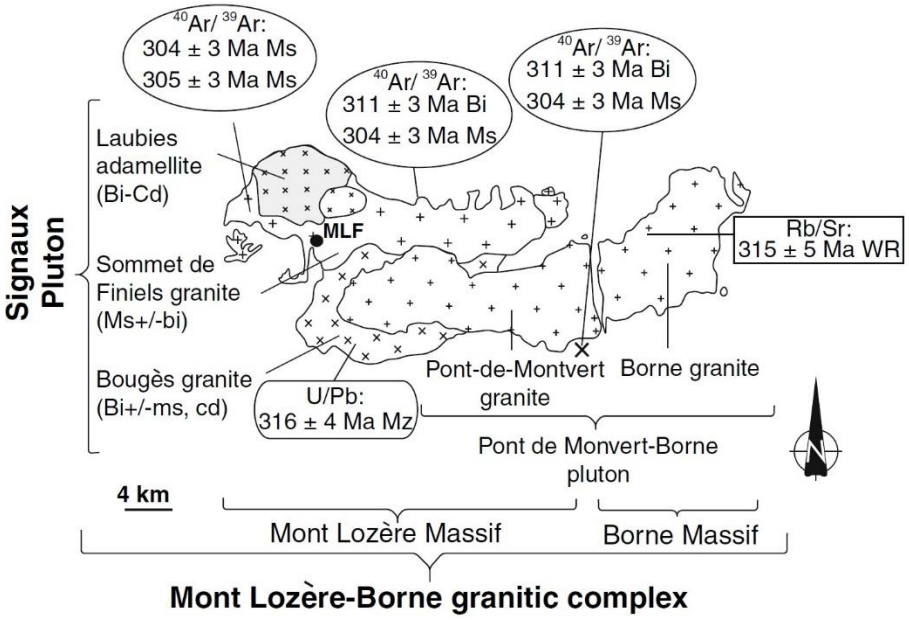

Figure 26 : Sketch map of the Mont Lozère batholith and summary of age constraints (Brichau et al., 2008).

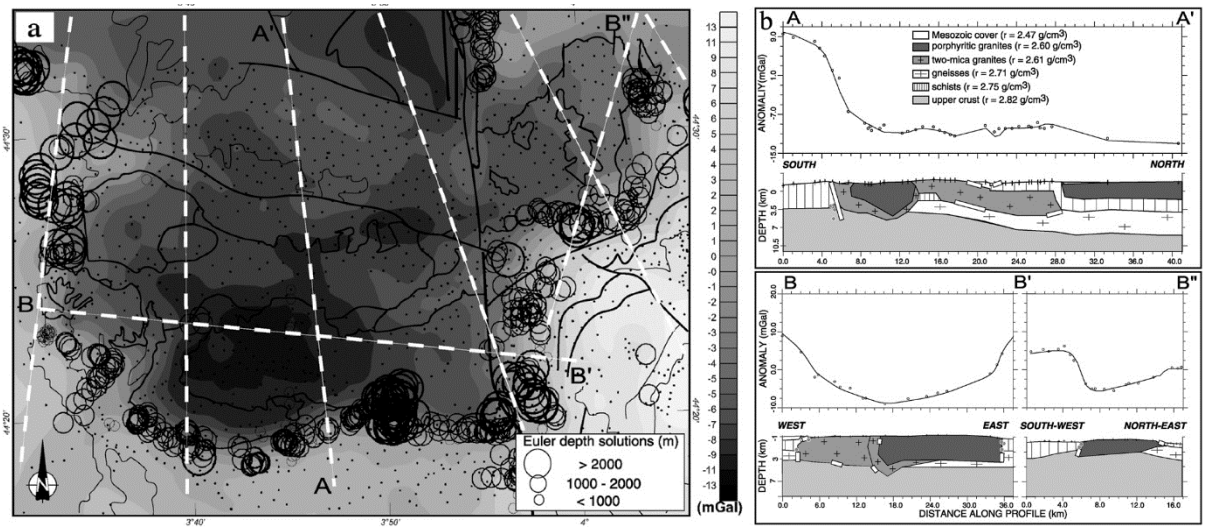

Figure 27 : Gravity data on the Mont Lozère batholith (Talbot et al., 2004). (a) Map of the residual Bouguer anomaly; black dots are the position of gravity stations, black lines correspond to the main geological limits, dashed white lines are profiles used for modelling and black circles show the location of Euler sources, with sizes proportional to their depth. (b) Direct 2D gravity modelling along A–A′ and B–B′–B″ cross-sections shown in (a).

On the map scale, the boundaries of the Pont-de-Montvert pluton cross-cut the internal contacts of the Signaux pluton (**Figure 26**) such that the former should be younger than the latter. However, geochronological data mentioned above show that the crystallization ages of the two plutons are undistinguishable within uncertainties (in the range 306–302 Ma); and the contact between them is very poorly exposed in the field. Where observable, this contact is rather transitional, for instance with a general increase of the abundance and size of K-feldspar megacrysts from the Bougès to the Pont-de-Montvert facies. In addition, the Bougès and Finiels facies are petrographically quite different from typical MPG, and the Bougès granite contains in fact relatively little, if any muscovite. Therefore, the different granite subtypes of the Mont Lozère batholith may correspond to distinct, yet genetically linked petrographic types within a single (KCG?) pluton.

The emplacement of the Mont-Lozère complex and the coeval, youngest extensional deformation event of the Cévennes domain, were accompanied by important hydrothermal activity associated with gold (± antimony) deposits. They belong to the regionally widespread event known as "*Or 300*" (Bouchot et al., 1997; Chauvet et al., 2012), a regional gold-forming period observed in all of the French Variscan outcrops. Evidence for hydrothermal activity and mineralization are concentrated along the southeastern margin of the Pont-de-Montvert pluton and extend away from it in the Cévennes schists along "mineralized corridors" (Faure et al., 2009a) (see map of **Figure 12**). Structural evidence indicates that fluid flow and mineralization happened synchronously to the regional extensional event that post-dates nappe stacking in the Cévennes schists (Charonnat et al., 1999; Chauvet et al., 2012).

Hydrothermal activity in the Cévennes area is characterized by **two, successive mineralizing systems**: a first **B–W–Sn event** and a subsequent **Au–As–Sb event** (see stop 2.4), both possibly related to the same source (Chauvet et al., 2012). The association of hydrothermal events with granitic intrusions (aplites, pegmatites), the concentration of alteration assemblages in the thermal aureole of the plutons and the structural context of the mineralized rocks clearly indicate a temporal and genetic link between these hydrothermal and ore-forming events, and the emplacement of the Mont Lozère batholith (Charonnat et al., 1999; Faure et al., 2001). This has been confirmed by direct Ar-Ar dating (**Figure 29**): in aplites/pegmatites, micas all yielded ages in the range 306–301 Ma, which, in addition to be in excellent agreement with crystallization ages obtained for the Mont Lozère batholith (see above), overlap those of micas from hydrothermal veins (Monié et al., 2000; Chauvet et al., 2012).

The aims of the day are primarily to discuss how the magmatic-hydrothermal transition is recorded in shallow granitic plutons and the nature of processes leading to the formation of ore (gold ± antimony) deposits associated with these intrusions. The investigated outcrops will also lead us to discuss the geometry of these plutons; the relationship between the regional stress field and magma emplacement / hydrothermal activity; and the origin of composite granitic complexes like the Mont Lozère batholith.

Stop 2.1 – The magmatic-hydrothermal transition in the Bougès facies

Coordinates: Lat. 44°21'5.8" N; Long. 3°37'51.1" E

Location: Bed of the Tarn river ca. 1 km East of Cocurès, access by a path starting from D998 road.

The Bougès granite, dated by LA-ICP-MS U-Pb on zircon at 304.0 ± 3.0 Ma (unpublished data) (**Figure 28**), is defined as a MPG based on the presence of biotite and muscovite, but muscovite is in fact practically absent (**Figure 30**). The rock exhibits a peculiar texture, characterized by the presence of euhedral quartz phenocrysts and locally of granophyric affinity. This, together with various petrological and structural characteristics exposed at stop 2.1 (**Figure 31**), collectively suggest that the Bougès facies represents a rather undercooled granite emplaced at shallow pressure (likely ≤2 kbar), at or near conditions of magmatic volatile phase saturation.

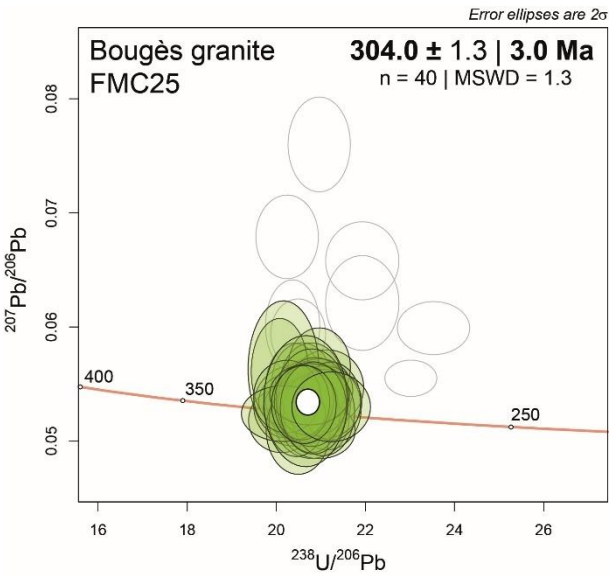

Figure 28 : Tera-Wasserburg diagram showing the results of LA-ICP-MS zircon U-Pb dating on a sample from the Bougès granite collected near stop 2.1 (O. Laurent & V. Janoušek; unpub. data).

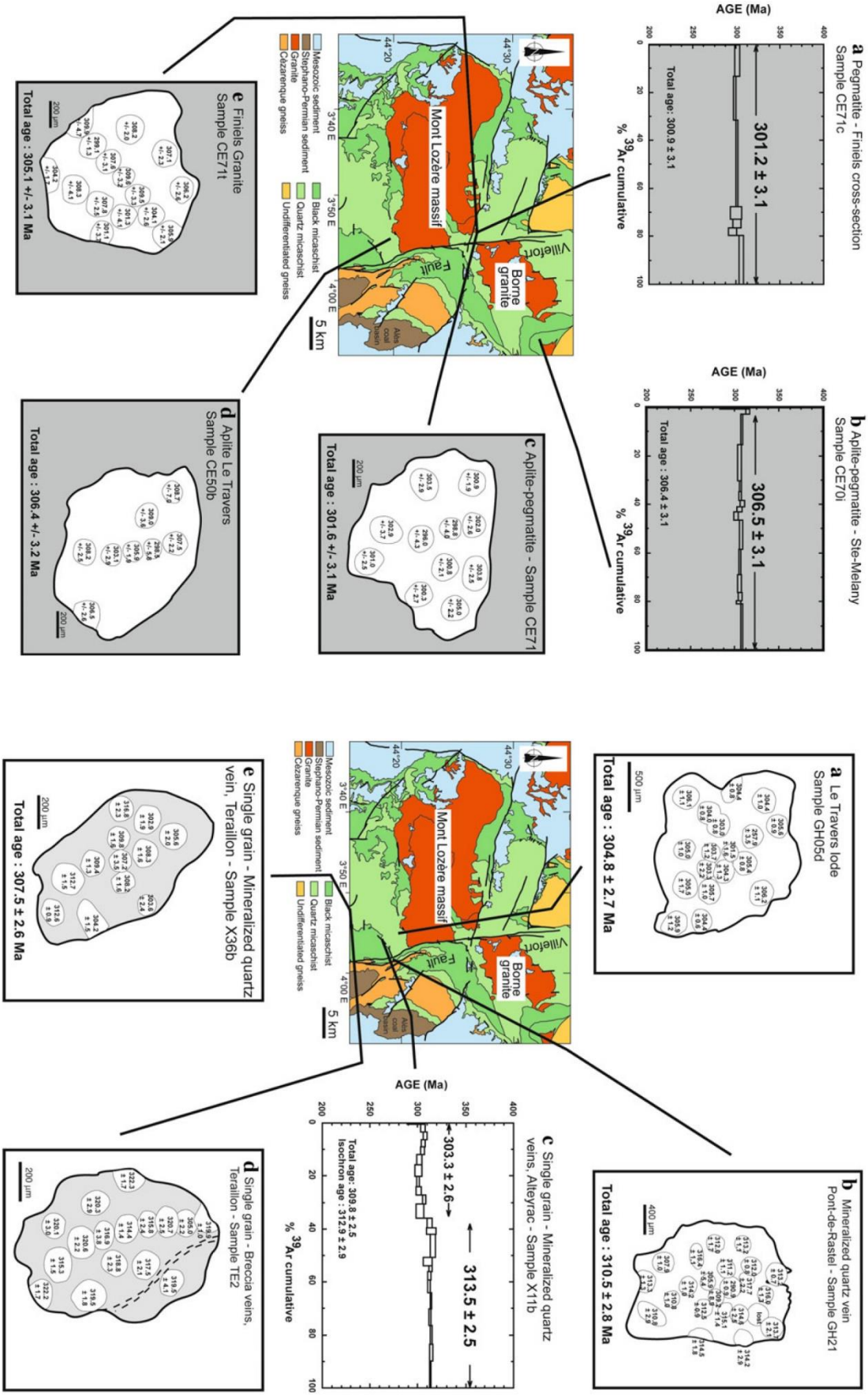

Figure 29 : Results of Ar-Ar dating on muscovite from aplite/pegmatite (bottom) and hydrothermal veins (top) associated with Au (± Sb) mineralization around the Mont Lozère batholith (Chauvet et al., 2012).

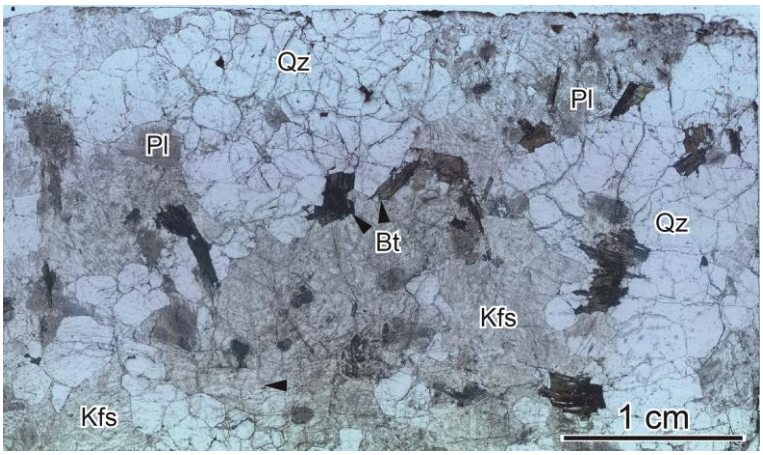

Figure 30 : Thin section scan of a sample of the Bougès granite at stop 2.1 (sample from H. Fest). Note the absence of muscovite and the aggregates made of euhedral quartz phenocrysts.

At the bottom of the path from the road, the contact between the Bougès granite and the Cévennes schists is exposed. There, the granite develops a thin border facies made of pegmatitic granite with crystals growing from the contact inwards (stockscheider) and aplitic granite (**Figure 31**b). Walking southwards (i.e. downstream) on the riverbed outcrop, one first encounters very fine-grained aplitic dykes and bodies. Those are characterized by irregular shapes and show digitated contact with the main granite (**Figure 31**c), suggesting a co-magmatic character. The aplites may thereby represent late-stage, volatile-rich residual melts expelled from the surrounding granitic mush.

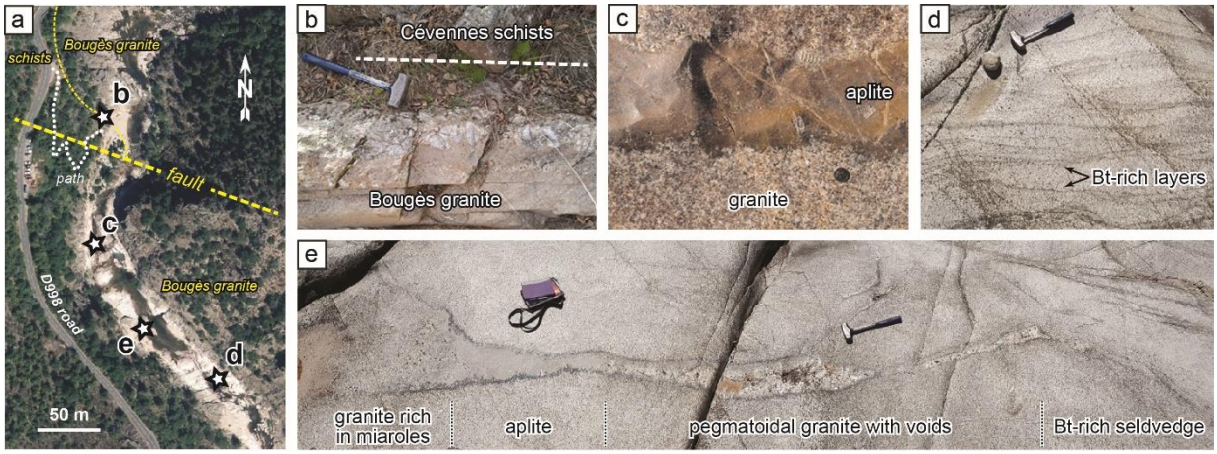

Figure 31 : (a) Aerial photograph of the site of stop 2.1 along the Tarn river, with location of main geological features and points of interest shown in b – e. (b) Stockscheider-like border facies of the Bougès granite at the contact with the Cévennes schists; (c) aplite dyke showing digitated contacts with the granite; (d) parallel biotite-rich layers in the granite; (e) granite body containing miarolitic cavities, grading into an aplitic/pegmatitic dyke.

Further downstream, a large pavement exposes a spectacular, funnel-shape body of granite which grades into an aplitic, then pegmatoidal granite dyke (**Figure 31**e). At the transition between the two structures, centimetric miarolitic cavities are developed in the granite, with inner surface covered by minute euhedral quartz. The whole structure of the dyke suggests that it may represent a former volatile-rich magma/fluid escape path, which fossilized volatile saturation of the granitic melt (miaroles; and at the transition from aplitic to pegmatitic granite in the dyke?). The location of miaroles at a bottleneck within the granite body may record either “boiling” of the magma through a sudden release of pressure when the dyke was opened, or a physical accumulation of bubbles trapped when the dyke was clogged.

Interestingly, the walls of the funnel-shape granite body, and the pegmatoidal dyke that extends it, are delineated by biotite-rich selvedges (**Figure 31**e). The selvedges can be traced as linear structures in the granite along strike of the closed dyke. This raises the question of the significance of mineral layering in granites, in particular the presence of biotite-rich layers – a set of such closely spaced, parallel layers is exposed further downstream on the outcrop (**Figure 31**d). Rather than accumulation of minerals through gravity- or flow-related processes in the magma, these may therefore represent “scars” after the closure of former volatile-rich magma conduits.

Stop 2.2 – the Pont-de-Montvert porphyritic granite

Coordinates: Lat. 44°21'47.6" N; Long. 3°44'53.9" E

Location: Bed of the Tarn river at the Eastern end of Pont-de-Montvert village, access by easy stairs.

The Pont-de-Montvert granite is a typical KCG (K-feldspar porphyritic, biotite- ± amphibole-bearing granite/granodiorite), forming an E–W trending body along the southern edge of the Mont Lozère batholith (see **Figure 26**). Magnetic fabrics suggest that this elongated shape results from magma emplacement above a feeder zone located on the western part of the pluton and eastward spreading in the same regional E–W extensional setting as the Aigoual pluton (Talbot et al., 2004) (**Figure 32**).

To the NE, the Borne pluton (see **Figure 26**) is traditionally regarded as the eastern extension of the Pont-de-Montvert pluton, offset towards the North by the strike-slip Villefort fault. This interpretation is supported by the continuity of magnetic fabrics defined by AMS between the Pont-de-Montvert and Borne plutons when restoring the latter in its purported original position (Talbot et al., 2004) (**Figure 32**). However, crystallization ages for the Borne massif are consistently older, i.e. 309.5 ± 3.6 Ma (Couzinié, 2017; LA-ICP-MS U-Pb on zircon) and 315 ± 5 Ma (Mialhe, 1980; Rb-Sr on whole rocks), indicating that it may actually represent a distinct intrusion, yet emplaced within the same regional stress field.

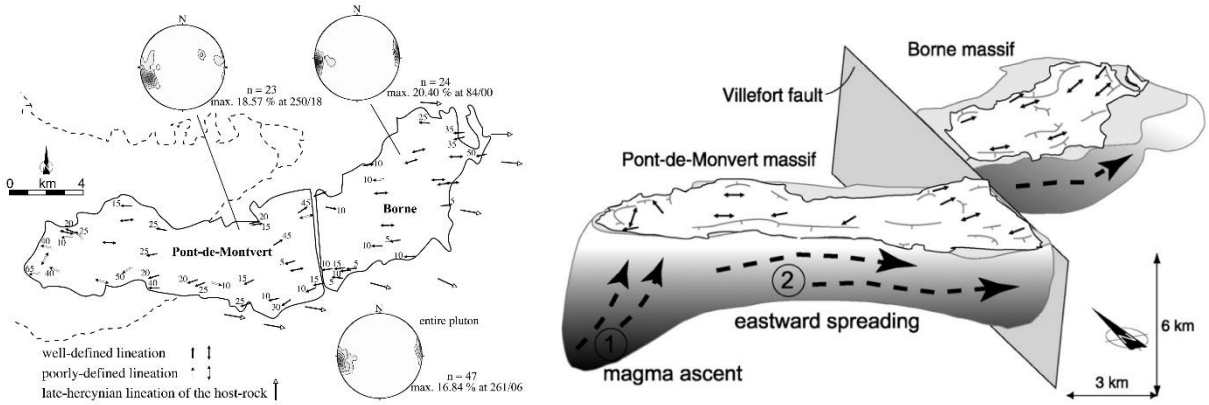

Figure 32 : Results of AMS studies (magnetic lineations) on the Pont-de-Montvert pluton and the nearby Borne pluton and interpretation in terms of magma emplacement and spreading (Talbot et al., 2004).

Stop 2.2 is located in the core of the Pont-de-Montvert pluton. It allows to examine the main petrographic facies of the granite and investigate its internal structure. A clear fabric is defined by the preferred orientation of K-feldpar megacrysts. In addition, aplite dykes, late hydrothermal features (such as carbonate-bearing veins cutting the granite) and alteration are observed.

Stop 2.3 – Intrusive contact of the Pont-de-Montvert granite with the Cévennes schists

Coordinates: Lat. 44°20'06.5" N; Long. 3°52'28.2" E

Location: Roadside and riverbed, D998 road ca. 2 km West of Vialas.

This outcrop is located along the southern contact of the Pont-de-Montvert granite with the Cévennes schists. The intrusive, basal contact of the granite is well exposed and demonstrates its laccolith nature. A sample of the granite taken along the road was dated by LA-ICP-MS U-Pb on zircon at 302.5 ± 3.1 Ma (Laurent et al., 2017) (**Figure 33**).

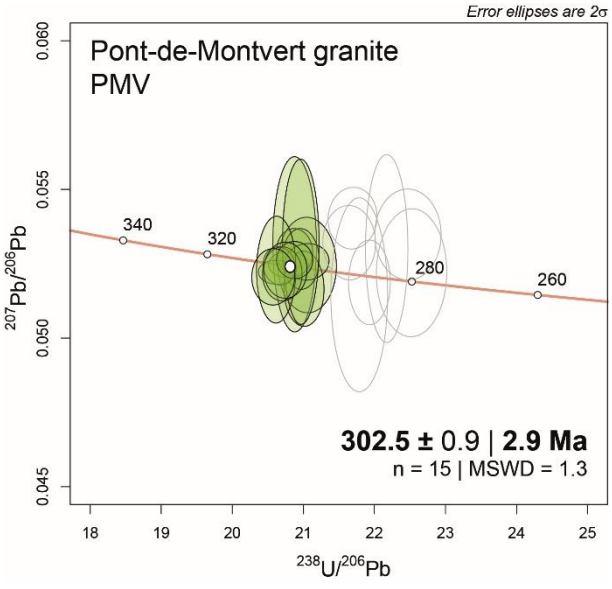

Figure 33 : Tera-Wasserburg diagram showing the results of LA-ICP-MS zircon U-Pb dating on a sample from the Pont-de-Montvert granite collected at stop 2.3 (redrawn from Laurent et al., 2017).

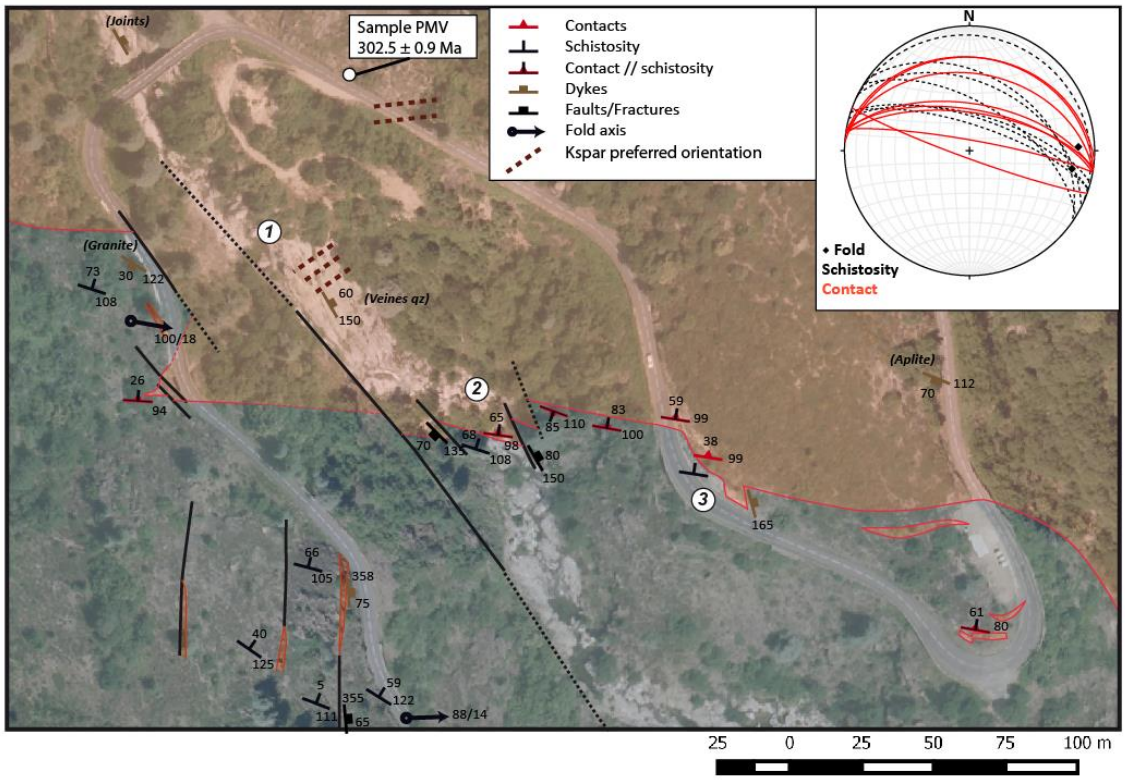

Figure 34 : Aerial photograph, sketch map and compilation of structural measurements of the southern intrusive contact of the Pont-de-Montvert granite (reddish shading) in the Cévennes schists (greenish shading) at stop 2.3 (J.F. Moyen, unpublished). The circled numbers refer to observation points described in the text.

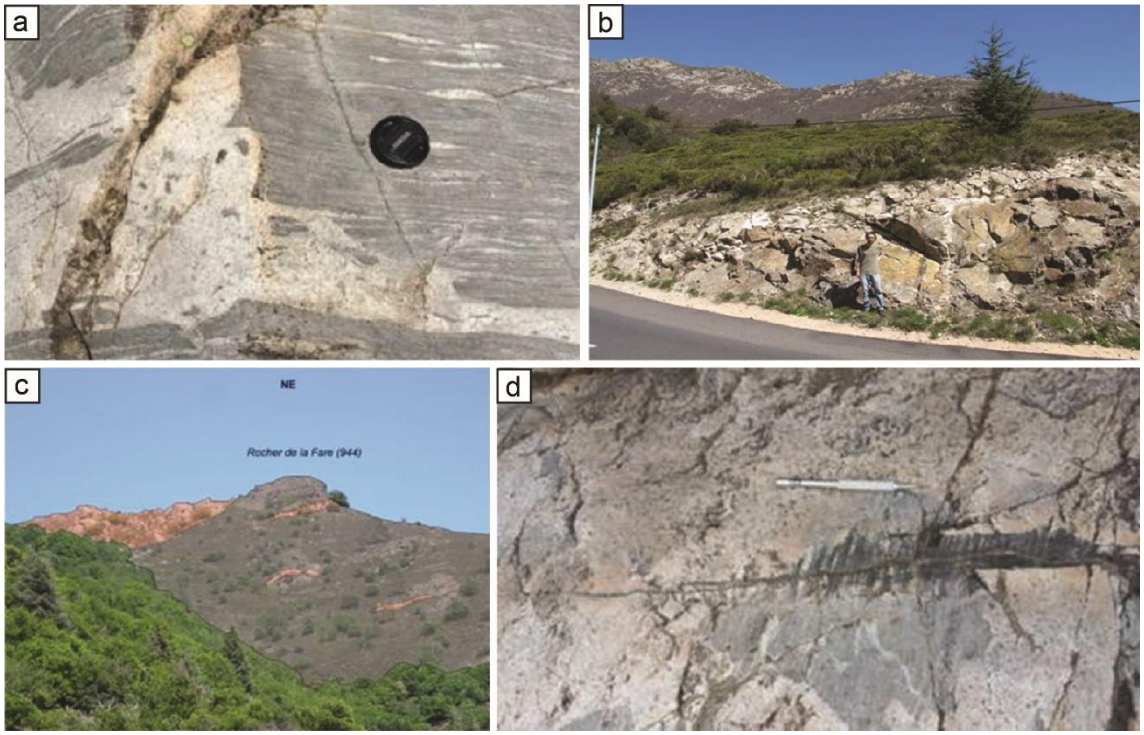

Figure 35 : Geometry of the intrusive contact of the Pont-de-Montvert granite in the Cévennes schists and associated structures. (a) Granitic dyke that cuts the foliation of the hornfels at high angle and then injects the sub-horizontal foliation. (b) Vertical dykes terminate in a horizontal sill; the summits in the background correspond to granites, overlying the schists in the foreground. (c) The “Rocher de la Fare” features a series of small, NW-dipping granitic sills below the main mass of the granite. (d) Tourmaline vein injecting the foliation of the schists and developing an alteration halo, best developed in the schists.

Fresh outcrops in the top part of the riverbed (**Figure 34**; observation point #1) allow to investigate the igneous texture of the granite. There, it shows a preferred orientation of K-feldspar phenocrysts, which is interestingly at angle to the contact. The granite contains rounded or irregular, dark mafic enclaves, but also angular or rounded xenoliths of country rocks. Late dykes of aplitic granite are also common, around which hydrothermal alteration is visible. Further upstream beyond the bridge (the site may be difficult to reach depending on the water level), carbonate-rich (brownish orange) veins cut the granite and clearly fill formerly open fractures, as shown by the directional growth of quartz and feldspars from the walls.

The intrusive contact of the granite into the schists (highly strained and metamorphosed to hornfels) is visible further down the creek (**Figure 34**; observation point #2) and along the road (**Figure 34**; observation point #3). Numerous pink aplites are present near the contact; although some are vertical, the dykes also infiltrate the sub-horizontal foliation planes and terminate in horizontal sills (**Figure 35**a,b). The surrounding hills show the same features, with a series of small sills below the main mass of the granite, occupying the topographic highs (**Figure 35**c). The agreement of structural measurements between the orientation of contacts in one hand, and the foliation in the schists (**Figure 34**), attests for the generally concordant nature of the contact. Later tourmaline-bearing veins cut across both lithologies and particularly develop alteration haloes in the schists (**Figure 35**d).

Stop 2.4 – Le Travers section, hydrothermal processes and ore deposits

Coordinates: from Lat. 44°19'56.8" N; Long. 3°55'20.9" E to Lat. 44°19'49.0" N; Long. 3°54'45.3" E

Location: ca. 500 m section along the D37 road ca. 2 km East of Vialas, near the Travers hamlet.

In the Cévennes area, five successive types of hydrothermal features have been identified (Charonnat et al., 1999; Charonnat, 2000) (**Figure 36**), which are from oldest to youngest: (i) Shallow dipping, East verging shear zones with essentially barren, quartz + chlorite + tourmaline + white mica ± arsenopyrite lenses; (ii) Quartz + cassiterite + wolframite veins, associated with aplites and pegmatites; (iii) Tourmaline + sulfide veins, also associated with aplites and pegmatites; (iv) Löllingite ($FeAs_2$)-bearing brecciated quartz; (v) Au (± Sb)-bearing quartz veins, main only type of economic interest in this area.

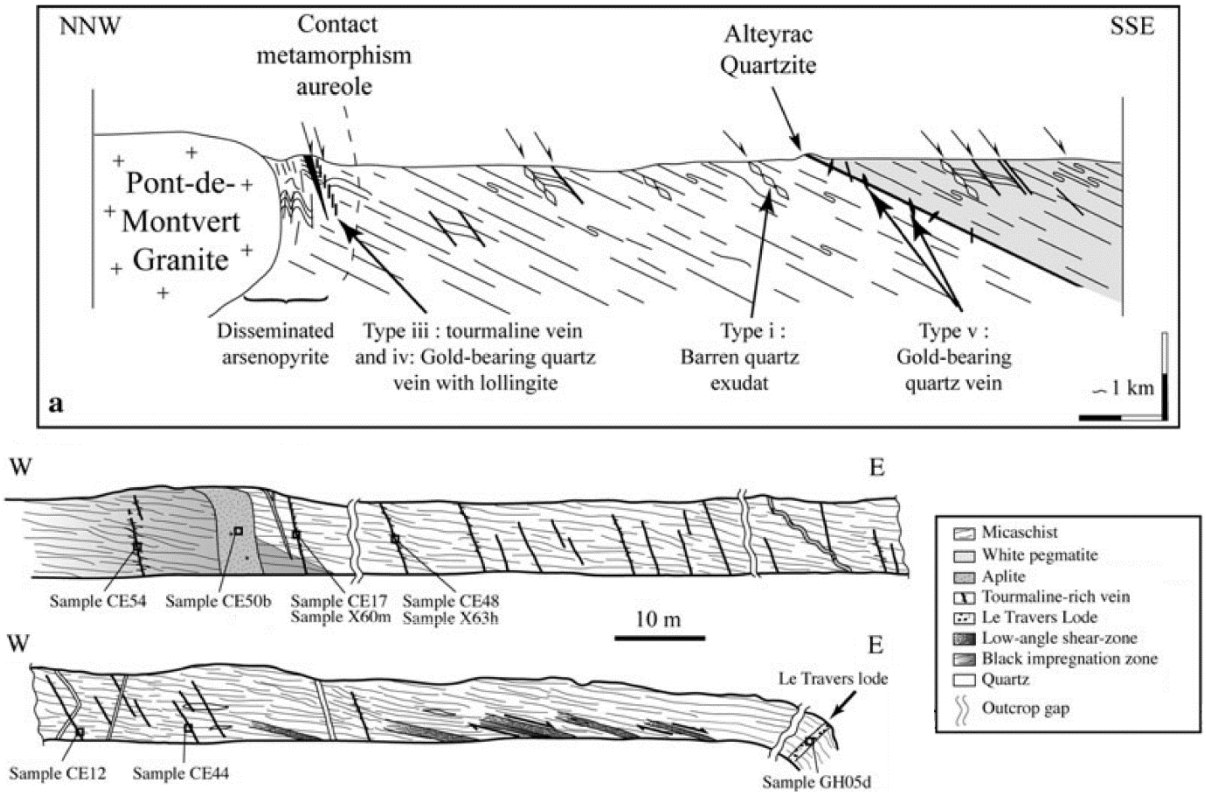

Figure 36: (a) Schematic NW–SE section extending from the southern edge of the Mont Lozère batholith showing the relations between the lithotectonic units of the Cévennes schists and hydrothermal features. (c) The Travers section of stop 2.4 (modified from Chauvet et al., 2012).

Structures and assemblages i to iii correspond to the B–Sn–W event; whereas iv and v belong to the Au–As–Sb event (Chauvet et al., 2012). This E–W section in the Cévennes schists is located <1 km to the South of the contact between the Pont-de-Montvert granite, within the thermal aureole of the latter. It allows to inspect the nature and structural context of emplacement of two of the type iii, tourmaline + sulfide veins (associated with aplites and pegmatites); and type iv, brecciated quartz + löllingite veins, in addition to the presence of disseminated arsenopyrite within the schists themselves.

A sketch of the Travers section is shown in **Figure 36**. At the easternmost end of the section, a gold-mineralized quartz + löllingite vein (type (iv)) (**Figure 37**) shows normal kinematics. Walking westwards, one successively encounters a set of low-angle (normal) shear zones within the schists, corresponding to the structures associated with type i veins (absent from this outcrop); and a wide zone rich in tourmaline- ± quartz- and arsenopyrite-bearing veins (type (iii)) (**Figure 37**), steeply dipping to the East. Occasionally, they are associated with structures showing a normal sense of shear and "en echelon" tension gashes filled with tourmaline. The veins are associated with aplite and porphyry granite dykes, which generally have the same orientation. Vein frequency increases in the vicinity of the largest of these dykes, found at the western end of the section, within a zone of sulfide impregnation in the schists.

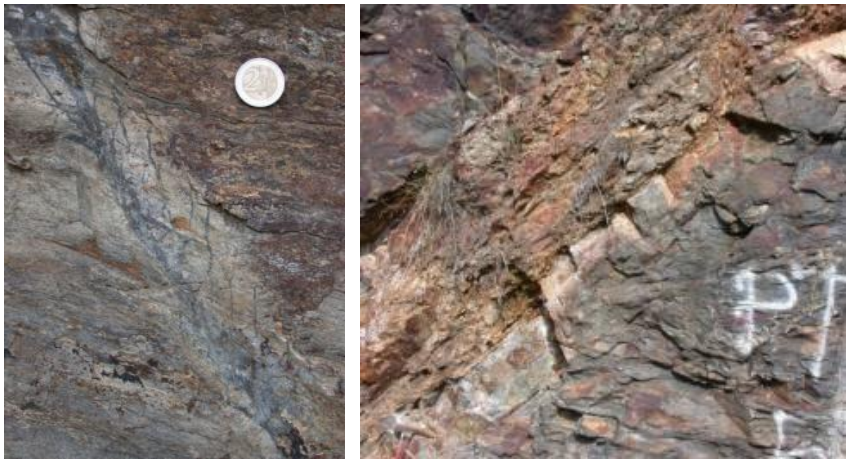

Figure 37: The two main types of hydrothermal veins cutting the Cévennes schists that can be found along the Travers section: tourmaline + quartz + arseno-pyrite veins and associated alteration haloes of the regional type (3) (left); and gold-bearing quartz-löllingite brecciated veins (about a meter wide) of the regional type (4) (right).

Stop 2.5 – The old Legal mine (optional)

Coordinates: Lat. 44°18'52.7" N; Long. 3°57'26.3" E

Location: on a trail ca. 1 km West of Pont-de-Rastel, ca. 250 m away from a minor tar road.

This stop is located within a quartz-rich gneiss unit of the Cévennes schists ("Gneiss d'Alteyrac"). Most of the (formerly) exploited gold-bearing quartz veins are found within this marker. They belong to the regionally defined type (v) (see above) and (in contrast with stop 2.4) are found in a distal position relative to the Pont-de-Montvert granite, whose southern contact is ca. 3 km away to the NW.

The Legal vein is found in a ca. 60 m long adit (**Figure 38**). It corresponds to vertical, NE–SW trending (N050°), and discontinuous quartz veins, exposed on the roof of the adit. The veins have a complex internal texture reflecting a polyphase history of opening and fluid flow (Nomade et al., 1999) (**Figure 38**). The mineralized paragenesis includes white quartz and gold-bearing arsenopyrite. Sphalerite, pyrite, chalcopyrite and Sb-minerals (bournonite and polybasite) are also observed in thin section. Kinematic indicators and minor arsenopyrite-bearing structures are present here and allow to discuss the tectonic regime. Pyrite, chalcopyrite and arsenopyrite from the vein in the adit all have $\delta^{34}S$ between 0 and +3 ‰, consistent with metamorphic fluids (H. Schmit, unpub. data).

Figure 38: Entrance to the adit (top) and petrographic aspect of the Legal quartz vein (bottom).

Day 3

Immediately to the North of the Cévennes domain, the Lower Gneiss Unit (LGU) and southern margin of the Velay dome are exposed (**Figure 39**). Based on the nappe model of the FMC (see Excursion notes – Geological background), the LGU and Velay dome should be tectonically emplaced above the Cévennes schists (which represent the PAU). However, the southward-dipping attitude of the two units at the contact and the relationships between metamorphic and granitic rocks (shallow intrusive plutons in the PAU; migmatites–diatexites in the LGU) are difficult to reconcile with this hypothesis. Alternatively, the PAU and LGU could be interpreted as two different structural levels of the same crustal column, respectively representing the upper- vs. mid-crust in the late Carboniferous (see **Figure 1**).

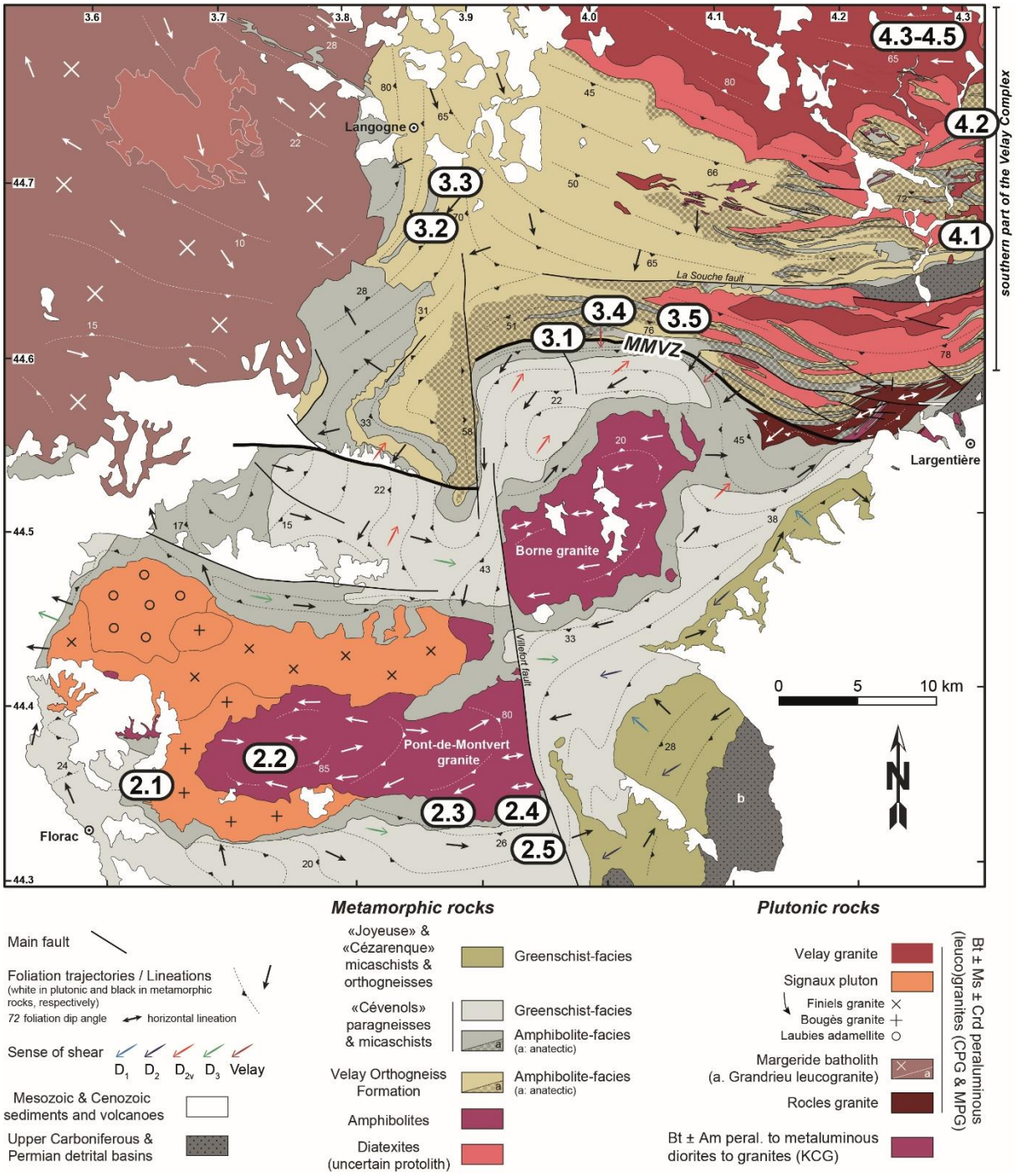

Figure 39 : Simplified geological map of the northern Cévennes domain and southern Velay complex (from S. Couzinié, unpublished), also showing the localities visited during days 2, 3 and 4 of this trip.

In the northern Cévennes and Monts d'Ardèche areas, the LGU is made of pre-Variscan basement rocks mostly formed coeval to the Cadomian orogeny in the late Neoproterozoic (Ediacaran) to early Cambrian (Couzinié et al., 2017; 2019) and metamorphosed under amphibole facies, up to partial melting conditions (4–6 kbar; 650–820 °C) in the Carboniferous to form the migmatites of the Velay dome (Montel et al., 1992; Barbey et al., 1999, 2015; Ledru et al., 2001; Villaros et al., 2018; Couzinié et al., 2021) (**Figure 39**). These rocks consist of two main lithologies: (i) **paragneisses**, corresponding to former sedimentary rocks deposited in the late Ediacaran (Couzinié et al., 2019); and (ii) **the Velay Orthogneiss Formation (VOF)**, gathering all meta-igneous felsic rocks that crop out in the region, mostly augen- and leucogneisses, and which intruded the former meta-sedimentary rocks (Ledru et al., 1994) near the Ediacaran-Cambrian boundary (Couzinié et al., 2017). These represent the oldest documented rocks and likely the main lithologies of the E-FMC at the scale of the entire crust, as lower crustal xenoliths brought up by Cenozoic volcanoes essentially correspond to higher-grade equivalents of the LGU meta-sedimentary and meta-igneous rocks (Leyreloup, 1992; Laurent et al., 2023). They must therefore have a fundamental significance for the formation and evolution of the E-FMC crust.

Paleogeographic reconstructions indicate that late Ediacaran sediments from the north Gondwana margin were deposited in back-arc basins located at the rear of the Cadomian subduction (Fernández-Suárez et al., 2000; Linnemann et al., 2000) (**Figure 40**). At the scale of the Variscan belt, the relatively short time span between late Ediacaran sedimentation (mainly 600–560 Ma) and magmatism (560–540 Ma) is consistent with a marginal orogenic setting where protracted periods of lithospheric extension and associated sedimentation are punctuated by contractional events leading to crust thickening and followed by anatexis (Collins and Richards, 2008). Hence, voluminous magmatism at the origin of the VOF was likely caused by the inversion of the back-arc basin at the end of the Cadomian orogeny (Linnemann et al. 2007), leading to limited stacking of supracrustal sequences in a high thermal regime that favored significant melting (Clark et al., 2011) (**Figure 41**).

As a consequence of this peculiar tectonic regime, the late Ediacaran events in the E-FMC feature both new crust formation and substantial crust reworking. The meta-sediments indeed include detritus from two end-members crustal components (Couzinié et al., 2019): (i) young and juvenile arc material, probably derived from the relatively proximal Cadomian arc; and (ii) ancient, Gondwana-derived cratonic crust, of Paleoproterozoic to Archean age. This mixture is at the origin of the "identity" of the E-FMC crust, reflected by the relative isotopic homogeneity that characterizes all subsequent igneous events (the VOF at ca. 545 Ma; Ordovician igneous rocks at ca. 480 Ma; and the Variscan granitoids at 340-300 Ma; see **Figure 6**).

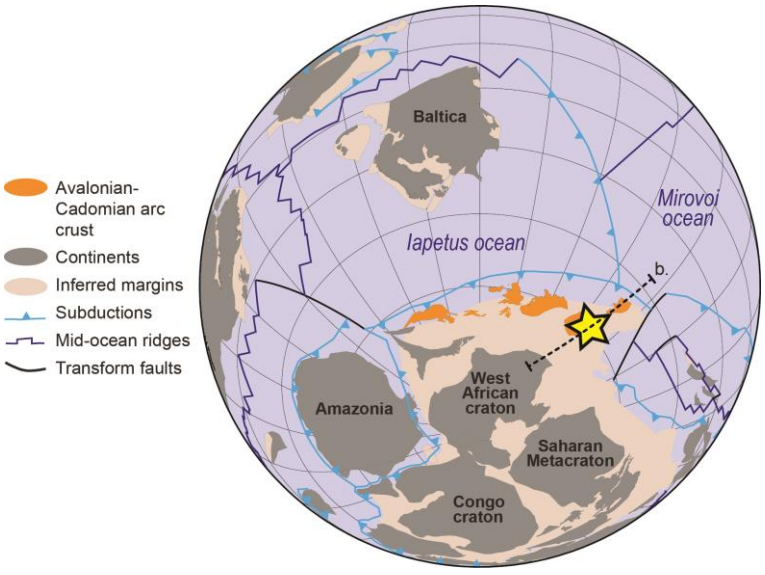

Figure 40 : Paleogeographic reconstruction centered on the southern hemisphere at 545 Ma, showing the approximate position of the E-FMC (yellow star) as a back-arc basin along the Cadomian convergent margin (modified from a figure courtesy of L. Doucet). The dashed line labelled (b) shows the approximate location of the cross-sections of **Figure 41**.

The first objective of the day is to observe the metamorphic and structural record of the transition from the low-grade Cévennes schists to the higher-grade LGU rocks. The second aim is to investigate the pre-Variscan crustal evolution of the E-FMC based on the nature and geodynamic significance of the Ediacaran protoliths of the LGU (ortho- and paragneisses). Finally, we will observe the onset of the Variscan melting event in these rocks, as an introduction to Day 4. This will also lead to discuss the role of these distinct lithologies as sources of melts during the regional Carboniferous anatectic event.

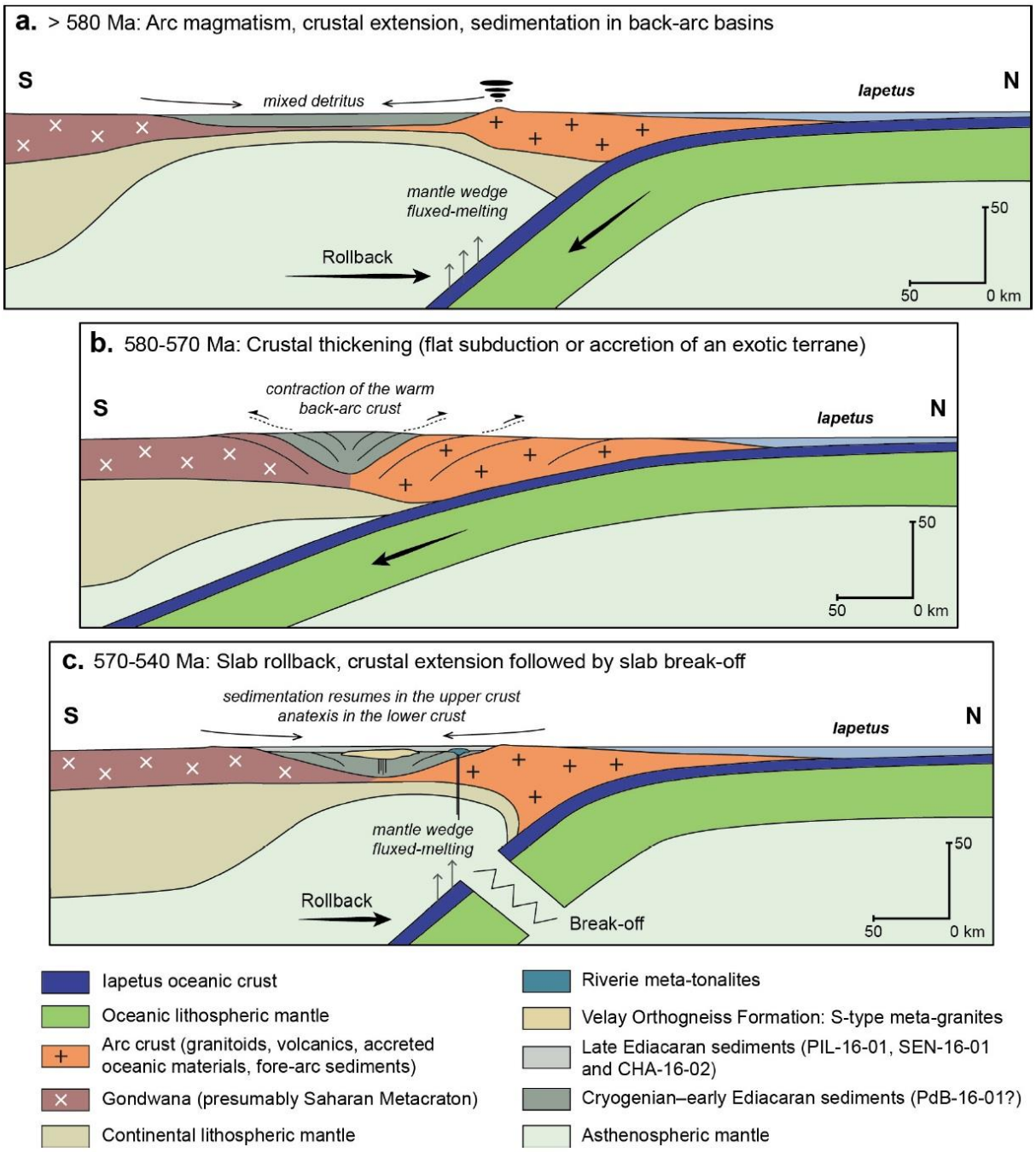

Figure 41 : Possible geodynamic situation explaining the formation of the E-FMC crust during the late Neoproterozoic to Cambrian (Couzinié, 2017).

Stop 3.1 – A section across the transition from the Cévennes schists to the LGU migmatites

Coordinates: from Lat. 44°35'31.8" N; Long. 3°58'27.7" E to Lat. 44°36'15.9" N; Long. 3°58'11.2" E

Location: a ca. 2 km section on a low-traffic country road from Tressol to Saint-Laurent-les-Bains.

The village of Saint-Laurent-les-Bains is a thermal resort, located on a minor N—S fault that operates as a drain for hydrothermal waters: a hot spring (53 °C) is present in the village. A fluorite body, which was mined from 1925 to 1970, also flanks the fault. The main local geological feature relevant for this field trip is the so-called Mylonitic Metamorphic Vellave Zone (MMVZ), corresponding to a roughly E–W trending zone of both complex structural record and rapid change in metamorphic grade, marking the

transition from the LGU high-grade rocks and the low-grade meta-sediments of the PAU (Bouilhol et al., 2006). The MMVZ is exposed along a ca. 2 km-long section through typical LP/HT metamorphic zones, from from South to North: **garnet-chlorite ($Z_{Grt-Chl}$)**, **cordierite-andalousite-biotite ($Z_{Crd-And-Bt}$)** and **biotite-sillimanite ($Z_{Bt-Sill}$)**, reaching anatexis at Saint-Laurent-les-Bains (**Figure 42**).

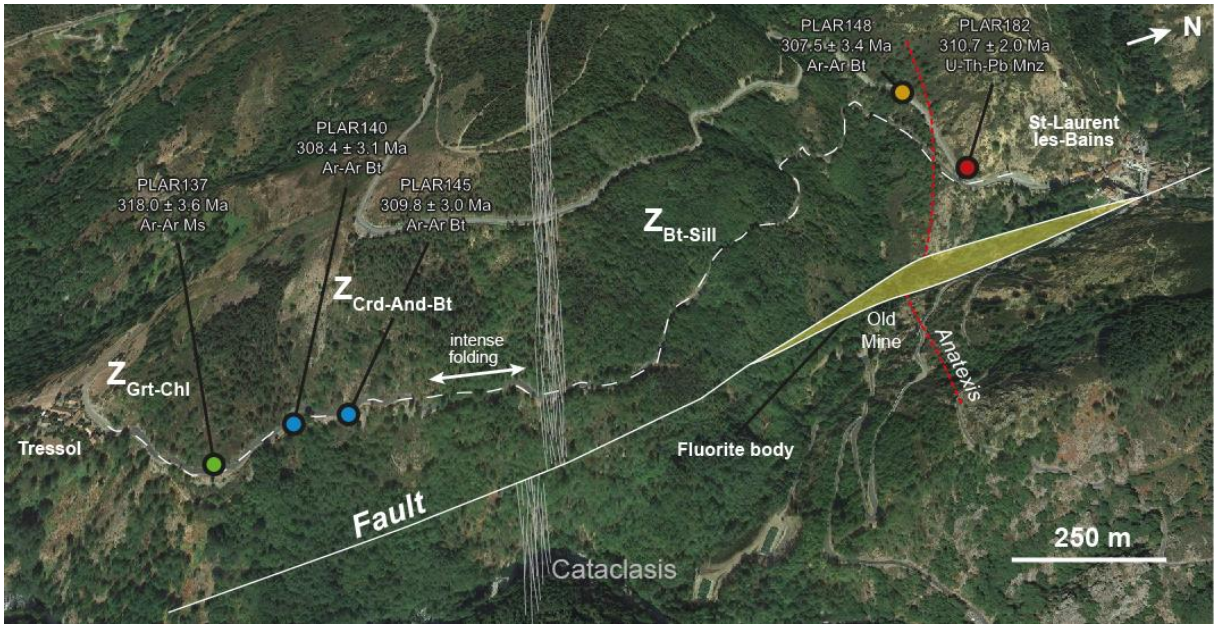

Figure 42 : Aerial photograph illustrating the main geological structures, metamorphic zones and available geochronological data (from Bouilhol et al., 2006) along the Tressol-Saint Laurent-les-Bains cross-section (dashed line). The yellowish area corresponds to the mined fluorite body.

Early top-to-the-NE deformation, dominated by simple shear, is observed in the $Z_{Grt-Chl}$ and in the $Z_{Crd-And-Bt}$ (**Figure 43** and **Figure 44**), and has been dated at 318.0 ± 3.6 Ma on synkinematic muscovites from the $Z_{Grt-Chl}$. The syntectonic Rocles granite (Be Mezeme et al., 2007; see **Figure 39**) yielded an identical emplacement age of 319.8 ± 3.8 Ma (LA-ICP-MS U-Pb on zircon, unpublished data from S. Couzinié). Within the $Z_{Crd-And-Bt}$ an intense deformation marked by constriction (fold axis parallel to the X and Y finite strain axis), with nice biotite aggregates marking the constant N240° lineation, is quickly followed by the appearance of sillimanite.

The $Z_{Bt-Sill}$ zone is characterized by the development of new, S-dipping mylonitic foliation associated with high-T top-to-the-South normal shearing (**Figure 43** and **Figure 44**), dominated by pure shear. Shearing was coeval with anatexis, dated at 310.7 ± 2.0 Ma (U-Th-Pb monazite, Bouilhol et al., 2006) and interpreted to reflect the vertical extrusion of the partially molten crust in the dome core. This is supported by the orientation of mineral stretching lineation, everywhere perpendicular to the edge of the dome (Bouilhol et al., 2006). Cooling of the $Z_{Crd-And-Bt}$ and $Z_{Bt-Sill}$ is constrained by Ar-Ar biotite ages ranging from 309.8 ± 3.0 Ma down to 307.5 ± 3.4 Ma, indicating fast uplift of the dome edge.

As a whole, this set of tectonic-metamorphic information points to a strong mechanical decoupling between the migmatitic mid-crust and its lower-grade meta-sedimentary roof, during buoyancy-driven uplift of the dome core. While the Cévennes schists locally preserve the record of an earlier tectonic event (top-to-the-NE thrusting?), the overprinting, strong top-to-the-South normal sense of shear associated with higher metamorphic grade are consistent with this process. Interestingly, a similar tectono-metamorphic record is symmetrically preserved on the far northern edge of the dome, in the Saint-Étienne area (ca. 100 km North). There, the Pilat shear zone, which can be regarded as an equivalent of the MMVZ, is characterized by top-to-the-North normal shearing (Malavieille et al., 1990) with emplacement of syntectonic granites and Ar-Ar mica cooling ages ranging from 306 to 299 Ma (Gardien et al., 2022).

The outcrop of migmatites near the village (PLAR182 on Figure 47) is altered and cut by sulfide veins forming a stockwork. $\delta^{34}S$ of pyrite and chalcopyrite at this locality are strongly negative (-12 to -15 ‰), consistent with meteoric water (H. Schmit, unpub. data). This alteration may be related to the recent (possibly Cenozoic; Leach et al., 2006) MVT deposits found in the region, and responsible for the numerous occurrences of Pb–Zn ore deposits. The nearby fluorite body is likely related to this event.

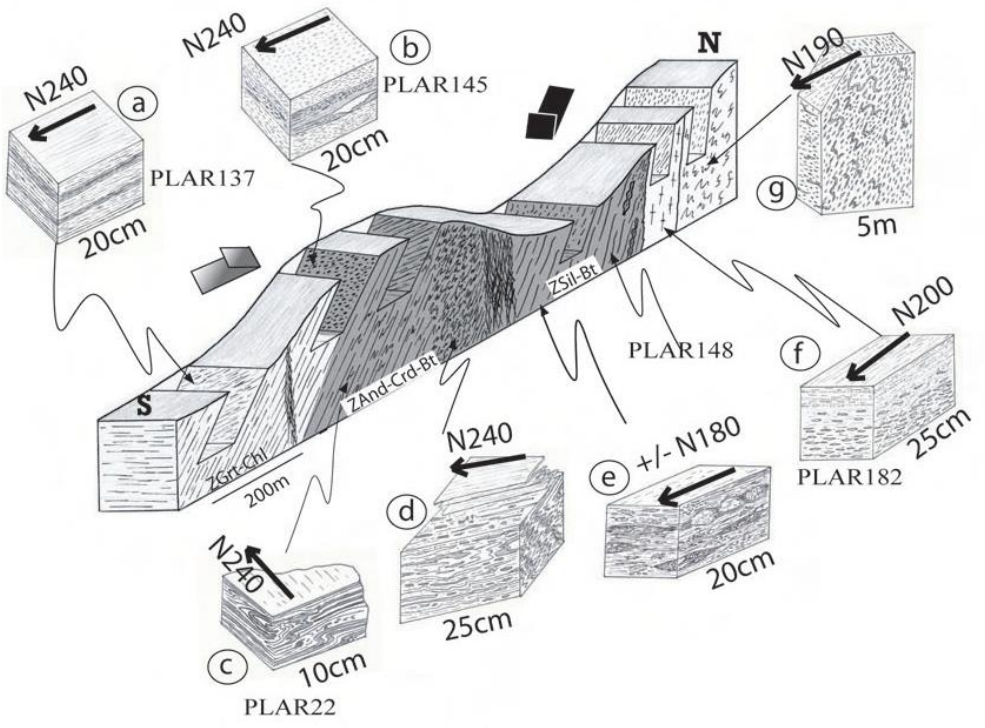

Figure 43 : 3D sketch of the structures observed along the Tressol – Saint-Laurent-les-Bains section (Bouilhol et al., 2006).

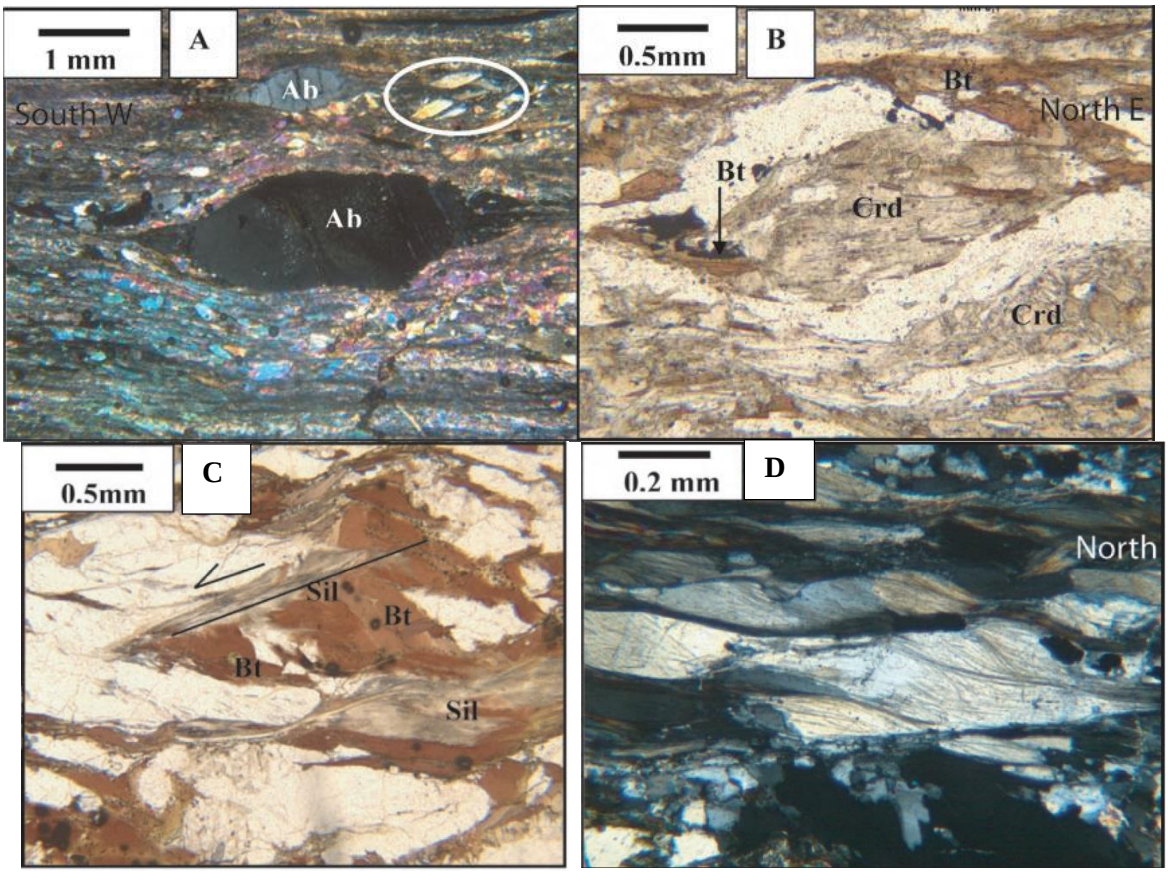

Figure 44 : (a) and (b) Top-to-the-northeast shear criteria. (a) $Z_{Grt\text{-}Chl}$. Cross-polarized-light view of mylonitic quartz-feldspar greenschist. Sigmoidal albite (Ab) and a muscovite fish (in the circle) indicate top-to-the-northeast shearing. (b) $Z_{Crd\text{-}And\text{-}Bt}$. Plane polarized view of a sigmoidal cordierite with biotite pressure shadows. (c) and (d) Evidence for ductile normal top-to-the South sense of shear in the $Z_{Bt\text{-}Sill}$: (c) sillimanite bearing shear planes cross cutting magmatic biotite and (d) quartz-sillimanite nodules with a sigmoid shape. From Bouilhol et al. (2006).

Stop 3.2 – Ediacaran paragneisses

Coordinates: Lat. 44°40'50.9" N; Long. 3°52'16.3" E

Location: roadcut along the RD906 road ca. 4 km North of Luc. **Mind the heavy traffic!**

Where the LGU is not affected by Carboniferous melting, it features interstratified augen- au leucocratic orthogneisses (the VOF, see stop 3.3) and paragneisses (this stop). Couzinié et al. (2019) undertook a regional survey of detrital zircon populations in the LGU paragneisses. A representative detrital zircon date distribution, from a meta-arkosic layer sampled ca. 15 km South of stop 3.2, is shown in **Figure 45**. Most E-FMC samples show comparable age patterns, which are typical of all Ediacaran meta-sediments from the northern Gondwana margin characterized by the predominance of Ediacaran-Cryogenian grains with additional populations of Tonian-Stenian (720-1100 Ma), Paleoproterozoic (1.8-2.1 Ga) and Archean (2.5-2.9 Ga, up to 3.4 Ga) age (**Figure 45**). A characteristic feature is also the absence of Mesoproterozoic detrital record, with a clear gap between 1.2 and 1.6 Ga. In the E-FMC, the ages of the youngest zircon populations give maximum deposition ages for the sedimentary protoliths between 553 and 592 Ma depending on the sample (Couzinié et al., 2019) (**Figure 45**).

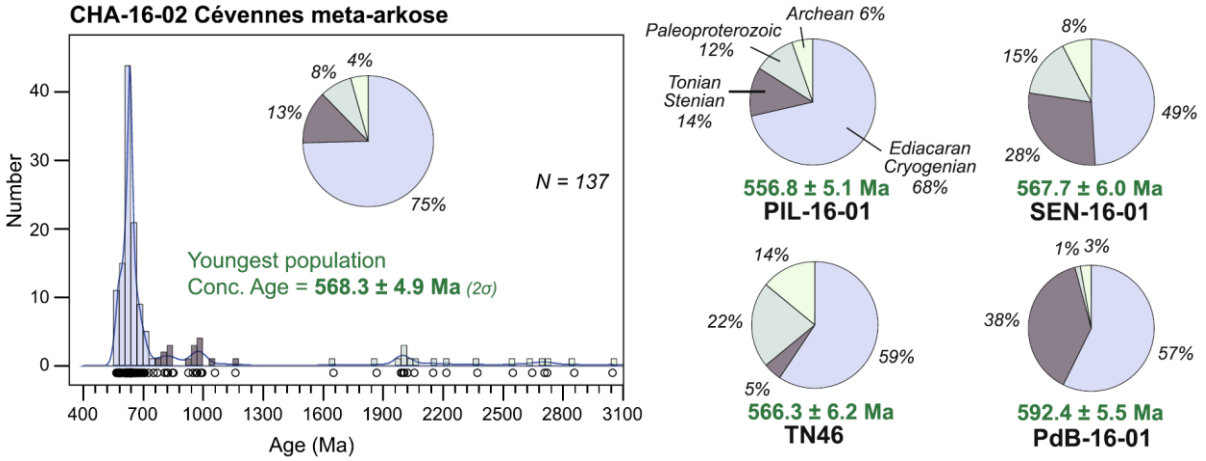

Figure 45 : Example of detrital zircon U-Pb date distribution of Ediacaran paragneisses from the LGU (e.g. meta-arkose from the Cévennes area). The pie charts indicate the proportions of the main age populations of detrital zircons in the sample as well as other paragneiss samples from the LGU in the E-FMC. Maximum deposition ages are indicated in green for each sample. Modified from Couzinié et al. (2019).

The obtained detrital zircon age distributions confirm the results of multi-methods studies, which have demonstrated that Ediacaran sediments deposited along the northern margin of Gondwana were of mixed origin, comprising detritus from the Avalonian-Cadomian magmatic arc; the Pan-African orogenies and terranes (e.g. Saharan metacraton, etc.); and an old (Paleoproterozoic to Mesoarchean), cratonic Gondwana-derived source (Denis and Dabard, 1988; Dabard et al., 1996; Linnemann et al., 2000). Zircon εHf_t vs. age relationships for FMC meta-sediments (**Figure 46**) further show that the dominant, Neoproterozoic detrital zircons population is characterized by an enormous range of εHf_t from ca. +10 to -40. Such a range hints that the sources of the parental igneous rocks correspond to a mixture in various proportions of juvenile Neoproterozoic crust and ancient (Paleoproterozoic to Archean) cratonic crust.

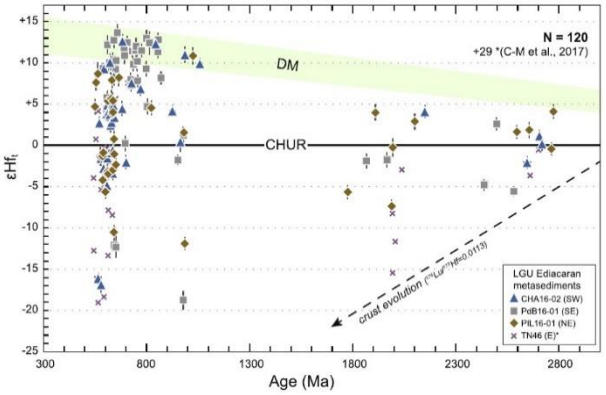

Figure 46 : Zircon εHf_t vs. age diagram showing the results of combined U-Pb and Lu-Hf isotopic analyses of detrital grains in the E-FMC Ediacaran paragneisses (from Couzinié et al., 2019). The εHf_t range for the Depleted Mantle (DM) reservoir is bracketed by the models of Næraa et al. (2012) and Griffin et al. (2000).

Stop 3.3 – Meta-igneous rocks of the Velay Orthogneiss Formation (VOF)

Coordinates: Lat. 44°41'43.3" N; Long. 3°53'01.4" E

Location: roadcut along the RD906 road ca. 4 km South of Langogne. **Mind the heavy traffic!**

The VOF is defined as a regionally consistent unit of meta-igenous lithologies cropping out all around the Velay dome, collectively dated at ca. 546–542 Ma and possibly representing a late-Cadomian large granitic batholith deformed and metamorphosed during the Variscan orogeny (Couzinié et al., 2017). The main lithologies of the VOF are (i) a volumetrically dominant biotite ± muscovite ± sillimanite augen gneiss featuring pluricentimetric K–feldspar porphyroblasts and accessory garnet, allanite, ilmenite, apatite and zircon; (ii) a muscovite ± biotite ± garnet fine-grained leucogneiss (locally called "leptynite") with similar accessory minerals; and (iii) a volumetrically subordinate banded orthogneiss.

The VOF samples display geochemical affinities to S-type granites (**Figure 47**) and likely originated from melting of sedimentary sources. Given the geochemistry and age of the VOF magmas, the surrounding Edicarian sedimentary rocks (now represented by the paragneisses) represent the most likely source material. Fractionation of plagioclase, biotite and accessory minerals from a magma compositionally similar to the augen gneiss accounts for the composition of leucogneisses.

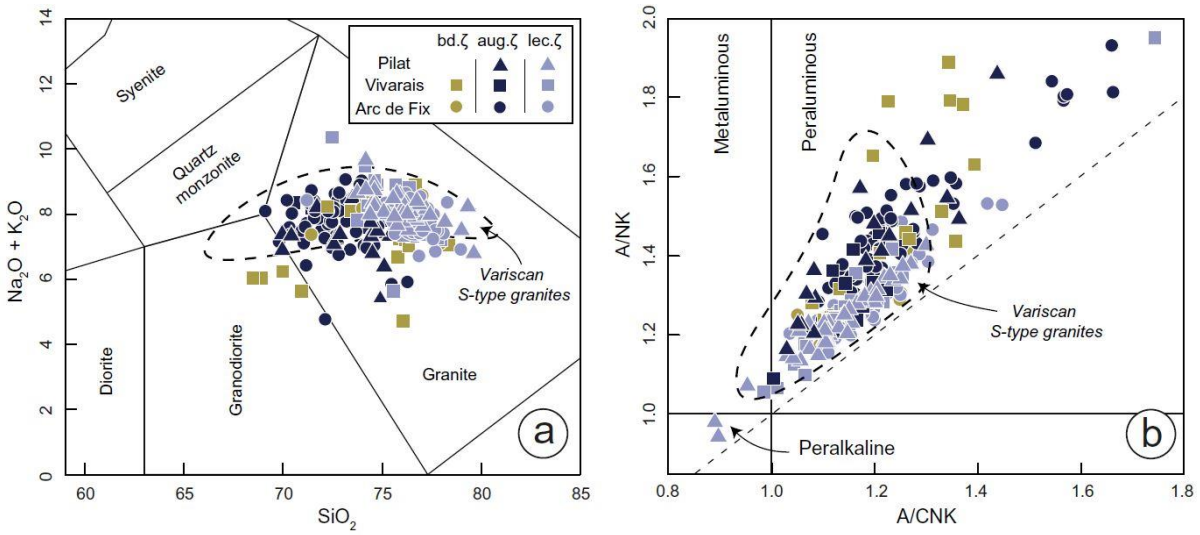

Figure 47 : Major elements compositions of samples from the Velay Orthogneiss Formation ("bd.", "aug." and "lec." refer to banded, augen- and leucogneiss respectively): (a) TAS classification diagram; (b) A/NK vs. A/CNK. From Couzinié et al. (2017).

The εHf_t variability of the VOF is small (**Figure 48**) indicating that zircons crystallized from a magma with relatively homogeneous Hf isotope composition, a feature rather uncommon for S-type granites (Appleby et al., 2009; Villaros et al., 2012; Farina et al., 2014). Such homogeneous signature strikingly contrasts with the huge range of εHf_t shown by the paragneisses, believed to be the source of the VOF magmas (**Figure 48**). This particular situation would result from (i) a relatively long residence time of the melt in the source under Zr-undersaturated conditions, favoring detrital zircon dissolution and isotopic homogenization of the melt by elemental/isotopic diffusion; followed by (ii) rapid extraction, transfer and cooling of the magmas, preventing further dissolution of inherited, isotopically disparate, grains (Couzinié et al., 2017).

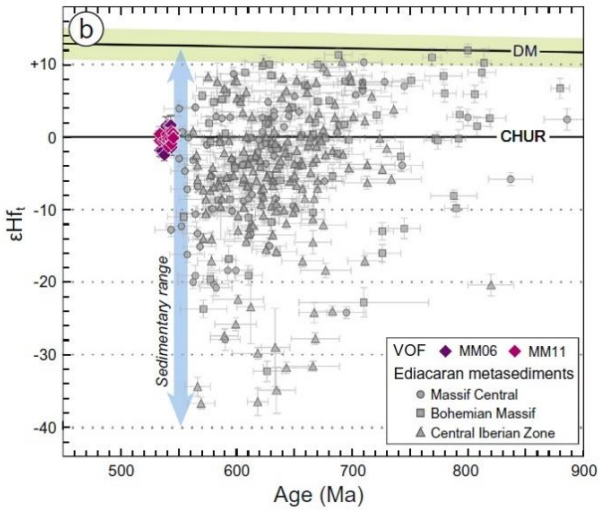

Figure 48 : Zircon εHf(t) vs. age diagram for two VOF samples compared with a compilation of data from detrital zircon in regional Ediacaran paragneisses (Couzinié et al., 2017).

The outcrop features coarse augen gneisses and leucogneiss (leptynite) enclaves,

representative of the two main lithotypes of the VOF. Both are cut by several generations of pegmatites and aplites, presumably Variscan in age (**Figure 49**). This is supported by the relative proximity of the Variscan melting front. A sample of leucogneiss was investigated here for LA-ICP-MS U-Pb zircon dating and yielded a crystallization age of 545.9 ± 4.3 Ma, identical to that of the augen gneisses on a regional scale (**Figure 49**). This confirms that the leucogneisses are coeval with the latter and probably represent differentiates of the VOF batholith, or hypovolcanic / extrusive felsic melts associated to them.

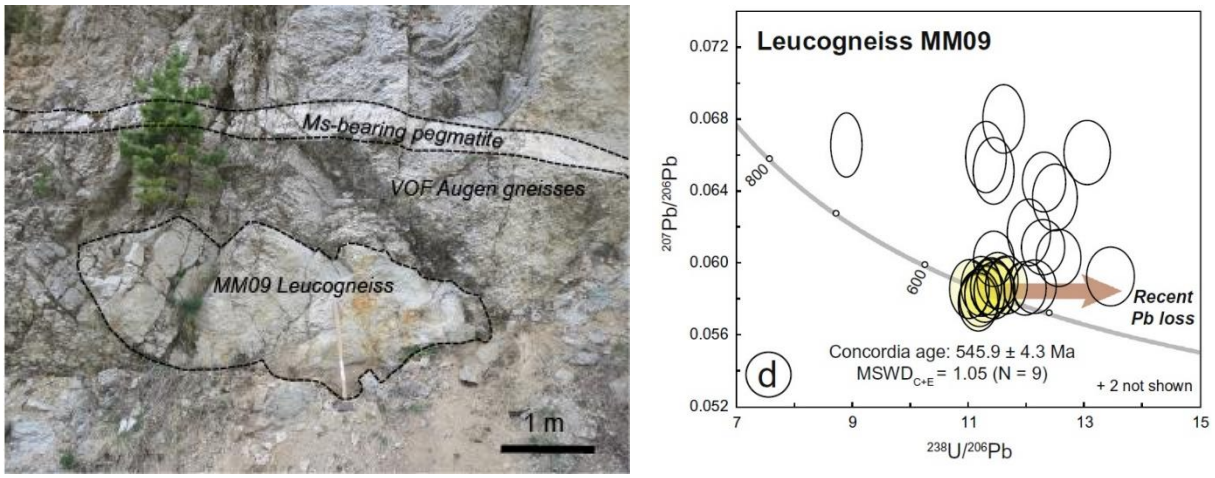

Figure 49 : Field relations at stop 3.3 and Tera-Wasserburg diagram showing the results of LA-ICP-MS zircon U-Pb dating of the leucogneiss enclave (sample MM09) (Couzinié et al., 2017).

Stop 3.4 – The onset of partial melting in orthogneisses

Coordinates: Lat. 44°36'51.6" N; Long. 4°01'16.3" E

Location: bed of the Borne river under the medieval tower of Borne, ca. 500 m East of the village.

The orthogneisses in the Borne area still belong to the late Edicaran VOF, but sit beyond the Variscan melting front, along the southern rim of the Velay dome. Although augen gneisses at this locality are still largely unmolten, localized and low-degree partial melting features are clearly visible on the outcrop (**Figure 50**). These are (1) thin (centimetric) quartz-feldspar leucosomes, commonly surrounded by biotite selvedges; (2) wider, apparently younger granite-textured zones (dykes?) and (3) late, cordierite-bearing leucocratic veins, slightly oblique on the main foliation.

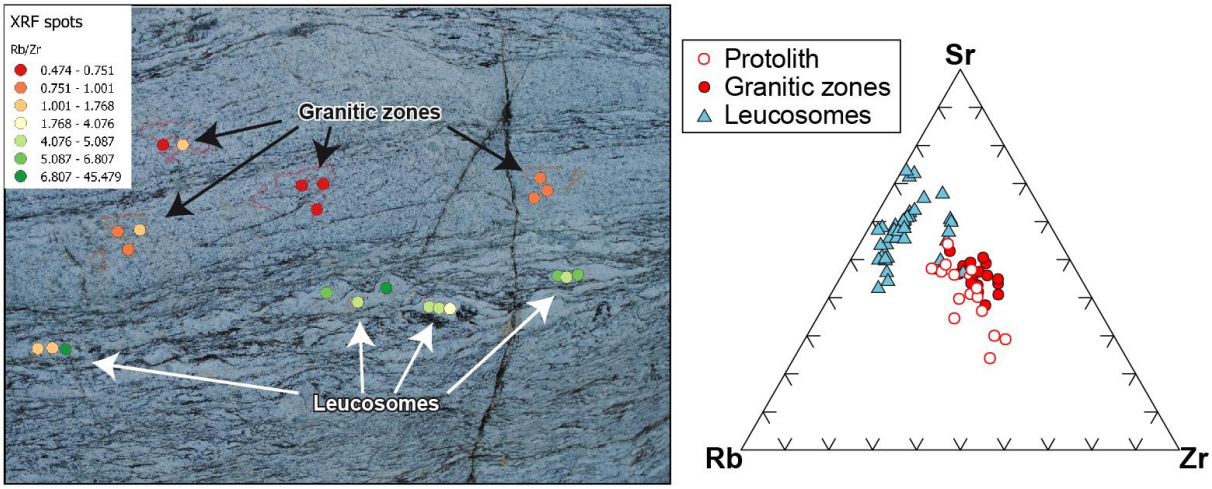

Figure 50 : Examples of the main anatectic features at stop 3.4 (thin leucocratic leucosomes and younger granitic zones) and results of in-situ geochemical analyses of the different zones by portable XRF on a Rb–Sr–Zr ternary diagram (S. Couzinié & J.F. Moyen, unpub. data).

A portable XRF study was undertaken to investigate the composition of the first two sets of anatectic features (**Figure 50**). The leucosomes show strikingly low Zr contents, suggesting that they represent "cold" melts that could not dissolve zircon from the protoliths. This is a distinctive peculiarity of the VOF rocks that may produce significant melt under water-fluxed melting conditions even at low temperatures (650–700 °C), owing to their near-eutectic bulk composition (Couzinié et al., 2021). Both leucosomes and granitic zones show the same Rb/Sr ratios as the unmolten augen gneiss (**Figure 50**), supporting congruent contributions of plagioclase and K-feldspar to the melting reaction (i.e. eutectic melting).

Stop 3.5 – Col de Meyrand lookout point

Coordinates: Lat. 44°36'23.7" N; Long. 4°04'33.2" E

Location: rocky summit ca. 150 m East of the Col de Meyrand montain pass (1372 m).

The Col de Meyrand lies right on the Atlantic-Mediterranean watershed. At this locality, the outcrops exhibit essentially unmolten augen gneisses of the VOF, but the melting front is located only a few hundreds of meters to the North. Although this is mostly a touristic stop (if the weather is clear, one may spot the Alps in the distance, as well as the iconic Mont Ventoux, of Tour de France fame, which sits ca. 100 km to the SE), the spectacular view to the East illustrates several features of the local geology, especially the (folded and faulted) southern margin of the Velay migmatite-granite complex and its relationship with Mesozoic cover rocks (**Figure 51** and **Figure 52**).

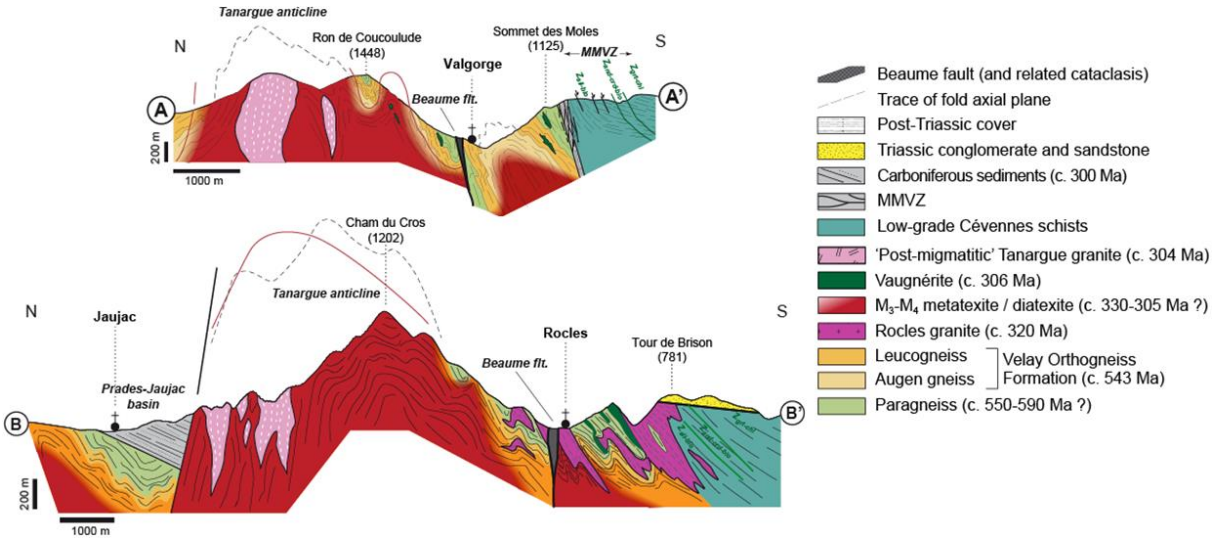

Figure 51 : Geological cross-sections across the Beaume Valley, corresponding to the view from Col de Meyrand (**Figure 52**). Drawn after geological map and partly after Barbey et al. (2015) and Bouilhol et al. (2006).

The Tanargue range (to the North, i.e. left-hand side) culminates at 1400–1500 m. It is armed by diatexites and granites (cordierite-bearing Velay granite and the late, 304 Ma-old sub-volcanic Tanargue granite; Couzinié et al., 2014). The flanks of the main valley (Beaume Valley) are made up of the typical Ediacarian association of para- and orthogneisses (VOF), affected by various extents of migmatization and folded along E–W trending, subvertical and syn-migmatitic folds. The sequence is partly duplicated by the late E–W trending Beaume brittle fault, a strike-slip fault with a minor vertical component.

To the South, the summit line of the Valgorge range (hardly reaching 1100 m) roughly coincides with the MMVZ (see stop 3.1). The contact was intruded by the Rocles laccolith (peraluminous biotite- and/or muscovite granites ± vaugnérites) at ca. 320 Ma (Be Mezeme et al., 2007 and S. Couzinié, unpublished data). The laccolith was tilted and deformed during the Upper Carboniferous doming of the Velay complex and associated top-to-the-South shearing (Be Mezeme et al., 2007).

Some lower summits further SE (i.e. the "Tour de Brison", a fire watch observatory) correspond to inliers of early Mesozoic (Triassic) sedimentary cover. The plain and modest hills in the background are formed by gently SE-dipping structural surfaces of the Jurassic and Cretaceous platform sequence, cut

by minor (normal fault-related) escarpments. This morphology illustrates the spectacular amplitude of the Cenozoic upflit that affected the E-FMC basement.

Sample MM11, a typical VOF augen gneiss, was taken opposite the lookout point along the road and yielded an age of 542.5 ± 3.1 Ma (Couzinié et al., 2017). Further South in the slopes, a body of vaugnérite embedded in migmatitic paragneisses was dated at 307.4 ± 1.8 Ma (Laurent et al., 2017).

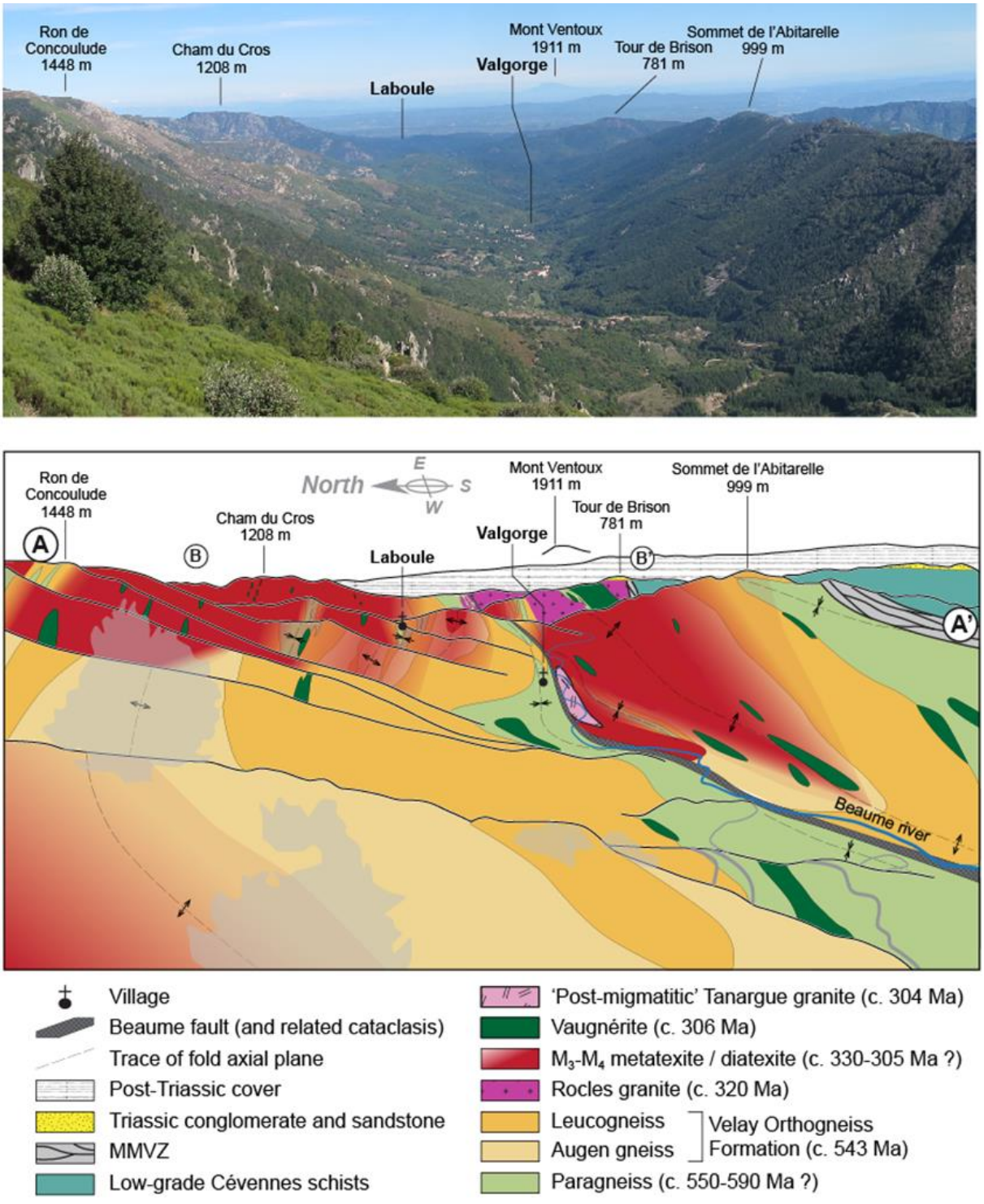

Figure 52 : View from the Col de Meyrand looking towards East (top), with geological interpretation (bottom, after BRGM 1/50 000 map, Sheet 0864 "Largentière"). Letters (A, A', B, B') show the approximate location of the sections presented in **Figure 51**.

Day 4

The Velay Complex is an asymmetric dome (**Figure 54**) bounded by ductile extensional shear zones (detachments), the top-to-the-North Pilat Shear Zone to the North (Malavieille et al., 1990) and the top-to-the-South MMVZ to the South (Bouilhol et al., 2006; stop 3.1). The Eastern side is truncated by the Rhône Valley. The southern and western sides are steeply dipping, to locally overturned to the South (Burg and Vanderhaeghe, 1993; Lagarde et al., 1994; Ledru et al., 2001). The strain pattern of the dome core reflect interaction between ductile vertical wrench shear zones (N—S sinistral and NE—SW dextral), and diapirism (Dupraz and Didier, 1988; Lagarde et al., 1994; Ledru et al., 2001). Altogether, the Velay dome would represent an extensive, partially molten layer formed by lateral flowing of the melt-bearing mid-crust and exhumed during late-orogenic extension (Vanderhaeghe et al., 1999, 2020).

Migmatites of the Velay dome develop at the expense of the main lithologies of the LGU (see Day 3), namely Ediacaran paragneisses (stop 3.2), lithologies of the VOF (augen- and leucogneisses; stops 3.3 and 3.4), and scarce amphibolites. The main regional foliation is reworked by prominent NW-SE to E-W trending asymmetric folds, broadly synchronous with anataxis (see stop 3.5). These lithologies underwent two successive and petrologically distinct stages of melting (Montel et al., 1992; Barbey et al., 1999, 2015) (**Figure 53**):

- A first, so-called « **M3** » **event** at relatively **low temperature (<750 °C)** and pressure above 5 kbar, produced metatexites and developed between 325 and 310 Ma (Montel et al., 1992; Be Mezeme et al., 2006; Bouilhol et al., 2006; S. Couzinié, unpub. data).
- It is followed in time (probably in continuity) by a **higher temperature (750-850°C)** but slightly lower pressure (ca. 4 kbar) « **M4** » **event** characterized by extensive biotite breakdown to melt and cordierite. It results in the generation of the cordierite-bearing Velay granite and diatexite (Weisbrod, 1970; Dupraz and Didier, 1988; Lagarde et al., 1994; Barbey et al., 1999, 2015), dated at 310–300 Ma (Mougeot et al., 1997; Didier et al., 2013; Couzinié et al., 2014; Chelle-Michou et al., 2017; Laurent et al., 2017).

The Velay granite s.s. is very heterogeneous (Dupraz and Didier, 1988; Williamson et al., 1992; Williamson et al., 1997). It ranges from an equigranular medium grained, to heterogeneous, banded or porphyritic granite, to leucogranite, and is always biotite- and cordierite-bearing. Cordierite develops a range of textures (Barbey et al., 1999), from euhedral (stop 4.3) to spectacular quartz-cordierite nodules up to 10 cm across (stops 4.2 and 4.5) and rimmed by a leucocratic quartz-feldspar zone. The granite is generally crowded with metamorphic enclaves of all sizes, from centimeter-long surmicaceous (restite?) enclaves, to rafts of migmatites tens of meters long.

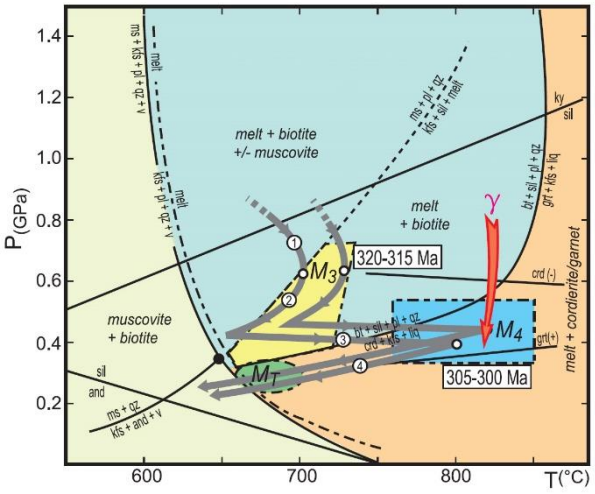

Figure 53 : Summary P–T conditions for the M3 and M4 events of Southern Velay migmatites and proposed evolution (from Barbey et al., 2015).

Due to the volumetric importance of the VOF at the regional scale, a sizeable fraction of migmatites develop at the expense of augen- and leucogneiss. They do however strongly contrast with migmatites developed at the expense of paragneisses. Thermodynamic calculations by Barbey et al. (2015) (**Figure 55**) show that melt volumes and mineral assemblage depends strongly on protolith composition, for instance while biotite remain stable at high temperature in paragneissic migmatite, biotite in leucogneiss is already out before reaching M4 conditions. In the same way, melting fertility varies dramatically from one lithology and paragneiss may produce twice the volume of melt of orthogneiss at M4 conditions. However, this proportion is reverse at lower (M3) temperatures if water-present melting takes place (Couzinié et al., 2021). In addition, strain and melt production interact in different ways in the contrasting lithologies, with melt being more diffuse in orthogneisses, and more readily extracted in fold hinges, shear zones, etc. in paragneisses.

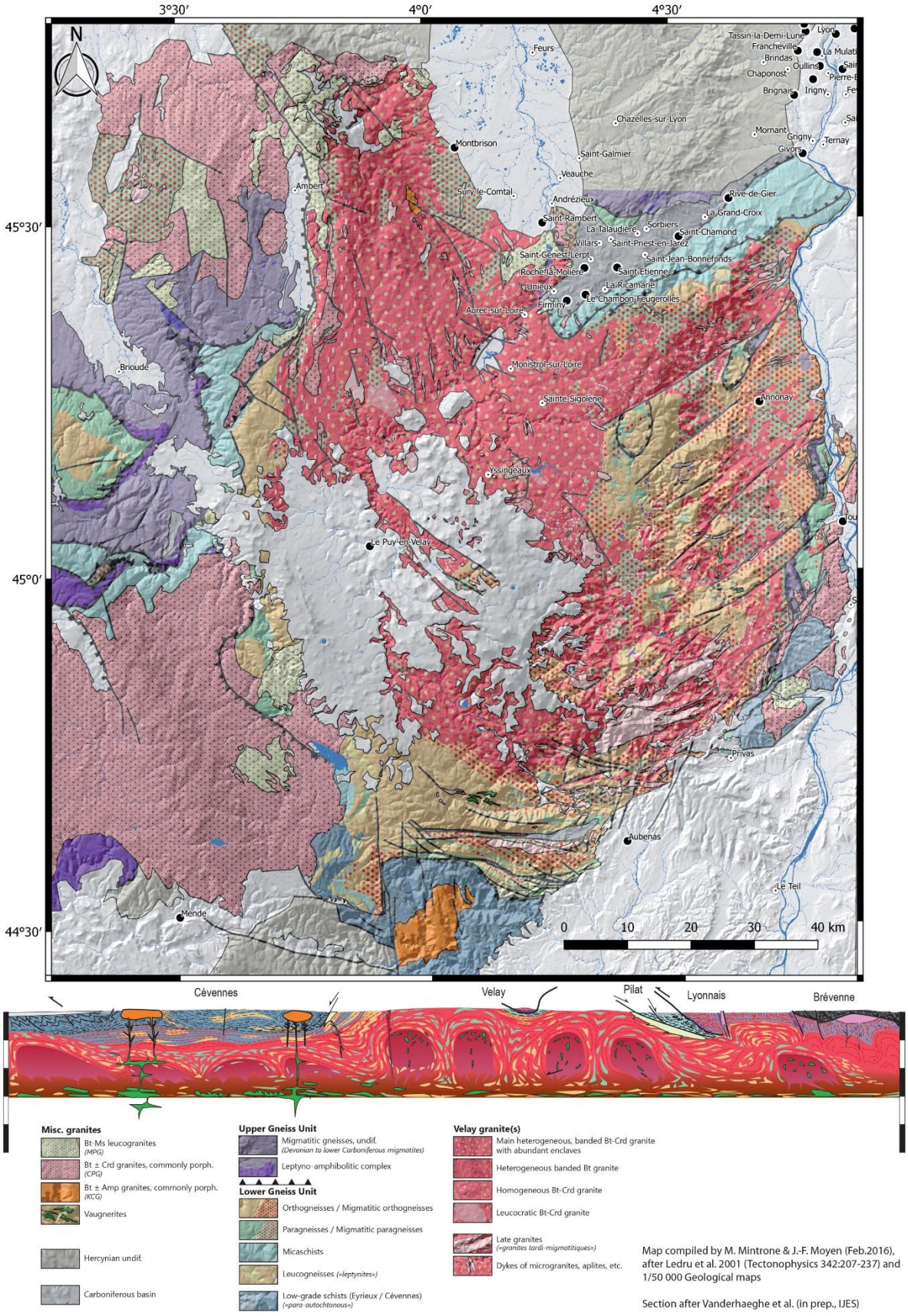

Figure 54 : Geological map (top, after Ledru et al., 2001) and interpretative South–North cross-section (bottom, from Vanderhaeghe et al., 2020) of the Velay dome.

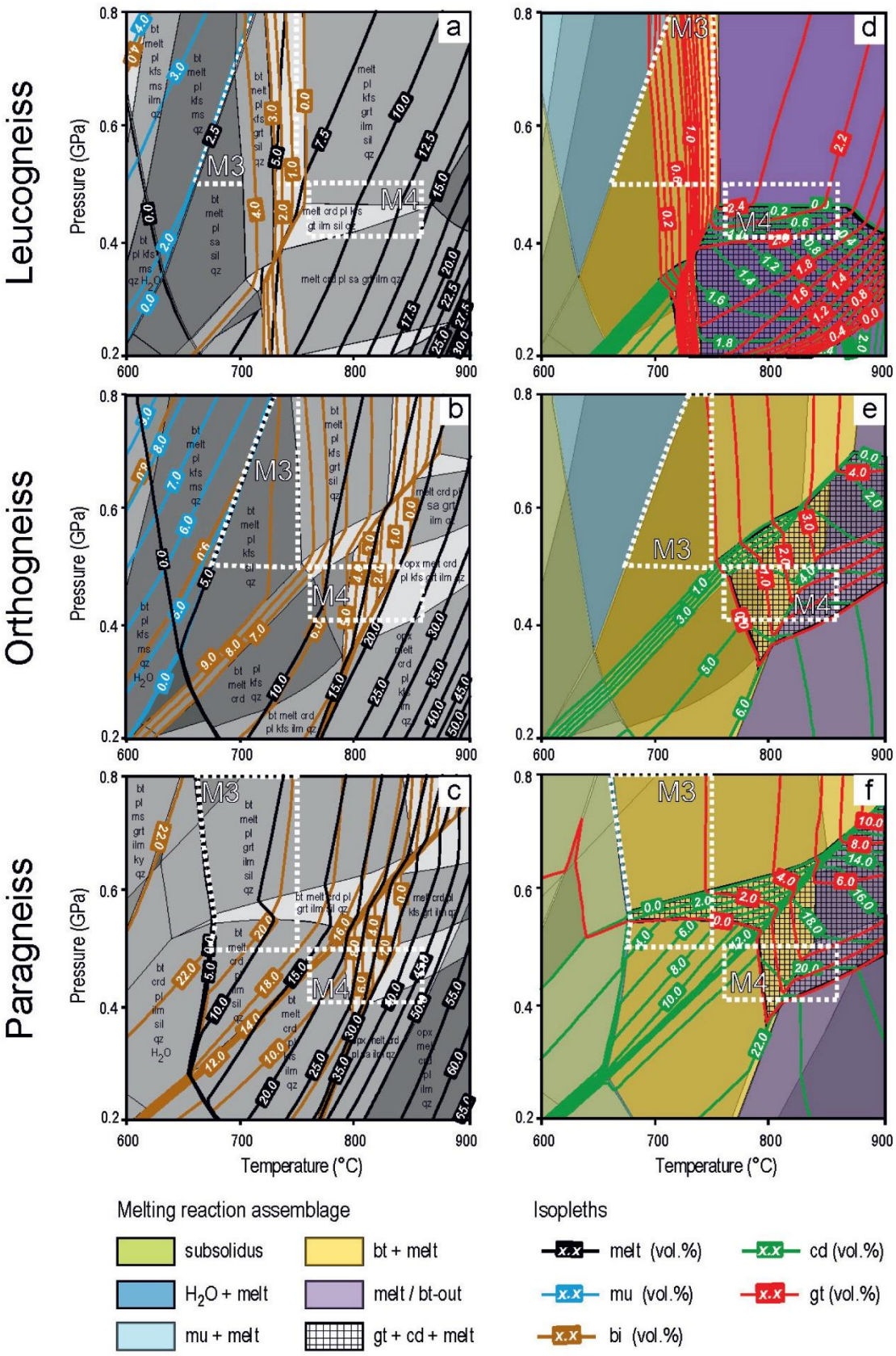

Figure 55 : (a) to (c) Pseudosections with isopleths of muscovite, biotite and melt, calculated using compositions of leucogneiss, orthogneiss and paragneiss. (d) to (f) Simplified pseudosections representing calculated isopleths for garnet and cordierite overlapping simplified assemblage in regard of melting reaction. White doted boxes represents the P-T range of the M3 and M4 events (Montel et al., 1992). From Barbey et al. (2015).

The temperature increase between M3 (<750 °C) and M4 (750-850°C) (**Figure 53** and **Figure 55**) could be related to the emplacement of large volume of granitic magmas produced by melting in the deeper part of the crust (Barbey et al., 2015; Villaros et al, 2018). Deep melting is also suggested by the composition of lower crustal xenoliths exhumed by Cenozoic volcanoes (Leyreloup et al., 1977; Downes et al., 1990; Williamson et al., 1992; Laurent et al., 2023), matching those of higher-pressure (≥8 kbar) melting residues as determined by thermodynamic modelling (Villaros et al., 2018; **Figure 56**a). The magmas extracted from the molten lower crust would either emplace at high crustal levels to produce CPG/MPG granitic plutons; or pond at 5–7 kbar owing to the presence of a physical barrier, probably the VOF, where they provide heat and H_2O upon crystallization to enhance partial melting of the mid-crust and generate the Velay diatexites (Villaros et al., 2018; Couzinié et al., 2021).

This model has been confirmed by recent geochronological data from the lower crustal granulite xenoliths and their comparison with mid- and upper crustal ages (Laurent et al., 2023). Zircons in the granulites show a continuous, 310–265 Ma range of ages correlated to a decrease of Ti contents (**Figure 56**b), indicating continuous cooling in the presence of melt, from the thermal peak at ultra-high temperature conditions (940-970 °C) down to the solidus. This indicates that most of (prograde and peak) melt production and extraction from the lower crust was completed by ca. 310 Ma. This readily explains crystallization ages of 335–310 Ma for upper crustal granites surrounding the Velay dome, consistent with magmas extracted along the prograde path of the lower crust; and the 310–300 Ma range of U-Pb ages in the Velay migmatites, corresponding to cooling and crystallization of the mid-crustal melt-rich layer (**Figure 56**c).

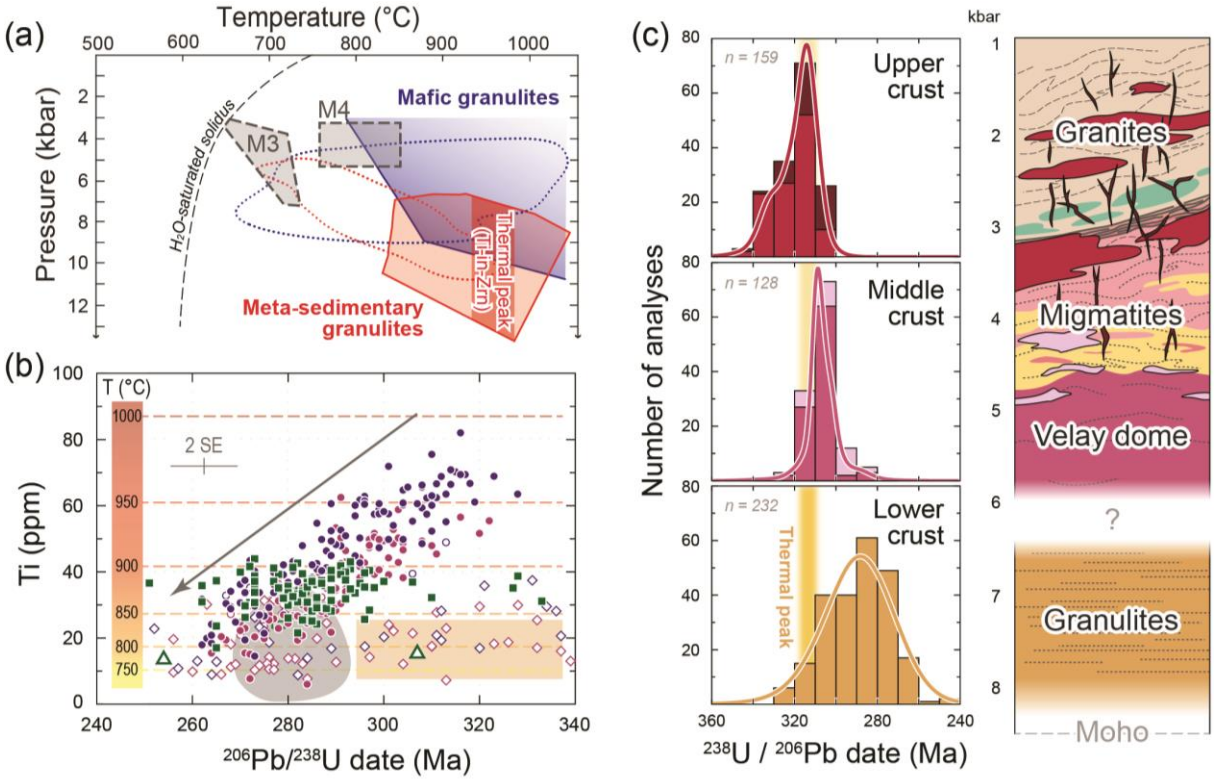

Figure 56 : Summary of investigations on lower crustal granulite xenoliths from the Velay area (modified from Laurent et al., 2023). (a) P–T diagram showing the conditions of equilibration of mafic (blue) and meta-sedimentary (red) granulites compared to M3 and M4 conditions; dashed fields are literature compilations (Leyreloup, 1992) and colored fields are new from this study (peak temperature conditions were obtained using Ti-in-zircon thermometry). (b) Ti vs. age plot for zircons in granulite xenoliths; full symbols are metamorphic zircons whereas empty symbols are detrital/inherited grains. (c) Comparison of U-Pb dates obtained at different crustal levels of the Velay dome.

Based on these results, the Velay Complex is the mid-crustal expression of a massive melting event that affected a large section of the crust. Its formation requires combined accumulation of magma produced by deep melting and nearly in-situ melting. The rheology of the resulting melt-rich mid-crustal layer was controlled by the magmatic liquid, such that it could flow laterally and move upwards to generate the present dome attitude (Burg and Vanderhaeghe, 1993; Vanderhaeghe et al., 1999, 2020).

Exhumation of the dome was probably fast. The ca. 310–300 Ma granites and migmatites (equilibrated at ca. 4 kbar) are cut by dykes of hypovolcanic microgranites whose ages are undistinguishable within uncertainty (between 307 and 297 Ma; Didier et al., 2013), and unconformably overlain by upper Carboniferous (301–295 Ma; Bruguier et al., 2003; Gardien et al., 2022) coal-bearing basins such as the small Prades-Jaujac basin locally and the larger Saint-Étienne and Alès basins on the North and South of the dome, respectively. Biotite ^{40}Ar-^{39}Ar ages of 305–300 Ma on Velay granites (Gardien et al., 2022) also demonstrate fast cooling and exhumation of the dome.

During this day, we will examine the petrological and structural expression of M3 and M4 melting events. The different stops will allow to move to the lower-temperature, M3 migmatites (stop 4.1) to the M3-M4 transition (stop 4.2), to the Velay granite proper (stops 4.3 to 4.5) to investigate the evolution of melting reactions, textures and influences of the pre-existing lithologies. This will allow to discuss broader-scale processes such as the formation of migmatite-granite domes and the nature of the complementary lower crust. An important aim of the day is also to discuss the significance of mantle-derived magmas (vaugnérites) and their role in the mid-crustal metamorphic evolution.

Stop 4.1 – Structures in M3 metatexites at Pont-de-Bayzan

Coordinates: Lat. 44°39’27.2” N; Long. 4°18’17.8” E

Location: bed of the Ardèche river under a footbridge near the crossroads between N102 and D119, ca. 1.5 km NW of Lalevade-d’Ardèche.

The M3 melting event, observed all along the southern margin of the Velay dome, is defined by the formation of biotite-bearing metatexites (Montel et al., 1992) at the expanse of both paragneisses and VOF lithologies. It has been proposed that M3 corresponds to water-fluxed melting (Montel et al., 1992) with reactions in the form quartz + plagioclase ± K-feldspar (depending on the protolith, i.e. para- or orthogneiss) + H_2O = melt. The presence of muscovite in unmolten paragneiss and its absence from M3 migmatites further suggests the contribution of muscovite dehydration melting (muscovite + quartz + plagioclase = Al-silicate + K-feldspar + melt) to melt production (Barbey et al., 1999, 2015). Minor cordierite may have formed at low temperature by incipient biotite breakdown, in particular in paragneiss lithologies (**Figure 55**). M3 melting has been collectively dated through different methods at 325–310 Ma (Aït Malek et al., 1997; Mougeot et al., 1997, Be Mezeme et al., 2006; Couzinié et al., 2014).

The Pont-de-Bayzan outcrop at stop 4.1 is located within the M3 melting “envelope” along the southern margin of the Velay dome (see **Figure 39**) and exhibits excellent examples of M3 migmatites. The main outcrop corresponds to the riverbed exposure under the footbridge (observation points 1 and 2 on **Figure 57**) and comprises two main domains (**Figure 58**):

- The bulk of the outcrop consists of spectacular M3 metatexites developed at the expanse of paragneisses, containing foliation-parallel quartz-feldspar leucosomes and including mica-rich enclaves and grey/greenish calc-silicate fragments. Locally, leucosomes form larger leucocratic and/or pegmatoidal bodies (observation point 2).
- A decametric granitic “corridor” containing large, rounded enclaves of vaugnérite (observation points 1 – and 3 if water level and time permits; **Figure 57**).

Figure 57 : Aerial photograph showing the location of observation points described in text and samples investigated for dating at stop 4.1.

The main components of the outcrop were investigated in detail both by portable XRF and through conventional bulk-rock geochemistry (Cadiou, 2023) (**Figure 59**). Interestingly, leucosomes do not match the composition of modelled melts from the regional paragneisses at M3 conditions, as they are either richer or poorer in K_2O. Therefore, upon crystallization these melts probably segregated a plagioclase-rich (low-K) cumulate (now forming trondhjemitic leucosomes in metatexite) and a K-richer liquid. Metatexites and restitic enclaves are chemically complementary with

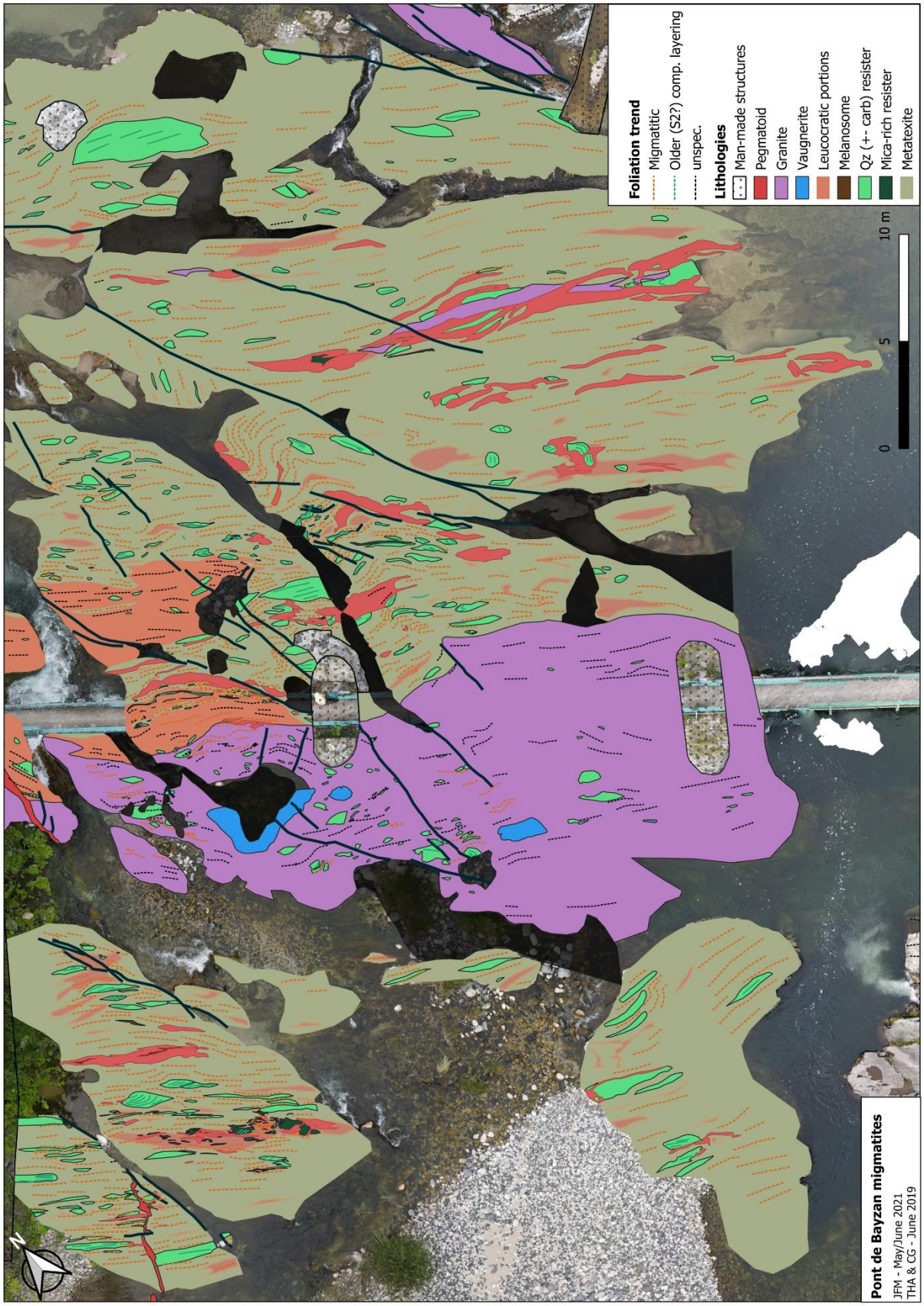

Figure 58 : Geological map of the Pont-de-Bayzan outcrop (corresponding to the area of observation points 1 and 2 of **Figure 57**) obtained by combining drone images with field mapping (J.F. Moyen, unpub. data).

the K-rich leucosomes and range from the composition of the protolith to a more melt-depleted component. The granitic corridor shows an intermediate composition, which could be explained by different processes: (i) restite unmixing, but this would require a very efficient mixing process to reach small-scale homogenization (i.e. at the scale of the volume analyzed by portable XRF, ca. 1 cm^3) ; (ii) a higher degree of melting with the granitic corridor corresponding to an intrusive magma body from a deeper crustal level; (iii) a higher degree of in-situ melting, enhanced locally by the intrusion of hot vaugnérite magmas (likely >1000°C; Montel and Weisbrod, 1986); (iv) mixing between K-rich local melts and the vaugnérite magmas, again requiring efficient homogenization.

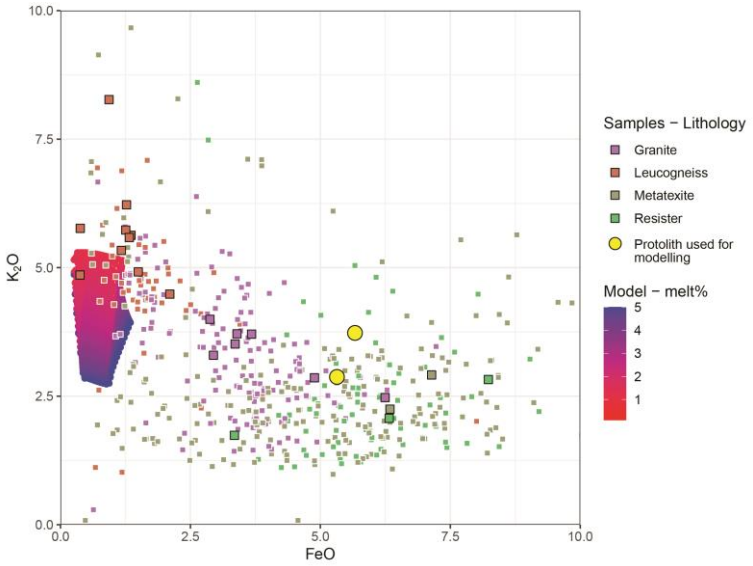

Figure 59 : K_2O vs. FeO diagram highlighting the geochemical variability of the key lithologies of the Pont-de-Bayzan outcrop and comparison with results of thermodynamic modelling (Cadiou, 2023). Data acquired by classical bulk-rock analyses (large squares) are compared to portable XRF data (small squares). The colored field corresponds to modelled melt compositions using different bulk starting H_2O contents between 650 and 800 °C, corresponding in general to H_2O-present melting.

Additionally, a sample of greywacke-like anatectic paragneiss (PdB-16-01; **Figure 57**) was taken from this locality for detrital zircon investigation (Couzinié et al., 2019). The maximum deposition age is ca. 592 Ma, making it the oldest rock dated so far in the E-FMC. In addition to be older than most regional paragneisses (570–550 Ma, see **Figure 45**), it contains a larger proportion of detrital Neoproterozoic (900–600 Ma) zircons with juvenile Hf isotopic compositions (**Figure 60**), possibly indicating a greater contribution of arc-derived material in the detritus.

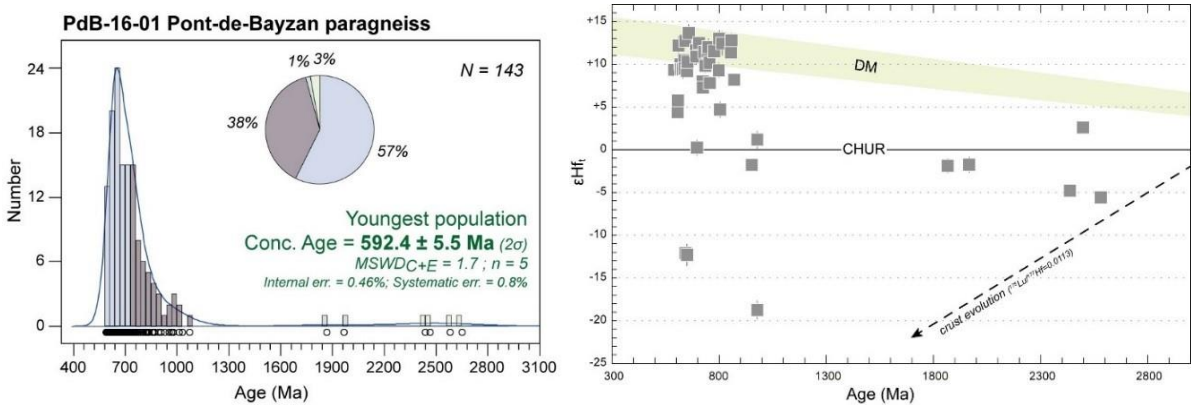

Figure 60 : Detrital zircon U-Pb date distribution of sample PdB-16-01 (left) and combined U-Pb and Lu-Hf isotopic data for the same detrital zircons in a εHf_t vs. age plot (right) (modified from Couzinié et al., 2019).

Migmatitic orthogneiss are exposed along the roadside (observation point 4; **Figure 57**). Although not spectacular, they illustrate the difference in behavior and melt productivity with the adjacent paragneisses. Vaugnérites are also intrusive in orthogneiss but instead of rounded masses, they form dykes a few tens of centimeters thick. One of them (SGC-12-29a) gave an age of 294.4 ± 3.9 Ma (Couzinié et al., 2014), whereas a rounded vaugnérite body in migmatitic paragneiss (SGC-12-26) yielded an age of 306.1 ± 3.0 Ma (Laurent et al., 2017).

Stop 4.2 – M4 diatexite rich in cordierite nodules overprinting M3 migmatites

Coordinates: Lat. 44°43'36.1" N; Long. 4°20'54.0" E

Location: bed of the Volane river ca. 750 m north of Antraigues (le Pont de l'Huile), accessible with a path starting from the D578 road.

The M4 event is defined by the extensive replacement of biotite by cordierite as the main ferromagnesian mineral, together with garnet (± spinel and tourmaline), depending on the rock compositions (Montel et al., 1992; Barbey et al., 2015). M4 migmatites correspond to higher-temperature (750-850 °C) and higher melt volumes than M3. In contrast with M3 metatexites that are clear metatexites, M4 migmatites are generally diatexites characterized by a progressive loss of the structures, more and more pronounced towards the North, i.e. approaching the Velay granite. The main melting reaction is incongruent and consumes biotite + plagioclase + sillimanite + quartz to produce abundant cordierite as the main mineral marker of M4 (± garnet, in particular in VOF lithologies) + K-feldspar + melt (Barbey et al., 1999; 2015). Melting takes place in an essentially extensional environment, synchronous to the development of large-scale upright folds with axial planes parallel to the dome contact (Ledru et al., 2001) and extensional (mainly top-to-the-South) shear zones (Laumonier et al., 1991; Bouilhol et al., 2006).

The outcrop at stop 4.2 is located within the M4 migmatitic envelope marking the transition between the southernmost domain affected by M3, and the Velay granite s.s. (see **Figure 39**). As a result, it shows M3 migmatites (biotite-bearing metatexites) overprinted by M4 leucosomes. The latter either form nearly concordant, quartzo-feldspathic bands; or discordant bodies and patches clearly secant on the foliation of the M3 migmatites defined by biotite. The M4 melting structures are associated with two types of cordierite (Barbey et al., 1999), namely small, prismatic cordierite crystals; or large, cordierite nodules (**Figure 61**). Tourmaline may also occur as subhedral crystals in leucosomes or as thin rims around cordierite nodules.

Prismatic cordierite in M4 leucosomes can be considered in equilibrium with melt and thus as a peritectic mineral, in agreement with biotite dehydration melting reactions. However, the cordierite nodules and "cockades" consist in fact of quartz + cordierite, which is puzzling as quartz is supposed to be a reactant of the melting process. These aggregates are therefore interpreted as late features, resulting from either fluid percolation (Weber et al., 1985) or out-of-equilibrium crystallization associated with diffusion-controlled biotite breakdown in the presence of melt and in the absence of Al-silicate (Barbey et al., 1999). The latter hypothesis would well explain the dendritic textures of some of these aggregates at this locality. The two types of cordierite would thus be markers of "in-source" M4 melts (prismatic cordierite) vs. deeper M4 melts injected in the mid-crust and therefore, overall favor a polybaric origin for the Velay diatexites and granites (Barbey et al., 2015).

Figure 61 : Two types of cordierites at stop 4.3: small, prismatic cordierite in M4 leucosome overprinting faintly foliated M3 (biotite-bearing) migmatites; and large cordierite-quartz nodules present both in and outside the leucosome.

Stop 4.3 – Complex M3/M4 diatexite–granite relationships in the Velay granite

Coordinates: Lat. 44°46'12.3" N; Long. 4°15'35.6" E

Location: roadcut along the D215 road ca. 1 km South of Péreyres.

This stop and the next are in the core of the dome, regionally mapped as Velay granite. As we will see, the granite is extremely heterogeneous in this area, and in fact "true" granite is uncommon. Rather, this region features diatexites together with banded and "dirty" granites, clogged with large rafts of gneisses, migmatites and displaying a variety of metamorphic textures. This is well illustrated by this complex outcrop, which features a range of distinct lithologies (**Figure 62**).

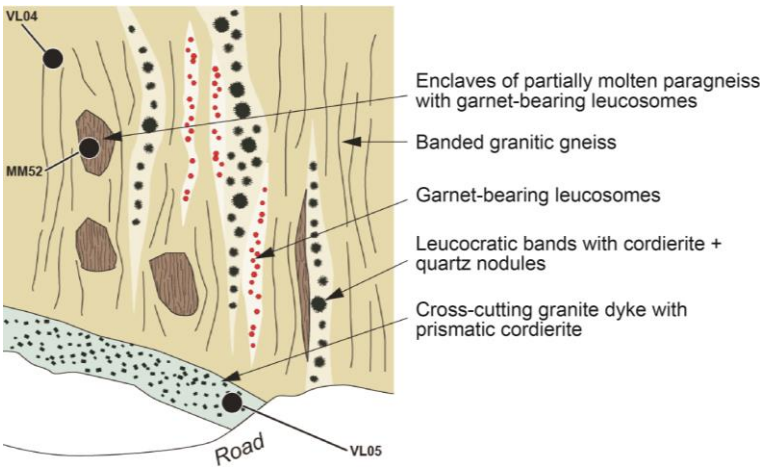

Figure 62 : Sketch of the field relationships between different lithologies at stop 4.3. The locations of dated samples discussed in text (VL04 and VL05) are also indicated.

The dominant rock type on the outcrop is a schlieric, banded granitic gneiss, of diatexitic character. It contains enclaves of darker, foliated paragneisses (similar to the regional, Ediacaran paragneisses) and shows the development of foliation-parallel, garnet-bearing leucosomes. It is unclear whether these relate to M3 or M4 as both events are superimposed in this area. Nonetheless, the leucocratic nature of the host rock suggests that the protolith may have been a leucogneiss, in which case early (M3) melting could have produced garnet (see **Figure 55**). This is partly confirmed by zircon U-Pb dating of one sample (VL04; **Figure 62**), which shows a dominant population at ca. 445 Ma with very few older grains (**Figure 63**). This is quite different from typical VOF lithologies (~545 Ma) and would make this rock a late Ordovician intrusive, uncommon in the LGU. Nevertheless, silicic orthogneisses of that age are commonly reported in the Cévennes domain (Faure et al., 2009a; Couzinié et al., 2022; see Day 1).

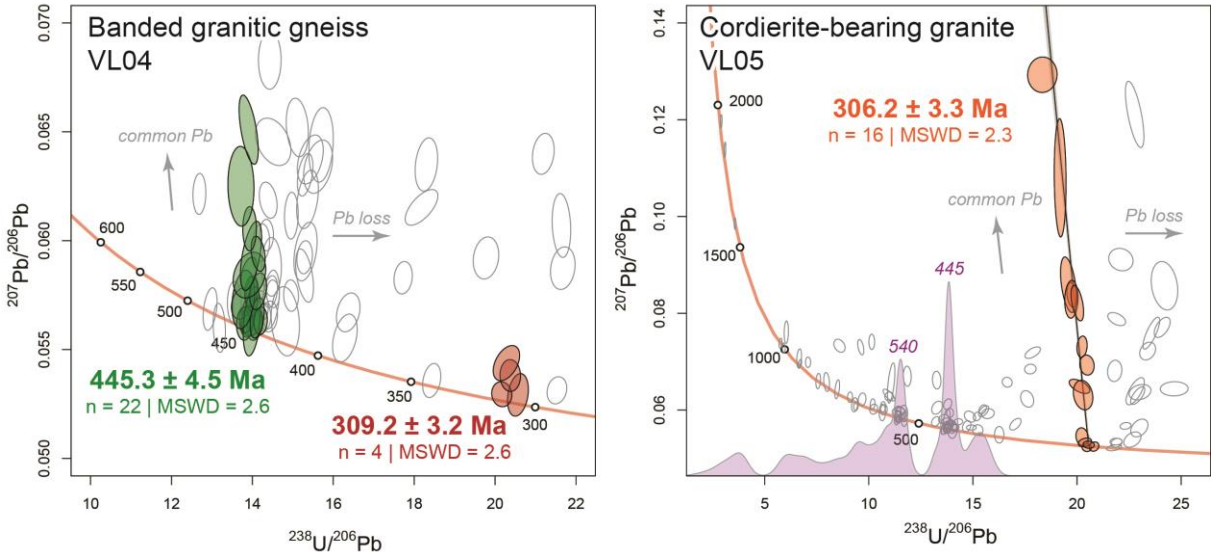

Figure 63 : Tera-Wasserburg diagrams showing U-Pb isotopic data obtained from zircons of samples VL04 and VL05 at stop 4.3 (see **Figure 62**) (C. Chelle-Michou, unpub. data). The red ellipses in VL04 correspond to some analyses of thin zircon rims; the Kernel Density Estimate in VL05 corresponds to the distribution of $^{238}U/^{206}Pb$ ratios from inherited zircon cores.

The garnet-bearing leucosomes are overprinted by M4 melting structures containing two distinct types of cordierite as observed at stop 4.2: (i) quartzo-feldspathic bands containing large cordierite + quartz cockades; (ii) a late dyke of granite containing euhedral, prismatic cordierite. The latter yielded a (poorly defined) zircon LA-ICP-MS U-Pb age of 306.2 ± 3.3 Ma (**Figure 63**). This M4 age is consistent with those obtained from a handful of concordant zircon rims in the banded gneiss (**Figure 63**). Inherited zircon ages in the granite dyke are consistent with those from regional lithologies (detrital grains from Ediacaran paragneisses and ~545 Ma VOF-like zircons) and the local gneiss (~445 Ma population).

Stop 4.4 – Garnet-bearing orthogneiss enclave and vaugnerite in the Velay granite

Coordinates: Lat. 44°46'57.2" N; Long. 4°15'24.2" E

Location: roadcut along the D215 road ca. 750 m North of Péreyres.

This outcrop still illustrates the heterogeneous nature of the Velay granite and uncovers some petrological curiosities associated therewith. This locality exposes a large (ca. 25 m) enclave of migmatitic augen- and leucogneisses, cut by sub-horizontal dykes of Velay granite. The granite itself yielded a monazite LA-ICP-MS U-Th-Pb age of 305.9 ± 1.4 Ma (Couzinié et al., 2014) (**Figure 64**). The most obvious landmark corresponds to a large (50 cm thick) plagioclase + quartz + sillimanite + garnet (and rare biotite) layer with spectacular, cm-sized garnets (**Figure 65**). Garnet is occasionally rimmed by green cordierite.

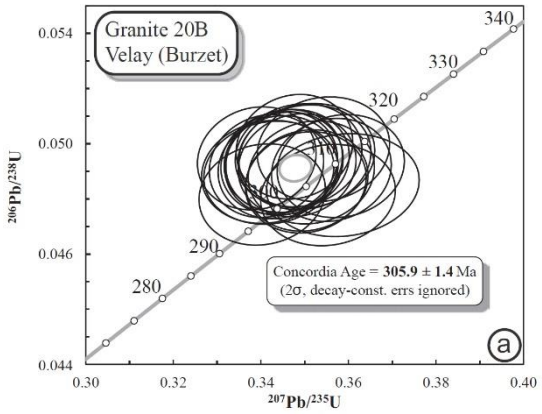

Figure 64 : Concordia diagram showing the results of monazite LA-ICP-MS U-Pb dating from the Velay granite at stop 4.4 (Couzinié et al., 2014).

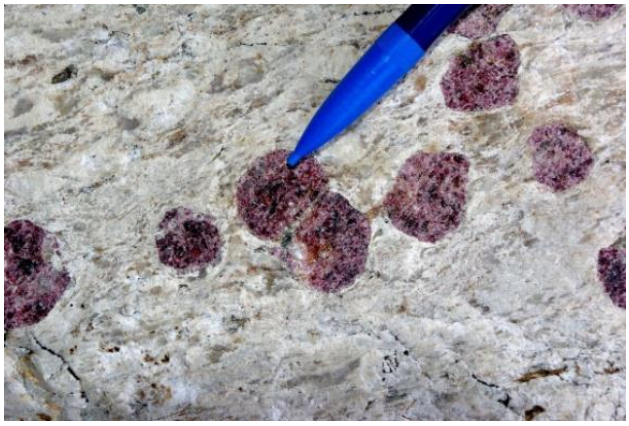

Figure 65 : Centimeter-scale, euhedral garnets in the large quartz + plagioclase + sillimanite band within the migmatitic orthogneiss enclave at stop 4.4.

The origin of the garnet-rich layer is unclear. The quartz shows evidence for high-temperature solid-state deformation, so this rock was solid early in its history (this is not a melt pocket). The garnets are unzoned and Mn-rich (ca. Sps_{20}). Portable XRF data shows that compared to the surrounding orthogneiss, the layer is depleted in both compatible (Cr, Ni, V) and incompatible (Ba, Th, LREE) elements. Speculatively, it could represent a (M4?) melting feature that has lost melt, as supported by the close petrological similarity with deep granulite xenoliths containing plagioclase + quartz + sillimanite + garnet and representing high-temperature melting residues (Laurent et al., 2023).

To the South of the garnet-bearing layer (ca. 100 m down the road), a vaugnérite body is surrounded by a pegmatoidal granitic zone containing biotite blades up to 15 cm long. This kind of pegmatitic aureole is common around vaugnérites in the Velay granite (Barbey et al., 2015) and possibly relates to the crystallisation of the vaugnérite and/or transfer of fluids from the latter. Vaugnérites are post-collisional mafic magmas (PCMM), an ubiquitous group of rocks in the late stages of continental collision since the end of the Archean (Couzinié et al., 2016). These magmas show a dual geochemical character (**Figure 66**): they are magnesian mafic rocks (SiO_2 <60 wt.%; FeO_t+MgO ≥10 wt.%; Mg# up to 70) rich in transition elements (Ni, Cr), but (ultra)potassic (2–8 wt.% K_2O) and rich in all incompatible trace elements. In addition, they show typically "crustal" isotopic signatures, both in terms of zircon Hf–O isotopes (Couzinié et al., 2016) and bulk-rock Sr–Nd isotopes (Turpin et al., 1988), overlapping with the coeval Variscan granitoids. Couzinié et al. (2016) hence proposed that the mantle source of these rocks was enriched by fluids/melts derived from regional continental rocks subducted in the Devonian.

Stop 4.5 – Giant cordierites and residual enclaves in Velay granite

Coordinates: Lat. 44°47'29.1" N; Long. 4°15'32.1" E

Location: bed of a tributary of the Bourges river, beneath a footbridge by the D215 road ca. 2 km North of Péreyres.

At this stop, the heterogeneous Velay granite is particularly rich in enclaves and cut by late homogeneous granite dykes (**Figure 67**a). The Velay granite contains the two, typical cordierite types: the classical cordierite + quartz cockades as well as crystals of (or pseudomorphs after) euhedral cordierite, particularly large at this locality (up to 5 cm across).

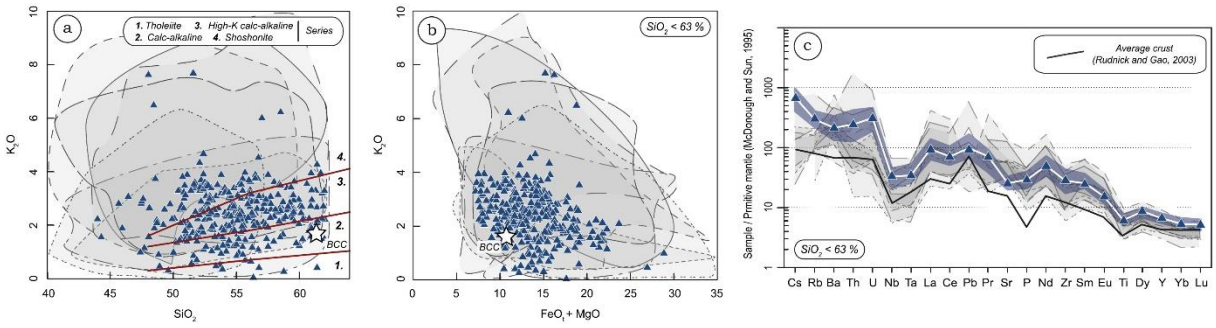

Figure 66 : Some geochemical characteristics of the E-FMC vaugnérites (blue triangles) and other PCMM from various orogenic systems worldwide (various fields; modified after Couzinié et al., 2016). (a) K2O vs. SiO2 and (b) K2O vs. FeOt+MgO diagrams; (c) Incompatible trace element concentrations plotted in multi-element pattern normalized to primitive mantle.

The enclaves in this area correspond to high-grade restitic material, probably sourced from deeper crustal levels, which are otherwise uncommon in the dome. A few km to the SW, such enclaves contain either (i) sillimanite + quartz + K-feldspar + plagioclase + corundum; or (ii) biotite + plagioclase + hercynite + garnet + corundum (Montel, 1985). This corresponds to decompression from ca. 10 kbar and 750 °C to 5–6 kbar, and could record fast ascent of an enclave-rich granite during the earliest stages of the dome formation.

At stop 4.4, the enclaves miss corundum and spinel but comprise: (i) “black restite” mainly composed of biotite + sillimanite; and (ii) “green restite” mainly made of cordierite + biotite + plagioclase + sillimanite + garnet + apatite ± ilmenite, with very few K-feldspar and quartz (<1 vol.%). A sample of such “green restite” (MM62; **Figure 67**b) was selected for petrological studies (Mintrone, 2016). In thin section, the rock is characterized by two very different textural domains corresponding to early M3 paragenesis partly overprinted by a higher-temperature M4 association (**Figure 68**a–d):

Figure 67 : (a) Field relationships at stop 4.5, with a granitic dyke cutting across the heterogeneous enclave-rich Velay granite; (b) Detail of the restitic enclaves and sampling site of sample MM62 discussed in text.

- Domain 1, a well-equilibrated texture of mainly polygonal plagioclase with biotite, garnet, sillimanite and very rare quartz and K-feldspar. These domains are similar to M3 parageneses in paragneisses (Barbey et al., 1999), and resemble the garnet-bearing layers at stop 4.3.
- Domain 2 consists of cordierite + biotite + plagioclase + sillimanite + garnet + ilmenite ± apatite ± K-feldspar and quartz. Cordierite is very abundant (up to 30 vol.%) and forms either anhedral grains associated with corroded sillimanite, plagioclase and biotite, consistently with the biotite dehydration melting reaction; or coronas around garnet, a classical decompression texture Biotite ranges from euhedral to partly resorbed, surrounded by cordierite and plagioclase. The plagioclase sometimes contains cordierite and sillimanite inclusions. Domain 2 assemblages overgrow domain 1 and could thus be attributed to M4.

Thermodynamic modelling points to P–T conditions for the peak assemblage of domain 2 between 730 and 830 °C (constrained by TiO_2 in biotite) and pressure between 5.3 and 6.3 kbar (**Figure 69**).

These conditions are consistent with the garnet-plagioclase barometer (Caddick et al., 2010) that yields pressures between 5.0 and 7.5 kbar for temperatures of 740–850°C. The retrograde part of the P–T path, defined by the increasing cordierite and decreasing garnet proportions (in agreement with textural relationships), records decompression and cooling to 600–700 °C and 3–4 kbar. The whole P–T evolution is at supra-solidus conditions, such that the rock must have lost substantial amounts of melt.

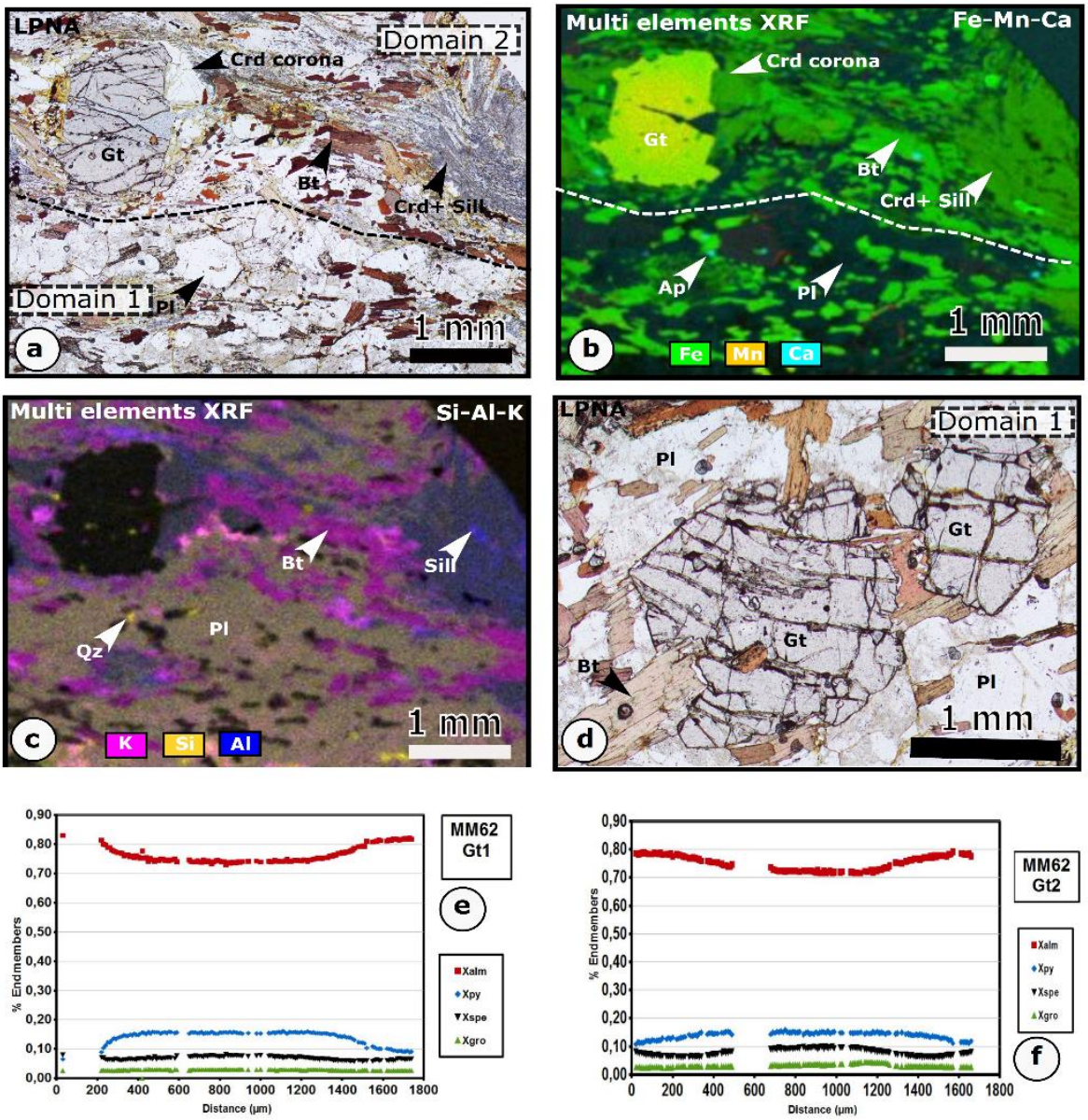

Figure 68 : Petrology of restite enclave MM62 from stop 4.5. (a) PPL view showing the two types of domains (1 and 2); (b) and (c) micro-XRF maps of the same area; (d) Close-up view of a Domain 1 garnet; (e) and (f) Zonation profiles across garnets in domain 1 and 2, respectively. From Mintrone (2016).

Garnet shows very similar composition and zoning profiles in both domains (**Figure 68**e–f). Using the diffusion rate of Fe, Mg, Ca and Mn, the duration necessary to reproduce this zoning can be determined (Caddick et al., 2010). This approach was applied to garnet from MM62 (Mintrone, 2016), using the above constrained P–T path (**Figure 70**). Although the prograde path cannot be accurately constrained, relict zoning in garnet is consistent with a maximum heating duration of ca. 5–15 Ma. The preservation of garnet zonation requires a time spent at peak temperature no longer than 1 Ma. The duration of the retrograde path is constrained to ca. 1 to 10 Ma. The entire duration of the P–T path for this sample is therefore between 7 and 26 Ma. This timing is in good agreement with the general temporal evolution of the Velay migmatites, with M3 dated between 325 and 310 Ma; and M4 between 310 and 300 Ma.

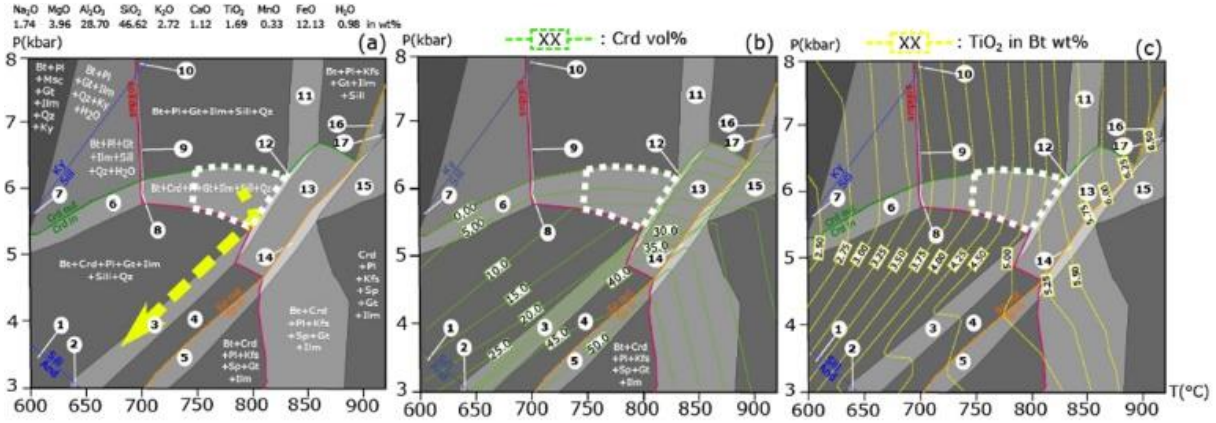

Figure 69 : Results of thermodynamic modelling for sample MM62 as P–T pseudosection including the proposed peak field for domain 2 and P–T path (a); and contoured with isopleths of cordierite proportion (b) and biotite TiO_2 content (c). From Mintrone (2016).

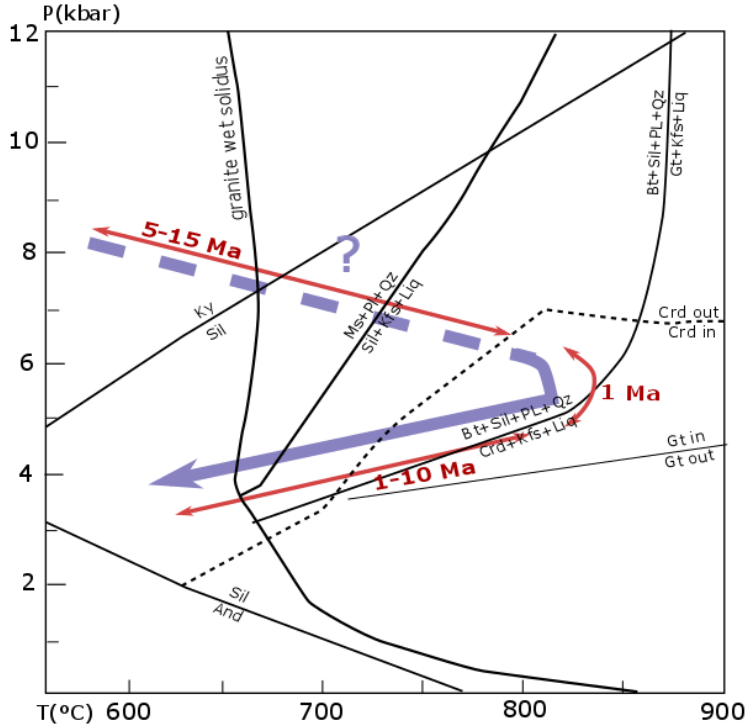

Figure 70 : Synthetic P–T path obtained from sample MM62 at stop 4.5, on which the approximate durations of each part of the path obtained by garnet speedometry are indicated (Mintrone, 2016).

References

Aït Malek, H., 1997. Pétrologie, géochimie et géochronologie U/Pb d'associations acides-basiques: exemples du SE du Velay (Massif central français) et de l'Anti-Atlas occidental (Maroc). Unpubl. Ph.D. thesis, Institut National Polytechnique de Lorraine, Nancy, 297 p.p.

Appleby, S.K. et al., 2009. Do S-type granites commonly sample infracrustal sources? New results from an integrated O, U–Pb and Hf isotope study of zircon. Contributions to Mineralogy and Petrology, 160(1): 115-132.

Arnaud, F., Boullier, A. and Burg, J., 2004. Shear structures and microstructures in micaschists: the Variscan Cévennes duplex (French Massif Central). Journal of Structural Geology, 26(5): 855-868.

Ballèvre, M. et al., 2014. Correlation of the nappe stack in the Ibero-Armorican arc across the Bay of Biscay: a joint French–Spanish project. Geological Society, London, Special Publications, 405(1): 77-113.

Barbarand, J., Lucazeau, F., Pagel, M. and Séranne, M., 2001. Burial and exhumation history of the south-eastern Massif Central (France) constrained by apatite fission-track thermochronology. Tectonophysics, 335(3): 275-290.

Barbarin, B., 1988. Field Evidence for Successive Mixing and Mingling between the Piolard Diorite and the Saint-Julien-La-Vetre Monzogranite (Nord-Forez, Massif Central, France). Canadian Journal of Earth Sciences, 25(1): 49-59.

Barbarin, B., 1999. A review of the relationships between granitoid types, their origins and their geodynamic environments. Lithos, 46(3): 605-626.

Barbey, P. et al., 1999. Cordierite growth textures and the conditions of genesis and emplacement of crustal granitic magmas: the Velay granite complex (Massif Central, France). Journal of Petrology, 40(9): 1425-1441.

Barbey, P., Villaros, A., Marignac, C. and Montel, J.M., 2015. Multiphase melting, magma emplacement and P-T-time path in late-collisional context: the Velay example (Massif Central, France). Bulletin De La Societe Geologique De France, 186(2-3): 93-116.

Be Mezeme, E., Cocherie, A., Faure, M., Legendre, O. and Rossi, P., 2006. Electron microprobe monazite geochronology of magmatic events: example from variscan migmatites and granitoids, Masif Central, France. lithos, 87: 276-288.

Be Mezeme, E., Faure, M., Chen, Y., Cocherie, A. and Talbot, J.Y., 2007. Structural, AMS and geochronological study of a laccolith emplaced during Late Variscan orogenic extension: the Rocles pluton (SE French Massif Central). International Journal of Earth Sciences, 96(2): 215-228.

Bea, F., Montero, P. and Molina, J.F., 1999. Mafic precursors, peraluminous granitoids, and late lamprophyres in the Avila batholith: a model for the generation of Variscan batholiths in Iberia. The Journal of geology, 107(4): 399-419.

Bébien, J., 1970. Etude pétrographique et géochimique des formations volcaniques dévono-dinantiennes de l'extrémité sud-ouest du faisceau synclinal du Morvan. , Nancy.

Benmammar, A., Berger, J., Triantafyllou, A., Duchene, S., Bendaoud, A., Baele, J.-M., Bruguier, O., Diot, H., 2020. Pressure-temperature conditions and significance of Upper Devonian eclogite and amphibolite facies metamorphisms in southern French Massif central. Bulletin de la Société Géologique de France 191(1), 28.

Berger, J., Femenias, O., Mercier, J.-C. and Demaiffe, D., 2006. A Variscan slow-spreading ridge (MOR-LHOT) in Limousin (French Massif Central): magmatic evolution and tectonic setting inferred from mineral chemistry. Mineralogical magazine, 70(2): 175-185.

Bernard-Griffiths, J. and Jahn, B.-M., 1981. REE geochemistry of eclogites and associated rocks from Sauviat-sur-Vige, Massif Central, France. Lithos, 14: 263-274.

Bernard-Griffiths, J., Gebauer, D., Grünenfelder, M. and Piboule, M., 1985. The tonalite belt of Limousin (French Central Massif): U-Pb zircon ages and geotectonic implications. Bull Soc Geol Fr, 8(14): 523-529.

Bouchot, V., Milési, J.P., Lescuyer, J.L. and Ledru, P., 1997. Les minéralisations aurifères de la France dans leur cadre géologique autour de 300 Ma. Chroniques de la Recherche Minière, 528(13-62).

Bouilhol, P., Leyreloup, A.F., Delor, C., Vauchez, A. and Monié, P., 2006. Relationships between lower and upper crust tectonic during doming: the mylonitic southern edge of the Velay metamorphic core complex (Cévennes-French Massif Central). Geodinamica Acta, 19(3-4): 137-153.

Briand, B., Piboule, M., Santallier, D. and Bouchardon, J., 1991. Geochemistry and tectonic implications of two Ordovician bimodal igneous complexes, southern French Massif Central. Journal of Geological Society, 148(6): 959.

Brichau, S., Respaut, J.P. and Monié, P., 2008. New age constraints on emplacement of the Cévenol granitoids, South French Massif Central. International Journal of Earth Sciences, 97(4): 725-738.

Brouder, P., 1963. Description d'une succession lithologique avec niveaux-repères dans les schistes cristallins des Cévennes près de Villefort (Lozère). Bullertin de la Société Géologique de France 7, 828-834.

Bruguier, O. et al., 2003. Application of in situ zircon geochronology and accessory phase chemistry to constraining basin development during post-collisional extension: a case study from the French Massif Central. Chemical Geology, 201(3-4): 319-336.

Burg, J.-P. and Matte, P., 1978. A cross section through the French Massif Central and the scope of its Variscan geodynamic evolution. Zeitschrift der Deutschen Geologischen Gesellschaft, 129: 429-460.

Burg, J.-P. and Vanderhaeghe, O., 1993. Structures and way-up criteria in migmatites, with application to the Velay dome (French Massif Central). Journal of structural geology, 15(11): 1293-1301.

Burg, J., Matte, P., Leyreloup, A. and Marchand, J., 1984. Inverted metamorphic zonation and large-scale thrusting in the Variscan Belt: an example in the French Massif Central. Geological Society, London, Special Publications, 14(1): 47-61.

Burg, J.P., Brun, J.P. and Vandendriessche, J., 1990. The Sillon-Houiller (French Massif-Central) - a Transfer Fault during Crustal Thinning of the Variscan Belt. Comptes Rendus De L Academie Des Sciences Serie Ii, 311(1): 147-152.

Caddick, M.J., Konopásek, J. and Thompson, A.B., 2010. Preservation of garnet growth zoning and the duration of prograde metamorphism. Journal of Petrology, 51(11): 2327-2347.

Cadiou, R., 2023. Migmatite : une évolution en système ouvert à l'origine d'un affleurement composite. M.Sc. thesis, Université Clermont Auvergne, Clermont-Ferrand.

Caen-Vachette, M., 1979. Age cambrien des rhyolites transformées en leptynites dans la série mé tamorphique du Pilat (Massif Central francais). CR Acad. Sci. Paris, 289: 997-1000.

Caron, C., 1994. Les minéralisations Pb-Zn associées au Paléozoïque inférieur d'Europe méridionale. Traçage isotopique Pb-Pb es gîtes de l'Iglésiente (SW Sardaigne) et des Cévennes, et évolution du socle enacissant par la géochronologie U-Pb, Ar-Ar et K-Ar, Université de Montpellier II.

Cartannaz, C. et al., 2007. Characterization of wrench tectonics from dating of syn-to post-magmatism in the north-western French Massif Central. International Journal of Earth Sciences, 96(2): 271-287.

Chantraine, J., Autran, A. and Cavelier, C., 1996. Carte géologique de la France à l'échelle du millionième (6e édition), BRGM, Orléans.

Charbonnier, S., Vannier, J., Gaillard, C., Bourseau, J.-P. and Hantzpergue, P., 2007. The La Voulte Lagerstätte (Callovian): evidence for a deep water setting from sponge and crinoid communities. Palaeogeography, Palaeoclimatology, Palaeoecology, 250(1): 216-236.

Charonnat, X., 2000. Les minéralisations aurifères tardi-hercyniennes des Cévennes (Massif central français): cadre structural, gîtologie et modélisation 3D, Orléans.

Charonnat, X., Chauvet, A., Faure, M., 1999. Contexte structural des minéralisations aurifères tardi-hercyniennes des Cévennes (Massif central français). Comptes-Rendus de l'Académie des Sciences, Paris, Sciences de la terre et des planètes 328, 463-469.

Chauvet, A., Volland-Tuduri, N., Lerouge, C., Bouchot, V., Monié, P., Charonnat, X., Faure, M., 2012. Geochronological and geochemical characterization of magmatic-hydrothermal events within the Southern Variscan external domain (Cévennes area, France). International Journal of Earth Sciences 101(1), 69-86.

Chelle-Michou, C., Laurent, O., Moyen, J.-F., Block, S., Paquette, J.-L., Couzinié, S., Gardien, V., Vanderhaeghe, O., Villaros, A., Zeh, A., 2017. Pre-Cadomian to late-Variscan odyssey of the eastern Massif Central, France: formation of the West European crust in a nutshell. Gondwana Research, 46: 170-190.

Clark, C., Fitzsimons, I.C.W., Healy, D. and Harley, S.L., 2011. How Does the Continental Crust Get Really Hot? Elements, 7(4): 235-240.

Collins, W.J. and Richards, S.W., 2008. Geodynamic significance of S-type granites in circum-Pacific orogens. Geology, 36(7): 559.

Couzinié, S., 2017. Evolution of the continental crust and significance of the zircon record, a case study from the French Massif Central. PhD thesis Thesis, Université Jean-Monnet, Saint-Etienne & Stellenbosch University.

Couzinié, S., Moyen, J.-F., Villaros, A., Paquette, J.-L., Scarrow, J.H., Marignac, C., 2014. Temporal relationships between Mg-K mafic magmatism and catastrophic melting of the Variscan crust in the southern part of the Velay Complex (Massif Central, France). Journal of Geosciences 59(1-4), 1-18.

Couzinié, S., Laurent, O., Moyen, J.-F., Zeh, A., Bouilhol, P., Villaros, A., 2016. Post-collisional magmatism: Crustal growth not identified by zircon Hf–O isotopes. Earth and Planetary Science Letters, 456: 182-195.

Couzinié, S., Laurent, O., Poujol, M., Mintrone, M., Chelle-Michou, C., Moyen, J.-F., Bouilhol, P., Vezinet, A., Marko, L., 2017. Cadomian S-type granites as basement rocks of the Variscan belt (Massif Central, France): Implications for the crustal evolution of the north Gondwana margin. Lithos, 286-287: 16-34.

Couzinié, S., Laurent, O., Chelle-Michou, C., Bouilhol, P., Paquette, J.-L., Gannoun, A.-M., Moyen, J.-F., 2019. Detrital zircon U–Pb–Hf systematics of Ediacaran metasediments from the French Massif Central: Consequences for the crustal evolution of the north Gondwana margin. Precambrian Research 324, 269-284.

Couzinié, S., Bouilhol, P., Laurent, O., Marko, L., Moyen, J.-F., 2021. When zircon drowns: Elusive geochronological record of water-fluxed orthogneiss melting in the Velay dome (Massif Central, France). Lithos 384, 105938.

Couzinié, S., Bouilhol, P., Laurent, O., Grocolas, T., Montel, J.-M., 2022. Cambro–Ordovician ferrosilicic magmatism along the northern Gondwana margin: constraints from the Cézarenque–Joyeuse gneiss complex (French Massif Central). Bulletin de la Société Géologique de France 193(1), 15.

Dabard, M.P., Loi, A. and Peucat, J.J., 1996. Zircon typology combined with Sm-Nd whole-rock isotope analysis to study Brioverian sediments from the Armorican Massif. Sedimentary Geology, 101: 243-260.

Denis, E. and Dabard, M.P., 1988. Sandstone petrography and geochemistry of late Proterozoic sediments of the Armorican Massif (France) – A key

to basin development during the Cadomian orogeny Precambrian Research, 42: 189-206.

Didier, A. et al., 2013. Disturbance versus preservation of U–Th–Pb ages in monazite during fluid–rock interaction: textural, chemical and isotopic in situ study in microgranites (Velay Dome, France). Contributions to Mineralogy and Petrology: 1-22.

Didier, J. and Barbarin, B., 1991. Enclaves and Granite Petrology. Elsevier, Amsterdam.

Downes, H., Dupuy, C. and Leyreloup, A.F., 1990. Crustal Evolution of the Hercynian Belt of Western-Europe - Evidence from Lower-Crustal Granulitic Xenoliths (French Massif-Central). Chemical Geology, 83(3-4): 209-231.

Downes, H., Shaw, A., Williamson, B.J. and Thirlwall, M.F., 1997. Sr, Nd and Pb isotopic evidence for the lower crustal origin of Hercynian granodiorites and monzogranites, Massif Central, France (vol 136, pg 99, 1997). Chemical Geology, 140(3-4): 289-289.

Dupraz, J. and Didier, J., 1988. Le complexe anatectique du Velay (Massif Central francais): structure d'ensemble et évolution géologique:. Bulletin du BRGM, v. Série "Géologie de la France" : . 73-88.

Duthou, J.L., Cantagrel, J.M., Didier, J. and Vialette, Y., 1984. Paleozoic Granitoids from the French Massif Central - Age and Origin Studied by Rb-87-Sr-87 System. Physics of the Earth and Planetary Interiors, 35(1-3): 131-144.

Farina, F., Stevens, G., Gerdes, A. and Frei, D., 2014. Small-scale Hf isotopic variability in the Peninsula pluton (South Africa): the processes that control inheritance of source 176Hf/177Hf diversity in S-type granites. Contributions to Mineralogy and Petrology, 168.

Faure, M., Charonnat, X. and Chauvet, A., 1999. Schéma structural et évolution tectonique du domaine para-autochtone cévenol de la chaîne hercynienne (Massif central français). Comptes Rendus de l'Académie des Sciences-Series IIA-Earth and Planetary Science, 328(6): 401-407.

Faure, M. et al., 2001. Tectonic evolution of the Cévennes para-autochtonous domain of the Hercynian French Massif Central and its bearing on ore deposits formation. Bulletin De La Societe Geologique De France, 172(6): 687-696.

Faure, M., Brouder, P., Thierry, J., Alabouvette, B., Cocherie, A., Bouchot, V., 2009a. Notice explicative, Carte géol. France (1/50 000), feuille Saint-André-de-Valborgne (911). Orléans : BRGM, 138 p. Carte géologique par Brouder, P., Alabouvette, B., Faure, M. (2009).

Faure, M., Lardeaux, J.M. and Ledru, P., 2009b. A review of the pre-Permian geology of the Variscan French Massif Central. Comptes Rendus Geosciences, 341(2-3): 202-213.

Fernández-Suárez, J., Gutiérrez-Alonso, G., Jenner, G.A. and Tubrett, M.N., 2000. New ideas on the Proterozoic-Early Palaeozoic evolution of NW Iberia: insights from U–Pb detrital zircon ages. Precambrian Research, 102: 185-206.

Feybesse, J.-L. et al., 1988. La série de la Brévenne (Massif central français): une unité dévonienne charriée sur le complexe métamorphique des Monts du Lyonnais à la fin de la collision varisque. Comptes rendus de l'Académie des sciences. Série 2, Mécanique, Physique, Chimie, Sciences de l'univers, Sciences de la Terre, 307(8): 991-996.

Finger, F., Roberts, M.P., Haunschmid, B., Schermaier, A. and Steyrer, H.P., 1997. Variscan granitoids of central Europe: their typology, potential sources and tectonothermal relations. Mineralogy and Petrology, 61(1-4): 67-96.

François, T., 2009. Contraintes géochimiques et géochronologiques sur l'origine et la mise en place des granites du Mont Lozère, Université des Sciences et Techniques du Languedoc (Montpellier II), 39 pp.

Franke, W., 2014. Topography of the Variscan orogen in Europe: failed–not collapsed. International Journal of Earth Sciences, 103(5): 1471-1499.

Gardien, V., 1993. Les reliques pétrologiques de haute à moyenne pression des séroies du Vivarais oriental (Est du Massif Central Français). Comptes Rendus de l'Academie des Sciences Serie IIa:Sciences de la Terre et des Planets, 316: 1247-1254.

Gardien, V., Tegyey, M., Lardeaux, J.-M., Misseri, M. and Dufour, E., 1990. Crust–mantle relationships in the French Variscan chain: the examples of the southern Monts du Lyonnais unit (eastern French Massif Central). journal of Metamorphic Geology, 8: 447-492.

Gardien, V. et al., 2011. Thermal maturation and exhumation of a middle orogenic crust in the Livradois area (French Massif Central). Bulletin De La Societe Geologique De France, 182(1): 5-24.

Gardien, V., Martelat, J.-E., Leloup, P.-H., Mahéo, G., Bevillard, B., Allemand, P., Monié, P., Paquette, J.-L., Grosjean, A.-S., Faure, M., Chelle-Michou, C., Fellah, C., 2022. Fast exhumation rate during late orogenic extension: The new timing of the Pilat detachment fault (French Massif Central, Variscan belt). Gondwana Research 103, 260-275.

Garfunkel, Z., 2015. The relations between Gondwana and the adjacent peripheral Cadomian domain—Constrains on the origin, history, and paleogeography of the peripheral domain. Gondwana Research, 28(4): 1257-1281.

Griffin, W. et al., 2000. The Hf isotope composition of cratonic mantle: LAM-MC-ICPMS analysis of zircon megacrysts in kimberlites. Geochimica et Cosmochimica Acta, 64(1): 133-147.

Gutiérrez-Alonso, G., Gutiérrez-Marco, J., Fernández-Suárez, J., Bernárdez, E. and Corfu, F., 2016. Was there a super-eruption on the Gondwanan coast 477Ma ago? Tectonophysics, 681: 85-94.

Henk, A., Von Blanckenburg, F., Finger, F., Schaltegger, U. and Zulauf, G., 2000. Syn-convergent high-temperature metamorphism and magmatism in the Variscides: a discussion of potential heat sources. Geological Society, London, Special Publications, 179(1): 387-399.

Holub, F.V., 1997. Ultrapotassic plutonic rocks of the durbachite series in the Bohemian Massif: petrology,

geochemistry and petrogenetic interpretation. Sborník geologických vìd, Ložisková geologie–mineralogie, 31: 5-26.

Janoušek, V., Bowes, D., Rogers, G., Farrow, C.M. and Jelínek, E., 2000. Modelling diverse processes in the petrogenesis of a composite batholith: the Central Bohemian Pluton, Central European Hercynides. Journal of Petrology, 41(4): 511.

Kroner, U. and Romer, R.L., 2013. Two plates — Many subduction zones: The Variscan orogeny reconsidered. Gondwana Research, 24: 289-329.

Lagarde, J.-L., Dallain, C., Ledru, P. and Courrioux, G., 1994. Strain patterns within the late Variscan granitic dome of Velay, French Massif Central. Journal of Structural Geology, 16(6): 839-852.

Lardeaux, J.M., Ledru, P., Daniel, I. and Duchene, S., 2001. The Variscan French Massif Central - a new addition to the ultrahigh pressure metamorphic 'club': exhumation processes and geodynamic consequences. Tectonophysics, 332(1-2): 143-167.

Lardeaux, J.M. et al., 2014. The Moldanubian Zone in the French Massif Central, Vosges/Schwarzwald and Bohemian Massif revisited: differences and similarities. In: K. Schulmann, J.R. Martinez Catalan, J.M. Lardeaux, V. Janousek and G. Oggiano (Editors), The Variscan Orogeny: Extent, Timescale and the Formation of the European Crust. Special publications. Geological Society, London.

Laurent, O., Couzinié, S., Zeh, A., Vanderhaeghe, O., Moyen, J.-F., Villaros, A., Gardien, V., Chelle-Michou, C., 2017. Protracted, coeval crust- and mantle melting during Variscan late-orogenic evolution: zircon U-Pb dating in the eastern French Massive Central. International Journal of Earth Sciences, 106(2): 421-451.

Laurent, O., Couzinié, S., Doucet, L.S., 2023. Timescales of ultra-high temperature metamorphism and crustal differentiation: Zircon petrochronology from granulite xenoliths of the Variscan French Massif Central. Earth and Planetary Science Letters 611, 118133.

Leach, D. et al., 2006. Precipitation of lead–zinc ores in the Mississippi Valley-type deposit at Trèves, Cévennes region of southern France. Geofluids, 6(1): 24-44.

Ledru, P. et al., 1989. Où sont les Nappes dans le Massif Central Francais? Bulletin De La Societe Geologique De France, 5(3): 605-618.

Ledru, P. et al., 1994. Notice explicative, Carte géol. France (1/50 000), feuille Craponne-sur-Arzon (767), BRGM, Orléans.

Ledru, P. et al., 2001. The Velay dome (French Massif Central): melt generation and granite emplacement during orogenic evolution. Tectonophysics, 342(3-4): 207-237.

Leyreloup, A.F., 1992. La croute métamorphique du Sud de la France (Massif Central, Languedoc). Géologie de surface et des enclaves remontées par les volcans cénozoïques : le rôle des intrusions mafiques basicrustales dans la croûte inférieure. Thèse d'Etat, Montpellier.

Leyreloup, A.F., Dupuy, C. and Andriambololona, R., 1977. Catazonal xenoliths in French Neogene volcanic rocks: constitution of the lower crust. Contributions to Mineralogy and Petrology, 62(3): 283-300.

Linnemann, U. et al., 2000. From Cadomian subduction to Early Palaeozoic rifting: The evolution of Saxo-Thuringia at the margin of Gondwana in the light of single zircon geochronology and basin development (Central European Variscides, Germany). In: W. Franke, V. Haak, O. Oncken and D. Tanner (Editors), Orogenic Processes: Quantification and Modelling in the Variscan Belt. London, Geological Society, Special Publications, pp. 131-153.

Linnemann, U., Pereira, F., Jeffries, T.E., Drost, K. and Gerdes, A., 2007. The Cadomian Orogeny and the opening of the Rheic Ocean: the diacrony of geotectonic processes constrained by LA-ICP-MS U–Pb zircon dating (Ossa-Morena and Saxo-Thuringian Zones, Iberian and Bohemian Massifs). Tectonophysics, 461(1): 21-43.

Linnemann, U., Gerdes, A., Hofmann, M. and Marko, L., 2014. The Cadomian Orogen: Neoproterozoic to Early Cambrian crustal growth and orogenic zoning along the periphery of the West African Craton—Constraints from U–Pb zircon ages and Hf isotopes (Schwarzburg Antiform, Germany). Precambrian Research, 244: 236-278.

Lotout, C., Pitra, P., Poujol, M. and Van Den Driessche, J., 2017. Ordovician magmatism in the Lévézou massif (French Massif Central): tectonic and geodynamic implications. Int J Earth Sci. doi, 10.

Lotout, C., Pitra, P., Poujol, M., Anczkiewicz, R. and Van Den Driessche, J., 2018. Timing and duration of Variscan high-pressure metamorphism in the French Massif Central: A multimethod geochronological study from the Najac Massif. Lithos, 308: 381-394.

Macaudière, J., Barbey, P., Jabbori, J., Marignac, C., 1992. Le stade initial de fusion dans le développement des dômes anatectiques: le dôme du Velay (Massif central français). – Comptes-Rendus de l'Académie des Sciences, Paris, 315, 1761-1767.

Malavieille, J., Guihot, P., Costa, S., Lardeaux, J.M. and Gardien, V., 1990. Collapse of the thickened Variscan crust in the French Massif Central: Mont Pilat extensional shear zone and St. Etienne Late Carboniferous basin. Tectonophysics, 177(1-3): 139-149.

Matte, P., 1986. Tectonics and Plate-Tectonics Model for the Variscan Belt of Europe. Tectonophysics, 126(2-4): 329-374.

Matte, P., 2001. The Variscan collage and orogeny (480–290 Ma) and the tectonic definition of the Armorica microplate: a review. Terra Nova, 13(2): 122-128.

Meinhold, G., Morton, A.C. and Avigad, D., 2013. New insights into peri-Gondwana paleogeography and the Gondwana super-fan system from detrital zircon U–Pb ages. Gondwana Research, 23(2): 661-665.

Melleton, J., Cocherie, A., Faure, M. and Rossi, P., 2010. Precambrian protoliths and Early Paleozoic magmatism in the French Massif Central: U-Pb data

and the North Gondwana connection in the west European Variscan belt. Gondwana Research, 17(1): 13-25.

Mercier, L., Lardeaux, J.M. and Davy, P., 1991. On the tectonic significance of retrograde P-T-t paths in eclogites of the French Massif Central. Tectonics, 10(1): 131-140.

Mialhe, J., 1980. Le massif granitique de la Borne, étude pétrographique, géochimique et géochronologique, Université Clermont II.

Michon, G., 1987. Les Vaugnerites de l'Est du Massif Central Français : Apport de l'Analyse Multivariée à l'Etude Géochimique des Eléments Majeurs Statistical Approach on Major Elements. Bulletin De La Societe Geologique De France, 3(3): 591-600.

Mintrone, M., 2016. Constraining the duration of metamorphic events by modeling of phase equilibrium and diffusion in garnet; Example from the French Massif Central, France. M.Sc. thesis, Université Blaise-Pascal, Clermont-Ferrand.

Monié, P., Respaut, J.-P., Brichau, S., Bouchot, V., Faure, M., Roig, J., 2000. $^{40}Ar/^{39}Ar$ and U-Pb geochronology applied to Au-W-Sb metallogenesis in the Cévennes and Châtaigneraie districts (Southern Massif Central, France). In Geode-GéoFrance3D workshop on orogenic gold deposits in Europe, with emphasis on the Variscides. Doc BRGM 297:77–79

Montel, J.M., 1985. Xénolithes peralumineux dans les dolérites du Peyron, en Velay (Massif Central, France). Indications sur l'évolution de la cropute profonde tardi-hercynienne. Comptes Rendus de l' Academie des Sciences Serie IIa:Sciences de la Terre et des Planets, 301: 615-620.

Montel, J.-M. and Weisbrod, A., 1986. Characteristics and evolution of “vaugneritic magmas”: an analytical and experimental approach, on the example of the Cévennes Médianes (French Massif Central). Bulletin of Mineralogy, 109(5), 575-587.

Montel, J.M., Marignac, C., Barbey, P. and Pichavant, M., 1992. Thermobarometry and Granite Genesis - the Hercynian Low-P, High-T Velay Anatectic Dome (French Massif-Central). Journal of Metamorphic Geology, 10(1): 1-15.

Mougeot, R., Respaut, J.P., Ledru, P. and Marignac, C., 1997. U-Pb chronology on accessory minerals of the Velay anatectic dome (French Massif Central). European Journal of Mineralogy, 9: 141-156.

Moyen, J.F, Laurent, O., Chelle-Michou, C., Couzinié, S., Vanderhaeghe, O., Zeh, A., Villaros, A., Gardien, V., 2017. Collision vs. subduction-related magmatism: two contrasting ways of granite formation and implications for crustal growth. Lithos, 277: 154-177.

Næraa, T. et al., 2012. Hafnium isotope evidence for a transition in the dynamics of continental growth 3.2 Gyr ago. Nature, 485(7400): 627.

Najoui, K., Leyreloup, A.F., Monié, P., 2000. Conditions et âges $^{40}Ar/^{39}Ar$ de mise en place des granitoïdes de la zone externe sud du Massif central français: Exemple des granodiorites de St-Guiral et du Liron (Cévennes, France), Bulletin de la Société Geologique de France 171, 495-510.

Nance, D.R., Murphy, B.J., Strachan, R.A., D’Lemos, R.S. and Taylor, G.K., 1991. Late Proterozoic tectonostratigraphic evolution of the Avalonian and Cadomian terranes. Precambrian Research, 53: 41-78.

Nance, R.D. et al., 2010. Evolution of the Rheic ocean. Gondwana Research, 17(2): 194-222.

Nomade, S., Chauvet, A., Barbanson, L. and Charonnat, X., 1999. Les minéralisations aurifères des Cévennes (Massif central français): étude comparative des filons d'Alteyrac/Pont-de-Rastel et du paléoplacer du Bulidou. Comptes Rendus de l'Académie des Sciences-Series IIA-Earth and Planetary Science, 328(12): 815-822.

Paquette, J.-L., Ballèvre, M., Peucat, J.-J. and Cornen, G., 2017. From opening to subduction of an oceanic domain constrained by LA-ICP-MS U-Pb zircon dating (Variscan belt, Southern Armorican Massif, France). Lithos, 294: 418-437.

Peiffer, M.-T., 1986. La signification de la ligne tonalitique du Limousin. Son implication dans la structuration varisque du Massif Central français. Comptes rendus de l'Académie des sciences. Série 2, Mécanique, Physique, Chimie, Sciences de l'univers, Sciences de la Terre, 303(4): 305-310.

Pin, C. and Lancelot, J., 1982. U - Pb Dating of an Early Paleozoic Bimodal Magmatism in the French Massif Central and of Its Further Metamorphic Evolution. Contributions to Mineralogy and Petrology, 79(1): 1-12.

Pin, C. and Paquette, J.-L., 1997. A mantle-derived bimodal suite in the Hercynian Belt: Nd isotope and trace element evidence for a subduction-related rift origin of the Late Devonian Brévenne metavolcanics, Massif Central (France). Contributions to Mineralogy and Petrology, 129(2-3): 222-238.

Pin, C. and Paquette, J.-L., 2002. Le magmatisme basique calcoalcalin d'âge dévono-dinantien du nord du Massif Central, témoin d'une marge active hercynienne: arguments géochimiques et isotopiques Sr/Nd: Sr-Nd isotope and trace element evidence for a Late Devonian active margin in northern Massif-Central (France). Geodinamica Acta, 15(1): 63-77.

R'Kha Chaham, K., Couturié, J.-P., Duthou, J.-L., Fernandez, A. and Vitel, G., 1990. L'orthogneiss œillé de l'Arc de Fix: un nouveau témoin d'âge cambrien d'un magmatisme hyper alumineux dans le Massif Central français. Comptes rendus de l'Académie des sciences. Série 2, Mécanique, Physique, Chimie, Sciences de l'univers, Sciences de la Terre, 311(7): 845-850.

Rossi, P. and Pin, C., 2008. Les magmatismes paléozoïques. Géochronique, 105: 53-56.

Sabatier, H., 1991. Vaugnerites: special lamprophyre-derived mafic enclaves in some Hercynian granites from Western and Central Europe. In: J. Didier and B. Barbarin (Editors), Enclaves and granite petrology. Developments in petrology, pp. 63-81.

Shaw, A., Downes, H. and Thirlwall, M., 1993. The quartz-diorites of Limousin: elemental and isotopic evidence for Devono-Carboniferous subduction in the

Hercynian belt of the French Massif Central. Chemical Geology, 107(1-2): 1-18.

Sider, H. and Ohnenstetter, M., 1986. Field and petrological evidence for the development of an ensialic marginal basin related to the Hercynian orogeny in the Massif Central, France. Geologische Rundschau, 75(2): 421-443.

Siebel, W. and Chen, F., 2009. Zircon Hf isotope perspective on the origin of granitic rocks from eastern Bavaria, SW Bohemian Massif. International Journal of Earth Sciences, 99(5): 993-105.

Solgadi, F., Moyen, J.-F., Vanderhaeghe, O., Sawyer, E.W. and Reisberg, L., 2007. The relative roles of crustal anatexis and mantle-derived magmas: Generation of Synorogenic, Hercynian granites in the Livradois area, French Massif Central. Canadian Mineralogist, 45: 581-606.

Squire, R.J., Campbell, I.H., Allen, C.M. and Wilson, C.J., 2006. Did the Transgondwanan Supermountain trigger the explosive radiation of animals on Earth? Earth and Planetary Science Letters, 250(1): 116-133.

Stampfli, G.M., Von Raumer, J. and Borel, G.D., 2002. Paleozoic evolution of pre-Variscan terranes: from Gondwana to the Variscan collision. In: J.R. Martínez Catalán, R.D. Hatcher, Jr., R. Arenas and F. Díaz García (Editors), Variscan-Appalachian dynamics: the building of the Late Paleozoic basement. Special publications. Geological Society of America, pp. 263-280.

Stampfli, G.M., Hochard, C., Vérard, C., Wilhem, C. and Von Raumer, J., 2013. The formation of Pangea. Tectonophysics, 593: 1-19.

Tait, J., Bachtadse, V., Franke, W. and Soffel, H., 1997. Geodynamic evolution of the European Variscan fold belt: palaeomagnetic and geological constraints. Geologische Rundschau, 86(3): 585.

Talbot, J.Y., Martelet, G., Courrioux, G., Chen, Y. and Faure, M., 2004. Emplacement in an extensional setting of the Mont Lozere-Borne granitic complex (SE France) inferred from comprehensive AMS, structural and gravity studies. Journal of Structural Geology, 26(1): 11-28.

Talbot, J.Y., Chen, Y., Faure, M., 2005. A magnetic fabric study of the Aigoual–Saint Guiral–Liron granite pluton (French Massif Central) and relationships with its associated dikes. Journal of Geophysical Research 110, B12106.

Thiery, V. et al., 2009. Visean sinistral wrench faulting along the Sillon Houiller in the French Massif Central: Late Variscan tectonic implications. Bulletin de la Société Géologique de France, 180(6): 513-528.

Toteu, S.F. and Macaudière, J. 1984. Complex synkinematic and postkinematic garnet porphyroblast growth in polymetamorphic rocks. Journal of Structural Geology 6, 669-677.

Turpin, L., Velde, D. and Pinte, G., 1988. Geochemical Comparison between Minettes and Kersantites from the Western European Hercynian Orogen - Trace-Element and Pb-Sr-Nd Isotope Constraints on Their Origin. Earth and Planetary Science Letters, 87(1-2): 73-86.

Turpin, L., Cuney, M., Friedrich, M., Bouchez, J.L. and Aubertin, M., 1990. Meta-Igneous Origin of Hercynian Peraluminous Granites in Nw French Massif Central - Implications for Crustal History Reconstructions. Contributions to Mineralogy and Petrology, 104(2): 163-172.

Vanderhaeghe, O., Burg, J. and Teyssier, C., 1999. Exhumation of migmatites in two collapsed orogens Canadian Cordillera and French Variscides. Exhumation processes normal faulting, ductile flow and erosion Geological Society Special Publications, 154: 181-204.

Vanderhaeghe, O., Laurent, O., Gardien, V., Moyen, J.-F., Gébelin, A., Chelle-Michou, C., Couzinié, S., Villaros, A., Bellanger, M., 2020. Flow of partially molten crust controlling construction, growth and collapse of the Variscan orogenic belt: the geologic record of the French Massif Central. Bulletin de la Société Géologique de France 191(1), 25.

Villaros, A., Buick, I.S. and Stevens, G., 2012. Isotopic variations in S-type granites: an inheritance from a heterogeneous source? Contributions to Mineralogy and Petrology, 163(2): 243-257.

Villaros, A., Laurent, O., Couzinié, S., Moyen, J.-F., Mintrone, M., 2018. Plutons and domes: the consequences of anatectic magma extraction—example from the southeastern French Massif Central. International Journal of Earth Sciences 107, 2819-2842.

Villaseca, C., Castiñeiras, P. and Orejana, D., 2015. Early Ordovician metabasites from the Spanish Central System: A remnant of intraplate HP rocks in the Central Iberian Zone. Gondwana Research, 27(1): 392-409.

von Raumer, J.F., Bussy, F., Schaltegger, U., Schulz, B. and Stampfli, G.M., 2013a. Pre-Mesozoic Alpine basements—their place in the European Paleozoic framework. Geological Society of America Bulletin, 125(1-2): 89-108.

von Raumer, J.F., Finger, F., Veselá, P. and Stampfli, G.M., 2013b. Durbachites–Vaugnerites–a geodynamic marker in the central European Variscan orogen. Terra Nova.

von Raumer, J.F., Stampfli, G.M., Arenas, R. and Martínez, S.S., 2015. Ediacaran to Cambrian oceanic rocks of the Gondwana margin and their tectonic interpretation. International Journal of Earth Sciences, 104(5): 1107-1121.

Weber, C., Pichavant, M., Barbey, M., 1985. La cordiérite dans le domaine anatectique du Velay (Massif central français): un marqueur de l'anatexie, du magmatisme et de l'hydrothermalisme. Comptes Rendus de l'Académie des Sciences, Paris, 301, 303-308.

Weisbrod, A., 1970. Pétrologie du socle métamorphique des Cévennes médianes (Massif central francais) : reconstitution sédimentologique et approche thermodynamique du métamorphisme, Université de Nancy, 355 pp.

Weisbrod, A and Marignac C., 1968. Sur l'origine des « schistes amygdalaires » des Cévennes (Massif

Central français). Comptes Rendus de l'Académie des Sciences, Paris, 266, 865-867.

Werle, M., Stevens, G., Moyen, J.-F., Laurent, O., Harris, C., Lana, C.C., Janney, P.E., 2023. Cryptic crustal growth identified through Variscan post-collisional lamprophyre-granite composite dykes, French Massif Central. Lithos 454, 107270.

Williamson, B.J., Downes, H. and Thirlwall, M.F., 1992. The Relationship between Crustal Magmatic Underplating and Granite Genesis - an Example from the Velay Granite Complex, Massif-Central, France. Transactions of the Royal Society of Edinburgh-Earth Sciences, 83: 235-245.

Williamson, B.J., Shaw, A., Downes, H., Thirlwall, M.F., 1996. Geochemical constraints on the genesis of Hercynian two-mica leucogranites from the Massif Central, France. Chemical Geology 127, 25-42.

Williamson, B., Downes, H., Thirlwall, M. and Beard, A., 1997. Geochemical constraints on restite composition and unmixing in the Velay anatectic granite, French Massif Central. Lithos, 40(2-4): 295-319.

Zeh, A., Brätz, H., Millar, I.L. and S., W.I., 2001. A combined zircon SHRIMP and Sm-Nd isotope study on high-grade paragneisses from the Mid-German Crystalline Rise: Evidence for northern Gondwanan and Grenvillian provenance. Journal of the Geological Society of London, 158: 983-994.